Engineering cytokine immunotherapies via cell surface targeting

by

Luciano Santollani
B.S. Chemical Engineering, Stanford University (2018)

Submitted to the Department of Chemical Engineering in partial fulfillment of the requirements for the degree of

Doctor of Philosophy in Chemical Engineering
at the
Massachusetts Institute of Technology
May 2024

Authored by: .....
Luciano Santollani
Department of Chemical Engineering
April 30th 2024

Certified by: .....
K. Dane Wittrup, PhD
Carbon P. Dubbs Professor of Chemical Engineering, MIT
Professor of Biological Engineering, MIT
Thesis Advisor

and by: .....
Darrell J. Irvine, PhD
Underwood-Prescott Professor of Biological Engineering, MIT
Professor of Materials Science, MIT
Thesis Supervisor

Accepted by: .....
Hadley Sikes, PhD
Willard Henry Dow Professor of Chemical Engineering
Chair, Committee for Graduate Students

Engineering cytokine immunotherapies via cell surface targeting

by

Luciano Santollani

Submitted to the Department of Chemical Engineering on April 30th, 2024 in Partial Fulfillment of the Requirements for the Degree of Doctor of Philosophy in Chemical Engineering

ABSTRACT

Cancer immunotherapy targets immune cells to trigger a highly specific, long-lasting anti-tumor response. With the clinical success of immune checkpoint blockade and the development of promising next-generation agents, immunotherapy is steadily growing as a key pillar of the oncology clinic alongside surgery, radiation, and chemotherapy. Cytokines, endogenous regulators of immune responses, have long been promising immunotherapy candidates due to their innate ability to modulate lymphocyte behavior. However, translation of cytokines as systemically administered immunotherapies has been severely limited by on-target/off-tissue toxicity. One approach to overcome this challenge is to engineer cytokines for intratumoral retention following local administration to isolate their activity to on-target tissue. In this thesis, we explore an immune cell-based localization strategy by designing, evaluating, and optimizing antibody-cytokine fusions targeting the ubiquitous leukocyte receptor CD45.

First, we engineer and profile an αCD45-IL15 fusion that exhibits significantly diminished receptor-mediated internalization relative to its wild-type counterpart. This extended surface half-life augments downstream pSTAT5 induction and enables both *cis* and *trans* signaling between lymphocytes. We demonstrate this enhanced cell-surface biology is consistent when this approach is applied to another pro-inflammatory cytokine, IL-12. Preliminary experiments additionally suggest conserved internalization behavior between mouse and human CD45. Intratumoral αCD45-cytokine administration at specified doses leads to decoration of leukocytes in the tumor and tumor-draining lymph node (TDLN) while sparing systemic exposure. Biodistribution experiments suggest dose-dependent drainage of CD45-targeted proteins from the tumor through the TDLN and into systemic circulation, allowing for compartment specific targeting.

In the second part of the thesis, we develop and deeply characterize a two-dose sequential cytokine therapy termed αCD45-Cyt that safely elicits profound anti-tumor immunity. In this paradigm, a single dose of αCD45-IL12 followed by a single dose of αCD45-IL15 is able to eradicate both treated tumors and untreated distal lesions in multiple syngeneic mouse tumor models. Mechanistically, the improved intratumoral and nodal retention driven by CD45 targeting enabled reprogramming of tumor specific $CD8^+$ T cells in the TDLN to exhibit an anti-viral transcriptional signature. Finally, we discuss preliminary data and plans for translating αCD45-Cyt therapy. Altogether, this thesis highlights the power of targeting host immune cells for use in immunotherapy and more broadly discusses the ability of multi-receptor targeting to elicit new signaling biology.

Thesis supervisor: K. Dane Wittrup, PhD; Darrell J. Irvine, PhD
Title: Carbon P. Dubbs Professor of Chemical Engineering and Biological Engineering (KDW); Underwood-Prescott Professor of Biological Engineering (DJI)

Thesis Committee Members

K. Dane Wittrup, PhD (*Thesis Advisor*)
Carbon P. Dubbs Professor of Chemical Engineering
Professor of Biological Engineering
Koch Institute for Integrative Cancer Research at Massachusetts Institute of Technology

Darrell J. Irvine, PhD (*Thesis Advisor*)
Underwood-Prescott Professor of Biological Engineering
Professor of Material Science
Koch Institute for Integrative Cancer Research at Massachusetts Institute of Technology

Paula T. Hammond, PhD
Institute Professor
Koch Institute for Integrative Cancer Research at Massachusetts Institute of Technology

Ulrich von Andrian, MD, PhD
Mallinckrodt Professor of Immunopathology at Harvard Medical School
Program Leader, Basic Immunology at Ragon Institute of MGH, MIT and Harvard

Acknowledgements

I remember moving to Boston in 2019, equally excited about the journey ahead and terrified at the thought of having to work again after a gap year traveling around South America. Fast forward to 2024 and I can confidently say that I couldn't have scripted a better 5 years for myself even if I tried. To the folks I had on my team throughout this adventure, thank you – I feel more fulfilled, happier, and compelled to make an impact than ever before.

To start, I want to express my gratitude to Dane and Darrell (D+D), the most legendary co-advisors you could ask for. Dane, thank you for the unwavering support from the very beginning. Our biweekly meetings are something I always looked forward to, guaranteed that the hour would be filled with a discussion spanning everything from scientific updates to biotech financings to food and wine. It's such an empowering feeling knowing you have my back and are always rooting for me. Darrell, thank you for helping to mold me into the scientist I am today. You are the most intentional and meaningful scientist I know – your ability to cut through to the core of complex biology is something I deeply admire and aim to emulate in my own thinking. The deep sense of purpose you both imbue the labs' science with is inspirational – not many people can say their labs have put 4+ novel technologies into the clinic. I am certain the three of us will continue to work together in the future, and I already look forward to it. To my committee members Paula Hammond and Uli von Andrian, thank you for all the insights and support throughout the journey. Your suggestions helped push the science to new and interesting places, and I'm very thankful you took the time to help train me into a better scientist.

My time at Stanford was truly formational and convinced me of my future as a researcher. I remember, as freshman, flagging down Gerry Fuller after a lecture to ask him for an opportunity to work in his fluid mechanics lab. It's been almost 10 years since that summer, but I still remember the experience so positively – thank you for making my initial research adventure such a great one. I want to thank Chaitan Khosla who ultimately sent me down the biotech rabbit hole (which I happily continue to go down today). The biotech entrepreneurship crash course that he and Zach Sweeney ran together on Tuesday nights put me on to this exciting field that I plan to pursue and contribute to.

To all of my labmates, past and present, in both the Wittrup and Irvine labs, thanks for fostering such an incredible community. A special shout out to Yash Agarwal, a previous Irvine + Wittrup grad student, who mentored me when I joined the labs. Yash taught me everything I needed to know to set myself up for success – I'll always be thankful for that. I've deeply enjoyed the collaborative and social nature of our labs. Anytime you need help, someone is there alongside you. Jordan Stinson, Laura Maiorino, Joseph Palmeri, Lauren Duhamel, Bri Lax, Kashif Qureshi – thank you for all the help and laughs along the way, especially when we were starting an 8AM experiment while listening to Joseph's *unique* music taste blasting through the lab speakers. A special mention to my Irvine lab mate and apartment neighbor, Asheley Chapman. Commiserating about failed

experiments and apartment maintenance together always made my day better. I also had the opportunity to work with an amazing MIT undergrad, Jack Suggs. Thanks for your incredible work ethic and commitment to the project over the year we worked together. Finally, a huge thank you to Stephanie Gaglione and Grant Knappe, two close friends from the 2019 Chemical Engineering cohort. I absolutely wouldn't have made it through this journey without you guys and I look forward to continuing our hang outs for years to come.

Throughout my PhD, I was able to contribute to and spend time with the biotech community in Boston. The friends and mentors I got to meet over the past 5 years have led to countless laughs, insights, and exciting opportunities. A special thank you to Tony & Thomas (T+T) at Pillar – your mentorship and support over the last few years were instrumental in helping me to be ready for what's to come.

Even though the PhD is earned through long days and experiments inside the lab, it's made possible by the support network you have outside of the MIT walls. Nate & Sayuri – from living in the same freshman dorm at Stanford to surviving the pandemic together in Boston to all of our adventures here and beyond, I'm so thankful for your friendship. Guillermo and Katie, even though we don't live close by anymore, our time together during Bay Area visits and back home in Texas are always a joy. Alborz, our battles on the squash court both at Stanford and now here in Boston kept me sane. Ryan and Laila, getting to see you guys during Texas visits was always a highlight. Ojas and Edward, I always look forward to our insane Korean BBQ reunions. To all the friends I've been fortunate enough to share many coffees and meals with over the last 5 years, thank you.

Oscar and Ceci…what a journey! Your encouragement and support from day 1 is what made this possible. Whether it was about my obsession with cars during elementary school or skateboarding during my teenage years or now starting my career, you guys have always been my biggest cheerleaders. Just as importantly, you've both taught me the value of building meaningful relationships and living an intentional life. Thank you for moving us from Argentina to the U.S. in 2002 – there's no way I would have these opportunities anywhere else. It was all worth it. Vamos!!!

Finally, and most importantly, Daria. Regardless of how good or bad a day in lab was, coming home to spend time together always was the best part. I'm the luckiest person in the world to get to do life with you by my side. Though a lot has changed since we met in CHEM 31X office hours in 2014, your support has remained an unwavering constant. Thank you for everything. Next time you tell me it might not be a good idea to defend a thesis, start a company, and get married all in 6 months, I promise I'll listen!

Table of Contents

List of Figures

List of Tables

Chapter 1 : Introduction

"That this seemingly simple mechanism—cell growth without barriers—can lie at the heart of this grotesque and multifaceted illness is a testament to the unfathomable power of cell growth. Cell division allows us as organisms to grow, to adapt, to recover, to repair—to live. And distorted and unleashed, it allows cancer cells to grow, to flourish, to adapt, to recover, and to repair—to live at the cost of our living. Cancer cells can grow faster, adapt better. They are more perfect versions of ourselves."

— **Siddhartha Mukherjee, The Emperor of All Maladies**

Parts of this chapter appear as published in Santollani and Wittrup, *Immunological Reviews* (2023)(*1*).

A Brief History of Cancer immunotherapy

Over the last two decades, cancer immunotherapy has emerged as powerful tool in the oncology arsenal. Whereas traditional chemotherapeutic agents act broadly and aim to kill tumor cells directly, cancer immunotherapies target our immune cells to elicit a highly specific anti-tumor response. This interplay between our immune system and cancer is canonically described in Chen and Mellman's cancer immunity cycle(*2*). In this model, cancer debris from dying tumor cells is picked up by professional antigen presenting cells (APCs) like dendritic cells (DCs). These DCs will traffic from the tumor to the nearest lymph node (tumor draining lymph node or TDLN). Here, DCs will present the cancer's molecular fingerprint, known as antigen or neoantigen, to a repertoire of $CD8^+$ T cells. A cognate match between DC-presented antigen and a given T cell receptor (TCR) will spur activation and proliferation of this T cell clone. Upon activation, this T cell will upregulate a genetic program that promotes lymph node egress and endows it with cytotoxic capacities. Circulating $CD8^+$ T cells will then infiltrate the tumor, and upon recognizing the cancer cell they were "trained" to kill, unleash cytotoxic molecules that kill the corresponding tumor cell. These freshly lysed tumor cells represent a new pool of antigen for DCs to present and begin the cycle again.

However, as Mukherjee's provoking quote above suggests, cancer is a formidable biological opponent. At every step in the cancer immunity cycle, tumor cells evolve to evade the immune system and dismantle the anti-tumor response. A canonical example is the downregulation of MHC-I by cancer cells(*2*). By shedding their surface of this recognition molecule, tumor cells avoid being targeted by $CD8^+$ T cells. Another key example is the upregulation of immune checkpoints by tumor cells. These regulatory proteins on the tumor cell surface interact with receptors on T cells to inhibit the immune response(*2*). Broadly, cancer immunotherapy aims to rescue specific pathways of the cancer immunity cycle and elicit a potent anti-tumor response.

The promise of immunotherapy has most recently been demonstrated by the clinical success of immune checkpoint blockade (ICB) – antibodies targeting PD-1, PD-L1, and CTLA-4 – against disseminated disease like metastatic melanoma where overall survival (OS) can reach up to 50%. In some indications, like subsets of non-small cell lung cancer (NSCLC), ICB has become a first-line therapy. However, apart from ICB, almost all immunotherapy agents that have been evaluated in the clinic for solid tumors have suffered from significant clinical challenges. Most notably, immunotherapies often trigger immune related adverse events (irAEs) that result in dose-limiting toxicities. Very simply, there is no dose that elicits strong activity without also triggering toxicity. Thus, much of the potential of immunotherapy remains untapped due to small therapeutic windows. Part of this undesired toxicity can be attributed to on-target/off-tumor stimulation of immune cells that occurs in bystander tissues. Furthermore, systemic delivery of these immunotherapeutic agents only leads to minimal tumor penetration before renal clearance, preventing enough payload accumulation in the tumor to achieve efficacy.

Ultimately, the development of successful immunotherapies requires striking a balance between efficacy and toxicity that is largely driven by biodistribution. In this thesis, we explore and engineer an immunotherapy strategy based on a class of naturally occurring proteins in the immune system known as cytokines.

Cytokines as immunotherapies

Cytokines represent a broad class of small proteins that serve as molecular messengers of the immune system. From Interferons (IFNs) to Interleukins (ILs), cytokines have long been promising candidates for cancer immunotherapy due to their ability to regulate immune signaling cascades(*3*, *4*). Notably, the cytokine family is involved in leukocyte activation and proliferation – key steps in mounting an anti-tumor response(*2*, *5*). In fact, IFNα and IL-2, two immuno-stimulatory cytokines, were first dosed in patients during landmark studies of the 1970s-80s, leading to their respective FDA approvals for hairy cell leukemia in 1986 and renal cell carcinoma (RCC) in 1992(*5*, *6*). These achievements, though initially promising, proved to not be a panacea for oncology. Narrow therapeutic windows and consequently low maximum-tolerated doses (MTDs) have significantly hampered clinical utilization of cytokines(*7*–*9*). The high systemic doses required to achieve therapeutic concentrations at tissues of interest lead to severe toxicity. As of the time of writing, only one new cytokine monotherapy, a locally delivered adenoviral vector encoding for the already-approved IFNα2b (Adstiladrin), had received FDA approval for cancer indications since that of Aldesleukin (IL-2) and Intron A (IFNα)(*10*).

The challenges in developing cytokines as exogenous therapies stem from their characteristics as fine-tuned signaling proteins of the immune system. Endogenous cytokine production is carefully regulated by various cellular processes and cues and is generally limited to specific tissues and timescales(*7*, *11*). This is in stark opposition to how cytokines are dosed therapeutically, often given systemically at high doses that lead to on-target/off-tissue toxicity, further compounded by cytokines' natural pleiotropy. The same cognate cytokine receptor can be found on multiple cell types, with sometimes counter-regulatory functions: notably, IL-2 will activate CD8 T cells and Natural Killer (NK) cells through the IL2Rβγ receptor, but additionally activate immuno-suppressive regulatory T cells (Tregs) through the higher affinity trimeric IL2Rαβγ complex. Thus, the same complex biology that underlies the ability of cytokines to maintain immune homeostasis presents an engineering challenge for therapeutic development.

Over the last two decades, protein engineering has emerged as a promising tool to address the shortcomings of these first-generation therapies. Breakthroughs in our understanding of cytokine signaling, tumor immunology, and ability to manipulate proteins have led to an explosion of preclinical, and now increasingly, clinical, development of next-generation cytokines. Approaches such as half-life extension, antibody-mediated targeting, and intratumoral anchoring are being explored to widen the narrow response curve that has plagued cytokine therapies (**Figure 1.1**).

In this thesis, we ultimately focus on engineering an intratumoral, antibody-targeted cytokine therapy whose mechanism is highly motivated by spatiotemporal programming. That is, we hypothesize that controlling the time, place, and duration of cytokine signaling is critical to maximizing both efficacy and safety. Using protein engineering to allow therapeutic cytokines to reproduce their endogenous immune system roles more closely may help unlock their therapeutic potential. To understand the specific therapy developed in this thesis, it is important to contextualize some previous work in cytokine engineering. Below I highlight select approaches that are relevant to the work in this thesis – for more comprehensive cytokine reviews, refer to the excellent reviews by Holder and colleagues, Pires and colleagues, and Saxton and colleagues(*11–13*).

Temporal programming by improving half-life

One of the first applications of protein engineering in cytokine development was to improve the poor pharmacokinetic (PK) properties they exhibit due to their small size. Cytokines, generally <50 kDa, are rapidly cleared from circulation, limiting duration of exposure and tumor uptake. This temporal regulation could be viewed as a feature subject to natural selection, limiting systemic exposure to cytokines from their local expression site. For example, IL-2 is sequestered to some extent by the local extracellular matrix (ECM) after inflammation for subsequent access by Tregs(*14*, *15*). However, in the therapeutic context, this rapid clearance following intravenous administration

necessitates high and repeated dosing to overcome the minutes-long half-life[4]. To address this, many preclinical studies, including ours, have used Fc-cytokine or albumin-cytokine fusions (**Figure 1.2A-B**) (*16–19*). In these strategies, the wild-type cytokine is fused with a flexible glycine-serine linker to the Fc portion of an IgG antibody or albumin (**Figure 1.2A-B**). This effective increase in molecular weight, together with neonatal Fc receptor(FcRn)-mediated salvage recycling, endows an extended half-life in vivo, with up to an order of magnitude increase reported for a mouse serum albumin (MSA)-IL-2 fusion in mice(*16*). MSA-IFNα has also been reported to be present in serum 5 days after administration(*20*). To maintain monovalent cytokine expression in an Fc-fusion format, co-transfection and orthogonal affinity tag purification or knob-in-hole mutations can be used(*16*, *18*, *21*). This can be important since monovalent cytokine Fc fusions have been reported to be more efficacious and less toxic in the context of IL-12(*21*). Additionally, effector-attenuating mutations in the Fc region have become commonplace to minimize any FcɣR interactions(*22*, *23*). We have additionally reported on a fully inert MSA variant with an H464Q mutation that abrogates FcRn-mediated recycling(*24*). For these fusion proteins, the longer half-life allows for lower and less frequent dosing, thus lowering the maximum drug concentration, C_{max}, which often associated with toxicity, while increasing the pharmacokinetic exposure (measured as area under the curve or AUC; **Figure 1.2A**)(*25*, *26*). Extended half-life strategies have become a standard part of the preclinical cytokine toolkit. Zhu et al. reported on a safe, efficacious treatment paradigm of extended half-life Fc/IL-2 in combination with either a tumor-targeting antibody or adoptive cell therapy (ACT) in multiple mouse models(*16*). This work was expanded upon in the context of extended half-life MSA-IL2 in combination with anti-PD1, a tumor targeting antibody, and a lymph-node draining cancer vaccine(*27*). This powerful combination, termed AIPV, was highly curative (>75%) in large (50mm^2) B16F10 melanoma tumors. Removal of the cytokine from this treatment ablated efficacy and led to no long-term survivors, highlighting the critical potential contribution of cytokines to combination therapies. More recently, Wang et al. mechanistically studied the subcomponents of AIPV therapy and found that a simplified regimen of single dose of MSA-IL2, αPD-1, and a

tumor-targeting component followed by subsequent checkpoint blockade immunotherapy (CBI) was as efficacious as the full AIPV treatment(*28*).

Despite their popularity and effectiveness in preclinical studies for over a decade, Fc and albumin fusions remain in early stages in the clinic. Albuleukin, a human serum albumin (HSA)-IL2 fusion showed promising preclinical data and was dosed in the clinic, but was ultimately discontinued(*29*, *30*). One of the most advanced half-life extension candidates, Dragonfly Therapeutics' DF6002, a monovalent IL-12-Fc fusion similar to that reported by Jung and colleagues(*21*), only recently entered a dose escalation Phase I/II trial, but results were not available at time of writing(*31*). Polymer conjugation has also been used for half-life extension, most notably in the context of Nektar Therapeutics' failed PEGylated IL-2, but we will refer readers to other reviews for more details on those strategies(*12*, *13*). While improving time-on-target will likely be required for successfully translating cytokine therapies, it will likely not be sufficient on its own. Much of the toxicity associated with cytokines stems from on-target/off-tissue stimulation of circulating immune cells. Simply extending circulation timescales will not ameliorate this, and in fact exacerbates it; however, half-life extension will play a critical role in enabling additional engineering strategies. For example, in the case of engineering the receptor specificity of a small cytokine like IL-2, half-life extension will still be needed to achieve a desirable pharmacokinetic profile.

Aside from half-life extension, it's also important to note that for small cytokines like IL-2 and IFNs, expression as an Fc or albumin fusion can significantly improve recombinant yields over wild-type cytokine in mammalian expression systems (unpublished results from our group, but also reported in literature by others(*32*)).

First-generation immunocytokines targeting tumors

One avenue attempted to improve the localization of cytokine responses has been to "target" them to the tumor via antibody fusions. By fusing wild-type cytokines to antibodies

(referred to as immunocytokines hereafter) directed at tumor-associated antigens (TAAs), it was hypothesized that systemic exposure and on-target/off-tumor toxicity could be reduced. However, we have previously shown that simple immunocytokine targeting does not solve this problem in the context of solid tumors(*33*, *34*). In the case of a systemically administered IL-2 immunocytokine targeted to the melanoma marker TRP1, Tzeng et al. demonstrated that the biodistribution of the fusion protein is entirely governed by cognate cytokine receptor expression patterns(*33*). For IL-2, this led to an appreciable systemic "sink" from NK and NKT cells, as opposed to the desired stimulation of intratumoral CD8 T cells. Substituting the targeting antibody with an untargeted control had no effect on the biodistribution or efficacy of this therapy, illustrating the dominance of cytokine-driven localization. Ultimately, this can be attributed to minimal antigen presence in circulation in comparison to that of the cytokine receptor, which can be found on many circulating lymphocytes (**Figure 1.2C**). Indeed, careful PK measurements and modeling of an IL-2 immunocytokine in clinical trials highlight the dominance of target-mediated drug disposition (TMDD) in the periphery, which is exacerbated further by IL-2 mediated expansion of the systemic off-tumor/on-target cellular pool(*35*). These findings likely explain the as-yet limited success of first-generation immunocytokines in the clinic. Even though these fusion proteins have been studied for decades, the majority remain in Phase I or Phase II. Immunocytokines have been studied in the clinic for IL-2, IL-12, TNF, IFNα and for targets such as GD2, FAP, tumor-specific matrix targets like EIIIB, and CD20(*13*, *36*). While additional engineering, such as affinity attenuation and *cis* targeting (discussed further below), will likely be needed for immunocytokines to deliver on their promise in solid tumors, leukemias and lymphomas present lower drug transport barriers and could therefore allow better therapeutic indices – for example, some current CD20-targeted immunocytokines such as DI-Leu16-IL2, could find an accessible therapeutic window(*37*).

Small-format immunocytokines, such as those designed with nanobody fragments instead of full-length IgGs, have been proposed to have improved tumor specificity over larger antibody-based immunocytokines due to their rapid renal clearance(*33*, *34*).

However, theoretical analysis of the fundamental rate processes of tumor localization suggests that with few exceptions, this may not be the case(*38–40*). Compartmental modeling balancing tumor antigen affinity with size-based clearance reveals a "valley of death" with regards to tumor penetrance for molecules between 10-100kDa(*40*). Indeed, full-length IgG antibodies show the optimal tumor penetrance for nanomolar binding affinities. The only exceptions to this rule are very small proteins (<10kDa) with very high affinity (pM), which are predicted to readily accumulate as well. Fusing a cytokine to the targeting moiety may only exacerbate this valley of death due to peripheral sinks before reaching the tumor. Lutz et al. recently demonstrated that even for a small format IL-2/domain antibody immunocytokine with picomolar affinity for EIIIB, a tumor-associated extracellular matrix component, no additional survival benefit was seen over an untargeted size-matched cytokine when dosed systemically(*34*). It should be noted, however, that intratumoral administration of these same agents was efficacious, with higher affinity leading to improved efficacy.

Next-generation immunocytokines targeting immune cells

Additional protein engineering strategies have enabled immunocytokine biodistribution governed by antibody rather than cytokine specificity. Originally proposed by Garcin et al., this approach relies on weakening the affinity of the cytokine for its receptor such that it is inert in solution at relevant doses(*41*). The attenuated cytokine is then fused to a high affinity antibody against a cell-surface receptor of choice. Antibody binding-driven high cytokine concentration at the cell surface, above its weakened EC50, suffices to rescue downstream signaling only on the antibody-targeted cell population (**Figure 1.2D**). Though tumor targeting is mentioned as a potential application of this approach, much of the recent development and translation in this area has been focused on targeting specific immune cells in circulation. Asher Biotherapeutics' lead molecule, AB248, is a CD8-targeted IL-2 mutein that has demonstrated promising mouse and non-human primate (NHP) data to date(*42*). A phase 1a/1b trial with AB248 dosed its first patient in early 2023. As opposed to other mutant IL-2 approaches, described in detail in section 4.1,

AB248 effectively avoids both Tregs and NK cells and isolates signaling to CD8 T cells. Enabling *cis*-signaling by cytokine attenuation and antibody-driven avidity could finally unlock the promise of immunocytokines.

Beyond lineage markers like CD8, phenotypic cell-surface markers are also being used to target cytokines to specific lymphocyte subsets. A team at Roche has recently reported a PD-1 targeted slightly-lowered affinity IL-2 mutein (IL-2v) to selectively expand activated and antigen-experienced CD8 T cells(*43*). In addition to minimizing off-tissue toxicity, these cell-surface displayed cytokines elicit different downstream effects than their wild-type counterparts. PD-1-cis IL-2v signaling is reported to drive CD8 T cells into less exhausted effectors in comparison to a combination of αPD-1 and IL-2v(*43*). Though it's not entirely understood what drives this altered downstream biology, it could be due to changes in the internalization behavior of the cytokine. PD-1 targeting antibodies have been reported to have relatively slow internalization(*44*), potentially anchoring the cytokine to the cell surface for longer periods over its native form and allowing for more sustained signaling. This concept of using multiple-receptor targeting to elicit new biology will be central to the thesis. Similar anti-PD1-IL-2 fusions have been reported by academic groups(*45*). Affinity attenuation and *cis* signaling is being tested for various other cytokines like IL-21 and IL-15(*46*, *47*).

Intratumoral immunotherapy

An alternate strategy to focus cytokine activity on the tumor is through direct intratumoral injection and retention. The idea of intratumoral delivery is as old as immunotherapy itself, with W.B. Coley injecting bacterial cultures directly into the tumor to drive an immunological response(*48*). Theoretically, delivering payloads directly into the tumor has the benefit of achieving an immediate high local concentration, though it's not often appreciated how quickly intratumorally delivered agents will diffuse into circulation. Locoregional delivery is further motivated by the hypothesis that an *in situ* immune response can lead to systemic anti-tumor immunity even if the treatment is administered locally(*49*–*51*). There have been encouraging clinical results from intratumorally delivered BCG vaccines and Toll-like Receptor (TLR) agonists and most notably, the approved oncolytic virus therapy talimogene laherparepvec (TVEC) is administered intratumorally(*52*–*56*). Advances in interventional radiology to access previously unreachable tumors have bolstered increasing popularity of these interventions. The number of new clinical trials per year involving intratumoral delivery has increased 6-fold over the last 2 decades and is projected to continue to increase(*51*).

Despite initial accumulation following intratumoral delivery, much of the injected payload will rapidly leak out and lead to systemic exposure. We and others have shown this to be true for cytokines and antibodies in preclinical models(*17*, *18*, *20*, *57*, *58*). Hence, simply changing the route of administration will not on its own ablate a cytokine's toxicity. However, additionally endowing these cytokines with the ability to bind a localized anchor has emerged as a promising strategy. Two anchoring approaches that have recently been explored are extracellular-matrix (ECM) binding cytokines and exogenous biomaterial depots. In both cases, the anchor prevents cytokine diffusion following intratumoral administration, providing a strong local response without systemic exposure.

Extracellular matrix (ECM) anchoring

ECM-based retention is a promising strategy for anchoring cytokines due to the overexpression of collagen in solid tumors(*59*, *60*). Furthermore, this strategy is actually biomimetic, as numerous cytokines (e.g. IL-2(*15*), IFN-gamma(*61*), and IL-12(*62*)) exhibit strong ECM interactions that keep their endogenous effects localized. Momin et al. reported on a collagen-anchoring platform that leverages these intratumoral collagen reserves for enhanced cytokine retention(*17*). In this approach, lumican, an endogenous collagen-binding protein, was fused to either IL-2 or IL-12. When dosed in combination, these anchored cytokines cured a majority of B16F10 melanoma tumor bearing mice without eliciting any toxicity-related weight loss. In comparison, the unanchored size-matched cytokines caused significant weight loss after intratumoral injection. These localized cytokines also safely synergized with other immunotherapies, including checkpoint blockade, anti-tumor antibodies, and CAR-T. One benefit of ECM anchoring is its tumor agnostic nature, given the presence of collagen in a majority of solid tumors(*59*, *60*). However, optimization of binding to specific collagen types may be necessary for some tumors where different expression patterns are reported. This technology has been licensed by Cullinan Oncology, where it is being translated as a single collagen-binding IL-2/IL12 fusion protein named CLN-617. This is likely due to ease of manufacturing of a single protein and evidence suggesting that IL-2 can sensitize T cells to IL-12 immunotherapy(*63*). The investigational new drug (IND) application was cleared by the FDA in 2023 to evaluate CLN-617 in a variety of solid tumors. Additionally, Stinson et al. reported on the use of this collagen-binding cytokine regimen in pet dogs with spontaneously occurring soft-tissue sarcomas(*64*). The intratumorally dosed cytokines were reported to be well tolerated with promising biomarker activity as shown by increased T cell infiltration and gene expression programs associated with a strong anti-tumor response.

Lutz et al. also reported on IL-2 targeted to the EIIIB domain of fibronectin, an ECM component that is specific to tumor tissue, unlike collagen(*34*). The tumor specificity of

EIIIB makes it a compelling target for systemic administration. However, as previously mentioned, without attenuating the affinity for its cognate receptor, the cytokine will govern the systemic distribution of the protein, which Lutz et al. demonstrate(*34*). Still, intratumoral administration of these EIIIB anchored cytokines was highly efficacious in comparison to their unanchored counterparts.

Other groups have further expanded on ECM binding by screening various peptides against different ECM components for cytokine retention. Chakravarti et al. reported on an engineered GM-CSF fused to ECM binding peptides targeting collagen I, hyaluronic acid, or fibronectin(*65*). In a head and neck squamous cell carcinoma model, the HA-binding peptide led to the longest retention and intratumoral administration of GMSCF-HA_p led to significantly improved tumor control over the un-anchored control, highlighting the broad applicability of ECM retention by fusion proteins.

Based on the promising preclinical data of ECM-based anchoring, Momin et al. developed an experimentally validated model that generalizes the timescale of intratumoral activity for anchored cytokines of various molecular weights and matrix affinities(*24*). The model incorporates the kinetic and transport dynamics that occur after intratumoral injection: initial volume displacement followed by various cytokine/matrix interactions, intravasation, and eventual clearance from the blood. Using IL-2 as a model cytokine, Momin et al. systematically modulate the cytokine's mass (as an MSA fusion) and collagen affinity (through multiple collagen binding domains) to experimentally confirm the model. Positron emission tomography (PET) imaging was used to quantify the intratumoral retention of these various cytokines. For reference, tumor half-life ($t_{1/2}$) ranged from 40 min for a small (15 kDa) untargeted protein to 8 hours for a large, tight binding protein (95 kDa, 20 nM collagen affinity). One notable pragmatic takeaway reported by Momin et al. is the small interstitial volume even within well established tumors in murine transplant models: B16F10 tumors between 200-300 mm^3 only held ~13 uL before spilling over into the periphery. Given that this size is comparable to some human melanoma lesions, this unexpected finding may be useful for optimizing dosing

guidelines for intratumoral therapies like T-VEC and other experimental cytokines. As expected, intratumoral retention scaled with increasing molecular weight and matrix affinity. Between the two key variables, size outweighed the contribution of affinity, highlighted by equivalent survival between an untargeted, large immunocytokine and a small, high-affinity immunocytokine. However, beneficial effects from increasing size and affinity were additive.

Efforts to leverage matrix binding through systemically administered therapies have also been reported. Ishihara et al. described a collagen-binding approach by repurposing the collagen-binding domain (CBD) of the von Willebrand Factor (VWF) A3 domain through direct fusions to IL-2(*66*). Systemically administered CBD-IL2 was shown to preferentially accumulate in tumors, though there was also noteworthy retention in the liver and kidney. CBD-IL2 showed a more favorable safety profile (less splenomegaly and pulmonary edema) and improved efficacy over untargeted IL-2. The same group built on these promising results by applying them to IL-12. Mansurov et al. reported a CBD-IL12 that was capable of eliciting a complete response in a majority of B16F10-bearing animals from a single 25µg dose(*67*). The authors characterize changes in serum IFNɣ and alanine transaminase (ALT) fold changes to show the enhanced safety profile of CBD-IL12 over untargeted cytokine. Arrow Immune was founded in 2018 to commercialize this technology but no information on their progress was readily available at the time of writing. While the preclinical data around this technology is compelling, the proposed mechanism of action of the CBD technology is at odds with some of the engineering principles we described earlier. The authors hypothesize that the tumor specificity of systemically administered CBD fusions comes from collagen's scarcity in blood (due to its insolubility) except in the case of leaky tumor vasculature, exposing collagen only at the tissue of interest. Thus, CBD-cytokine fusions could face similar challenges to first generation tumor-targeting immunocytokines, where lack of tumor antigen in circulation led to biodistributions governed by the cytokine and subsequent off-tissue toxicity. Systemically administered CBD-cytokine fusions closely mimic the EIIIB immunocytokines reported by Lutz et al. Similar to our commentary on that approach, we believe cytokine attenuation

or masking, additionally demonstrated by further work from Mansurov et al(*68*), would be necessary to safely and effectively translate the promise of systemically administered CBD-cytokine fusions.

Exogenous Depots

While collagen anchoring enables retention of intratumoral proteins for hours to days, using exogenous biomaterial depots has extended this timescale to multiple days and even weeks. Agarwal et al. reported on an intratumoral cytokine retention strategy using the traditional vaccine adjuvant aluminum hydroxide (alum, or Alhydrogel)[71]. The approach relies on alum's ability to undergo ligand exchange with phosphorylated proteins, resulting in long-term linkages[119]. Agarwal et al. leverage this by developing an in-cell phosphorylation strategy, capable of inducing site-specific phosphorylation on engineered alum-binding peptides (ABPs). Specifically, co-transfection of Fam20C, a well-characterized kinase responsible for phosphorylating a majority of the secreted phosphoproteome, with an ABP-tagged protein allows for phosphorylation of serine residues within the ABP. Fusing an ABP to IL-12 (IL-12-ABP) led to robust retention on alum while maintaining cytokine bioactivity. A single low dose of alum-bound IL-12-ABP with CBI led to complete responses in a majority of B16F10-bearing mice. Whole animal IVIS imaging revealed the presence of the intratumoral depot up to 3 weeks after injection. Measurement of IL-12 in serum 5 hours after administration revealed rapid leakage of unanchored IL-12 in comparison to alum-anchored cytokine. ALT measurements, serum IFNg, and weight loss data further support the claim that intratumorally dosed anchored cytokines do not leak into circulation. In comparison to the collagen anchoring work, a key benefit of exogenous depots like alum is being able to circumvent the variability in collagen abundance between tumor types and patients. Additionally, alum is a Generally Recognized As Safe (GRAS) material used in over 20 clinically licensed vaccines, paving the way for translation of this technology. Ankyra Therapeutics was formed to commercialize this work and is expected to file an IND in 2023 to evaluate ANK-101 (ABP-IL-12) as a monotherapy and in combination with CBI in solid tumors.

Lutz et al. applied the alum-binding platform to type I IFNs, another cytokine family known both for its potency and toxicity(*20*). Unlike interleukins, type I IFNs can directly interact with tumor cells through the IFNAR receptor, opening up additional mechanisms for anti-tumor immunity. Alum anchoring significantly improved the efficacy of IFNα and IFNβ monotherapy in B16F10. Of note, however, in the more inflamed MC38 model, anchoring of IFNβ did not improve efficacy and in fact, anchored IFNα was more efficacious than anchored IFNβ despite being an order of magnitude less potent. The authors hypothesize this is due to the higher basal type I IFN signaling in MC38 tumors and that there may be a ceiling on productive signaling. This result highlights the complexity of spatiotemporal cytokine regulation and suggests that for IFN engineering, more is not always better. Alum-interferon therapy directly increased MHC-I and PD-L1 levels, sensitizing them to subsequent doses. Lutz et al. additionally analyzed the nonhematopoietic compartment through bone marrow chimeras and saw a significant loss of efficacy, highlighting the dependence on the non-immune compartment to this therapy.

One of the benefits of strong retention strategies like alum-anchoring is the potential to safely deliver toxic immunotherapy combinations that would otherwise be impossible to dose. Lutz et al. combine their alum-interferon therapies with extended half-life MSA IL-2 or CBI (αPD1). The combination with MSA-IL2 was shown to be highly synergistic for both alum-anchored IFNα and IFNβ, eliciting a 90%+ complete response rate in B16F10 tumors. In contrast, the unanchored cytokine combinations only led to modest delays with no survivors. Alum anchoring was able to widen the therapeutic window in both directions as it ablated the toxicity-related weight loss induced by the unanchored cytokine combination. Despite this robust efficacy, mice rechallenged 100 days after initial tumor challenge mostly succumbed to tumor burden, suggesting poor immune memory formation from the double cytokine therapy. This is attributed to a large skewing of the CD8 T cell pool towards a short-lived effector (SLEC, KLRG1+CD127-) phenotype at the expense of the memory-precursor effector cells (MPEC). Similarly to the hypothesis that there is a threshold for productive IFN signaling in tumors, overstimulation from anchored

cytokines may harm memory formation. By contrast, combination of alum-anchored IFNα with anti-PD-1 led to majority cures and memory formation.

Abscopal effects

A key topic for discussion around intratumoral therapies is their ability to drive abscopal effects. First described in the context of radiation by RH Mole in 1953, abscopal effects describe responses at untreated lesions after local therapies (like radiation or in the present case, anchored cytokines)(*69*). In theory, antigen generation and drainage from the treated lesion to the TDLN should allow for a wave of *de novo* T cell priming, which could then disseminate activated T cells agnostically through circulation. Various preclinical data suggest that localized monotherapies and combinations with systemic agents like tumor-targeting antibodies or CBI can elicit strong abscopal effects. Agarwal et al. showed abscopal effects from alum-anchored IL-12 monotherapy in a two-tumor Ag104 fibrosarcoma model, where only one lesion is treated(*57*). In the neoadjuvant setting for the 4T1 triple negative breast cancer model, which is known to metastasize, alum-anchored IL-12 monotherapy led to a complete response in a majority of animals after tumor resection. A team from OncoSec reported robust abscopal effects in a metastatic i.v. B16F10 model from their intratumoral in vivo electroporation of IL-12(*70*). Momin et al. demonstrated strong abscopal potential of collagen-anchored IL-2 in a two-tumor B16F10 model in combination with the tumor specific antibody TA99(*17*). Cullinan additionally tested this in combination with CBI, leading to a 90% complete response rate in a two-tumor MC38 model for their IL-2/IL-12 collagen-binding fusion protein. T-VEC, the locally delivered oncolytic virus encoding GM-CSF, has been shown to completely resolve 30% of uninjected lesions, clinically supporting the systemic abscopal effects of locoregional administration(*71*). An intralesionally administered EIIIB-targeting IL-2 (L19-IL-2 or “Darleukin”), in combination with a targeted TNFα, led to complete responses in over half of non-injected lesions in a Phase II trial(*72*). Because of the propensity of many cancers to metastasize, eliciting abscopal effects is an important goal for the effective translation of localized cytokines, either as a monotherapy or in combination with a

systemic component. Thus, while there have been some reports highlighting abscopal effects, effective control of untreated lesions remains a key problem for the field.

Temporal impact of cytokine therapies

It has become increasingly appreciated that combination immunotherapies present a very promising approach. However, toxicity from immunotherapy combinations is often as additive as efficacy. Many of the approaches described here offer solutions to this problem by spatially controlling cytokine signaling to specific cells or tissues. Another key variable to consider for combination cytokine therapies is their temporal programming, both for maximizing efficacy and minimizing toxicity. Tzeng et al. reported on a combination of IFNα, extended half-life IL-2 (FcIL2), and TA99 (TRP1 targeting antibody)(*73*). Strikingly, while simultaneous dosing of all 3 components only led to a modest delay in survival (and no long-term survivors), staggering the IFNα dose 48 hours after the FcIL2 + TA99 dose elicited a 60-100% complete response rate in B16F10 tumors. This schedule dependent synergy was generalized to various tumor models and a wide range of combination immunotherapies. Mechanistic studies revealed CD8α+ dendritic cell (DC) activation as the key determinant of efficacy in this temporally programmed combination therapy. Dosing IFNα, which is known to activate DCs, concurrently with antigen generation from the FcIL2 + TA99 bolus, led to lower antigen capture and poor CD8 T cell priming by DCs. Maturation of DCs after antigen generation allowed for an optimal response. While this study highlights immunotherapy scheduling as an underappreciated variable for efficacy, toxicity remained a drawback in this combination. Further work by Rothschilds et al. sought to understand the toxicity drivers of this combination more deeply and elucidated further temporal programs that decouple efficacy and toxicity(*74*). Because the relationship between DC maturation and antigen generation seemed to be critical, Rothschilds et al. maintained the delay between the tumor-targeting antibody and IFNα, but varied the timing of FcIL2 dosing. Interestingly, delaying the FcIL2 dose to not be concurrent with the antibody (either 1, 2, or 3 days after), preserved the efficacy while minimizing toxicity as shown by weight

loss. This was shown to be true in additional tumor models. Importantly, depletion of NK cells via antibody-mediated depletion in the original therapy showed equivalent efficacy with reduced toxicity. This suggests that NK cells are implicated in toxicity but do not contribute to efficacy in this cytokine combination therapy.

Cytokine therapies can play key roles outside the context of cancer, especially in many immunological conditions. While this chapter has focused on oncology applications of cytokines, there are rich insights on temporal considerations from the vaccine literature that we will highlight. In a series of papers from Barouch and colleagues, the timing of an extended half-life IL-2/Ig plasmid in relation to an HIV DNA vaccine is explored(*75*–*77*). The authors find that injection of the IL-2/Ig plasmid before or concurrently with the vaccine suppressed the immune response, while delaying the cytokine dose by 2 days after the vaccine led to an amplified immune response. This temporal dependency suggests that an optimal immune response may be found through initial antigen generation which is then amplified by cytokines. This was confirmed in a Phase I trial where the delayed cytokine administration led to an increased immune response compared with simultaneous dosing in patients(*78*). We believe these principles may be directly applicable in guiding the design of immunotherapy combinations. One potential parallel could be to delay amplifying or proliferative cytokines like IL-2 after initial doses of antigen-generating therapies like tumor-targeting antibodies or even other cytokines like IL-12. These examples, while not explicitly addressing temporal regulation through protein engineering, highlight the importance of this key variable for designing safe and efficacious cytokine therapies. New engineering approaches or further optimization of current ones to control the release kinetics or bioavailability for cytokine combinations may help unlock their potential.

CD45 as a cell surface anchor

In this thesis, we explore targeting cytokines to CD45 through heterofunctional fusion proteins. Thus, understanding CD45 biology, especially as it relates to cytokine signaling, will be crucial. Structurally, CD45 is a 180–220 kDa transmembrane protein with two cytoplasmic PTP domains, and a variable-length, highly glycosylated, extracellular domain(*79*, *80*). It is expressed at very high levels, accounting for up to 10% of all surface area on T and B lymphocytes(*81*). CD45 is expressed in multiple isoforms as a result of alternative splicing of exons 4, 5, and 6 (corresponding to A, B, and C protein domains). Though the combinatorial possibilities are high, only six are observed at reasonable levels: CD45RO (lowest molecular weight), CD45RB, CD45RAB, CD45RBC, CD45RABC (highest molecular weight)(*80*, *82*). This variable extracellular domain contains O-linked glycan chains and is responsible for all the diversity across isoforms. After the variable region, there is a cystine-rich domain, followed by three type III fibronectin domains (fnIII) before the transmembrane domain(*80*).

Because of its ubiquity and variability, human CD45 isoform regulation is dependent on cell type, developmental stage, and activation state(*83*). For example, stimulation of naive T cells will shift their expression profile from CD45RB to the shorter CD45RO. Memory T cells have also been shown to predominantly express CD45RO(*83*, *84*). This regulation has also been described in natural killer (NK) cells, where CD45RA and CD45RO expression correlates with high anti-tumor activity(*85*). While being able to potentially target specific leukocyte populations by their distinct CD45 isoform expression is a compelling idea, these isoform-phenotype relations have not been shown in mice.

CD45 was identified as the first transmembrane protein tyrosine phosphatase (PTP) and was thought to exclusively serve as a regulator of T cell signaling by dephosphorylation of Src family kinases(*79*). In some cases, CD45 has been reported to be a negative regulator of cytokine receptor signaling by being a Janus Activated kinase (JAK) phosphatase, dephospohorylating Jak1, Jak2, Jak3 and Tyk2 *in vitro*(*82*, *86*). CD45's

natural phosphatase activity has been repurposed by the Garcia Lab at Stanford in multiple ways: in an *in vitro* membrane model, they segregate CD45 receptors to impact pMHC-TCR signaling dynamics(*87*), and more recently, they have developed diabodies to enforce dephosphorylation of target proteins(*88*). This approach, which the authors describe as receptor inhibition by phosphatase recruitment (RIPR), uses fusion proteins to induce proximity between CD45 and inhibitory receptors like PD-1 to enforce basal dephosphorylation of downstream inhibitory cascades. Though this work suggests that signaling cascades near bound CD45 could be dampened, it's important to note key differences between the RIPR mechanism involving inhibitory synapse receptors and the one described in this work involving cytokine receptors. Namely, RIPR was applied to synapse-driven signaling like PD-1/PD-L1 and was used to modulate receptors that rely on membrane-bound kinases. Recent work exploring the mechanics of effective agonist signaling highlight the necessity for CD45 exclusion from the synapse(*89*). However, cytokine receptors use soluble cognate ligands and rely on cytosolic kinases like JAKs. Based on these key differences, we hypothesized that cytokine signaling could remain functional in close proximity of CD45.

Our lab has previously explored the concept of CD45-mediated cell targeting in the context of cytokine biomaterials (*90*). In this work, IL-15 "nanogels" were functionalized with CD45 antibodies for the "backpacking" of cell therapies. CD45 was chosen as a cell surface anchor due to its unique ability to be bound to without triggering internalization, potentially lengthening surface half-life of tethered molecules. Upon soluble cytokine release triggered by TCR signaling, JAK-STAT signaling was unaffected (*90*). Key initial experiments in this thesis were focused on validating active cytokine signaling for CD45-targeted cytokines. As will be described in depth later, CD45 immunocytokines as they are described in this work do not suffer from dephosphorylation despite induced proximity between CD45 and cytokine receptors.

Putting it all together: Outline of thesis

To summarize, we are now almost three decades into an engineering campaign aiming to extend the therapeutic window of cytokine therapies and ultimately harness them effectively in the clinic. Despite many promising technologies, clinical translation of cytokine therapies remains challenging. One engineering approach that our labs have focused on in recent years is engineering cytokines for local retention after intratumoral administration. We have previously leveraged this cytokine "anchoring" approach by retention through the extra-cellular matrix (ECM)(*17*) or biomaterial depots(*57*). In this work, we explore a third approach – cytokine anchoring directly to immune cells via targeting of a prevalent cell-surface receptor, CD45. We hypothesized that due to CD45's abundant expression and slow internalization, engineering cytokines to target this large cell surface receptor could elicit novel signaling biology.

In Chapter 2, we introduce the rationale for CD45-targeted cytokine fusions and initial optimization work on their design and dosing scheme. This chapter focuses on in vitro validation of these cell surface targeted cytokines, highlighting the hallmark ability of CD45 to minimize cytokine internalization on T cells. This chapter also includes biodistribution and dose optimization experiments that ultimately led us to the dosing paradigm used in Chapter 3, which we refer to as αCD45-Cyt therapy. We show that locally delivered CD45-targeted cytokines have a unique ability to be retained at the TDLN. Finally, in the discussion, we put forward a conceptual framework for drainage of intratumoral cytokines after local administration.

Chapter 3 builds on the optimized αCD45-Cyt therapy and focuses on evaluating its efficacy and in vivo mechanism of action. We show that αCD45-Cyt therapy is not only able to eradicate single tumors but also elicit substantial abscopal responses in both MC38 and B16F10 tumors. Mechanistically, we show that efficacy is primarily driven by CD8 T cells and *batf3*+ dendritic cells. To profile the CD8 response with more resolution, we performed RNA-sequencing on TDLN tumor-specific CD8 T cells after therapy. This

uncovered a unique gene signature triggered by αCD45-Cyt therapy that was akin to that of an acute anti-viral response. We also profile the $CD8^+$ T cell response by flow cytometry to confirm the transcriptomic signature.

Finally, in Chapter 4, we focus on future directions for this work, highlighting our most recent work to further translate αCD45-Cyt therapy. We explore an all-in-one molecule to simplify translation of the original two-part αCD45-Cyt therapy, which we validate in mice. We also evaluate the ability of CD45-targeted cytokines to synergize with other therapies such as alum-anchored IL-12. We discuss some ongoing work to generate a canine CD45 binder through yeast surface display for the translation of αCD45-Cyt therapy into canine patients. Finally, we conclude with future outlooks on the engineered cytokine field.

.

Figures

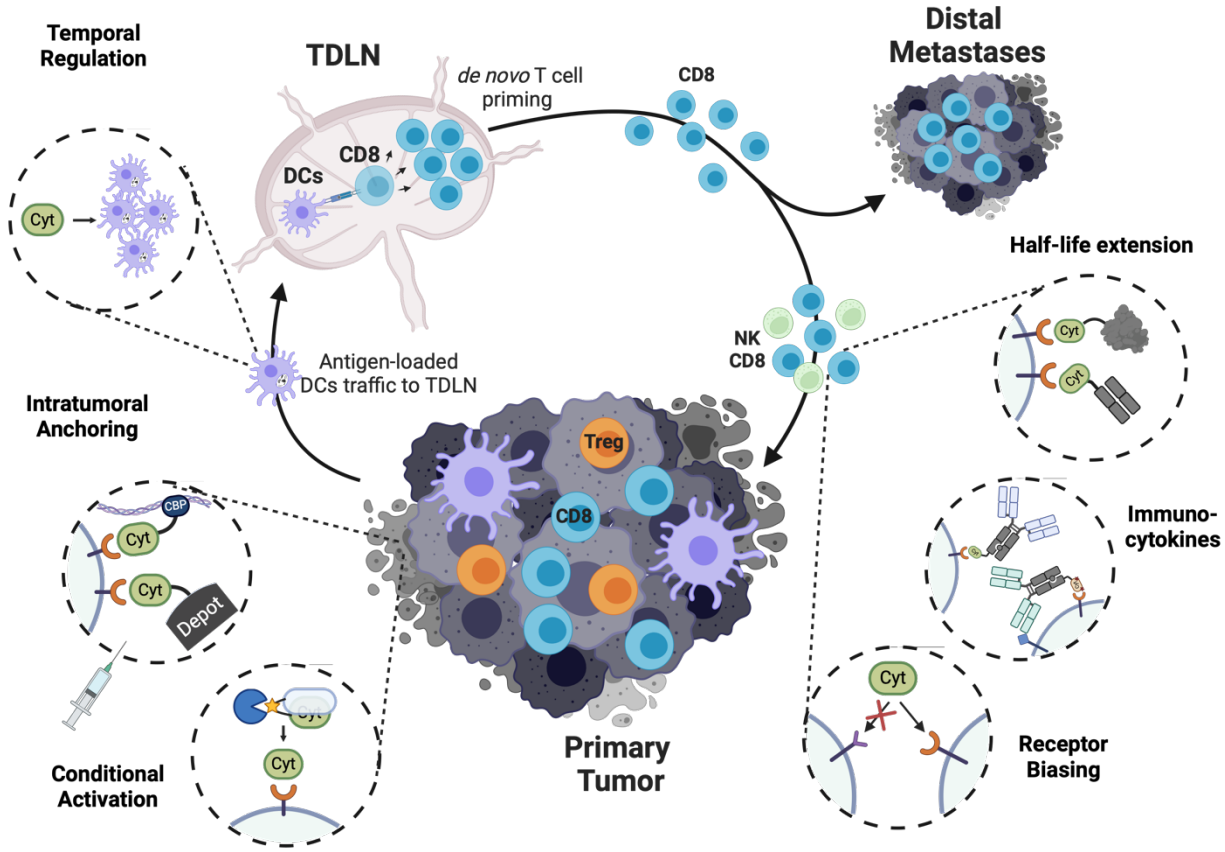

Figure 1.1. Summary of cytokine engineering efforts for cancer immunotherapy.

Different spatiotemporal engineering strategies aim to rescue and amplify different parts of the cancer immunity cycle. Select examples are discussed in the text and contextualized within the canonical anti-tumor response. The schematics are meant to be generalizable to any cytokine but specific examples for each section are described throughout the text. **Abbreviations**: CBP, collagen binding protein; cyt, cytokine; TDLN, tumor draining lymph node; NK, Natural Killer cell; DC, Dendritic Cell.

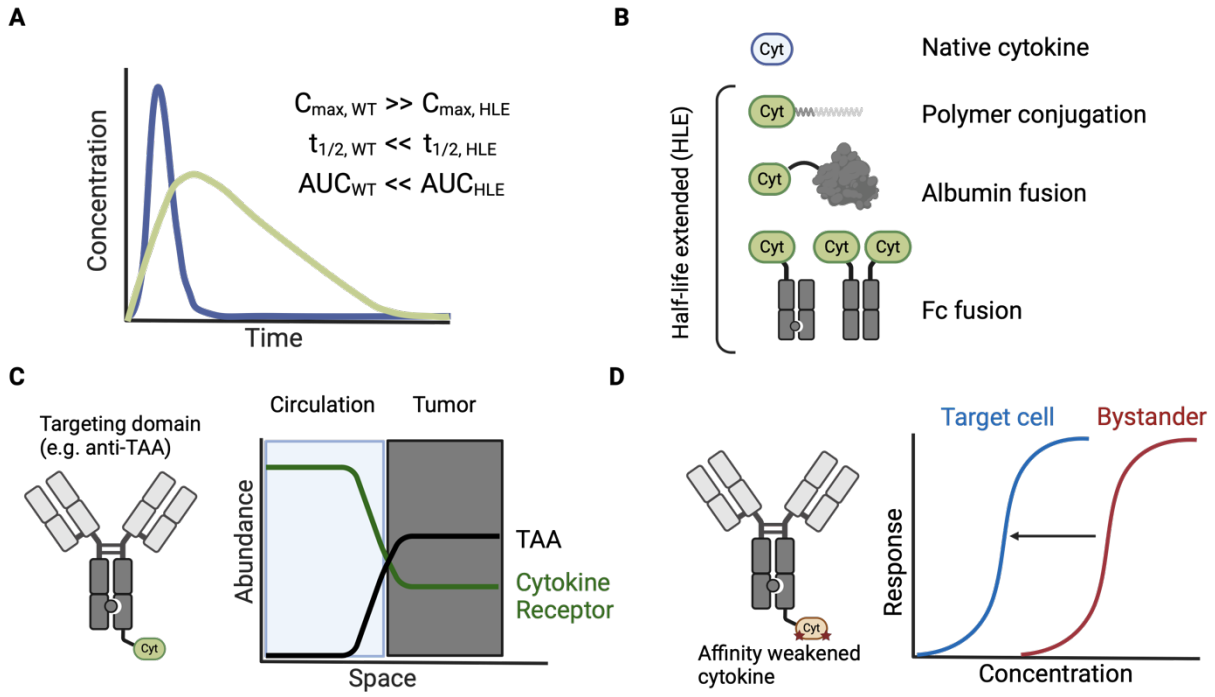

Figure 1.2. Cytokine fusion proteins extend half-life and can address specificity concerns.

A, Temporal programming via half-life extension (HLE) strategies alter the pharmacokinetic properties of cytokines to decrease their maximum serum exposure (Cmax) and extend their half-life ($t_{1/2}$) and area under the curve (AUC). **B,** Cytokines can be fused to polymers, albumin fusions, and antibody Fc domains to accomplish half-life extension. Fc fusions are commonly made monovalent through knob-in-hole (KiH) mutations. **C,** First generation immunocytokines attempted spatial programming by "targeting" tumors through tumor-associated antigens (TAAs); but their biodistribution was ultimately dominated by the cytokine due to minimal solid tumor antigen in circulation. **D,** Newer immunocytokines using affinity-weakened cytokines isolate productive signaling to target cells (dictated by antibody or targeting moiety), achieving effective cell-level spatial programming.

Chapter 2 : CD45-targeted cytokine fusions

Parts of this chapter appear as described in Santollani et al., *bioRxiv* (2024).

Introduction

As described in the introduction, cytokines are a class of small proteins that serve as modulators of immune signaling cascades. Because of their multifunctional roles in lymphocyte migration, activation, and proliferation, cytokines have been long recognized as promising cancer immunotherapy agents(*3*, *4*, *7*). In fact, interleukin-2 (IL-2) was the first efficacious immunotherapy for advanced cancer, eliciting a 17% overall response rate as a monotherapy in metastatic melanoma leading to its FDA approval in 1998(*5*). Despite this clinical validation, dose-limiting toxicities and severe immune-related adverse events significantly hinder the clinical utilization of cytokines for oncology. This can be attributed to systemic lymphocyte activation triggered by the high doses that must be administered to achieve meaningful tumor concentrations.

Over the last 20 years, protein engineering has emerged as a tool to address the shortcomings of native cytokine therapies(*1*, *11*, *12*). One strategy to increase both safety and efficacy is to engineer cytokines for local delivery and retention within tumors and/or tumor-draining lymph nodes (TDLNs). We and others have previously demonstrated that potent cytokines and other immune agonists that exhibit high levels of toxicity when administered systemically can safely and effectively drive anti-tumor immunity when administered intratumorally (i.t.) to accessible lesions, by “anchoring” these drugs to intratumoral collagen, or to injected materials such as liposomes or alum particles(*17*, *18*, *20*, *57*, *58*, *67*, *91*). These approaches are enabled by modern interventional radiology methods that make intratumoral administration feasible in virtually any type of cancer(*91*–*93*).

In this chapter, we introduce a localized immunotherapy strategy targeting cytokines to the universal leukocyte receptor CD45. We have previously shown that antibodies against

the ubiquitous leukocyte surface receptor CD45 bind to the surface of T cells and other lymphocytes without triggering internalization(*94*, *95*). Analogous to recent reports of the altered biology achieved when IL-2 is targeted to lymphocytes via anti-PD-1(*43*), we hypothesized that cell surface-displayed cytokines using CD45 targeting might exhibit new biological effects relative to the native forms of these cytokines.

We begin the chapter by highlighting the development of CD45-targeted immunocytokines. Through a variety of *in vitro* assays, we show that the immunocytokine formats we developed can simultaneously bind both CD45 and cognate receptor, eliciting novel internalization and signaling biology. We characterize the ability of CD45 immunocytokines to remain on the cell-surface, thus lengthening their signaling timescale. Through co-culture assays, we also demonstrate the ability of cells decorated with CD45-targeted cytokines to signal in both *cis* and *trans*. From there, we test CD45-targeted cytokines in initial *in vivo* studies aimed at understanding their biodistribution and tolerable doses. Throughout the chapter we apply the strategy to both IL-15 and IL-12 fusions. Ultimately, optimizing dose level, tissue localization, and timing results in a highly efficacious and non-toxic cytokine therapy capable which we refer to as αCD45-Cyt therapy. The mechanism of the therapy is detailed in Chapter 3.

Results

Engineering CD45 immunocytokines

To develop CD45 targeted cytokines, we employed an immunocytokine approach where we fused cytokines to an anti-CD45 antibody. Using a publicly available sequence for an anti-CD45 clone, 30-F11, we grafted the variable regions onto a mouse IgG2c backbone with effector-attenuating mutations (hereafter, αCD45). We also synthesized a non-targeted size-matched control immunocytokine using an irrelevant fluorescein-specific antibody (clone: 4-4-20, hereafter IgG). Using ELISA, we confirmed binding of αCD45 to plate-bound recombinant mouse CD45 as well as validated IgG as a proper control antibody (**Fig 2.1A**). We next profiled binding to cell-surface CD45 using a T cell derived cell line in a competition flow cytometry experiment. The recombinantly produced mouse IgG2c αCD45 antibody was competed off by a commercially available antibody of the same clone, confirming cell surface CD45 binding (**Fig 2.1B**).

With validated binding and relevant controls, we designed and built initial antibody-cytokine fusions using the αCD45 and IgG antibody scaffolds. We first generated αCD45 or IgG immunocytokine fusions with IL-15 as a testbed payload. A murine superagonist IL-15 (IL-15 linked to a domain of its α receptor chain, IL-15Rα$_{sushi}$) was fused to the C terminus of a murine IgG2c isotype heavy chain carrying LALA-PG effector attenuating mutations (hereafter, αCD45-IL15 or IgG-IL15) (**Fig. 2.2A-B**)(*23*). We verified that recombinantly expressed αCD45-IL15 was able to bind plate-bound CD45 and both immunocytokines triggered proliferation of IL-15 receptor-expressing reporter cells (**Fig 2.2C-D**).

As described in the introduction to this chapter, CD45 can be bound to without triggering internalization. On the contrary, cytokine receptors tend to be rapidly internalized. Thus, we wanted to profile how binding CD45 would affect cytokine receptor mediated internalization. Using dye-labeled constructs and fluorescence quenching, we assessed the binding and internalization behavior of these IL-15 immunocytokines incubated with

activated primary $CD8^+$ T cells. Control IgG-IL15 fusions bound to the cells and were rapidly internalized, while αCD45-IL15 had a cell-surface half-life of 24 hours, suggesting that CD45 binding can maintain cytokines on the cell surface irrespective of the rapid internalization typical for the native cytokine (**Fig 2.3 A-B**). CD45-targeted IL-15 bound to T cells at far higher levels than IgG-IL15, suggesting that CD45 increases the immunocytokine target receptor pool due to its high expression level (**Fig 2.3 C**).

To evaluate whether this extended surface retention altered cytokine activity, we pulsed primary $CD8^+$ T cells with IL-15 immunocytokines for 1 hr, then washed to remove unbound cytokine and evaluated downstream signaling over time. Strikingly, T cells briefly pulsed with αCD45-IL15 exhibited robust pSTAT5 and CD25 expression levels 24 hours later that were almost as high as cells incubated continuously in IL-15 (**Fig. 2.4**). By contrast, these markers of IL-15 signaling had all returned to near baseline by this timepoint for cells pulsed with non-targeted IgG-IL15 (**Fig. 2.4**). We next tested whether CD45-anchored cytokines could signal to neighboring cells *in trans*. CFSE-labeled $CD8^+$ T cells were pre-loaded with AlexaFluor-labeled αCD45-IL15 by pulsing for 1 hour with the construct, then washed and mixed with non-loaded $CFSE^-$ "bystander" $CD8^+$ T cells for an additional hour. The presence of just 1 pre-loaded T cell per 20 total cells led to pSTAT5 induction in a majority of both the preloaded and bystander cultures, though at a higher level in the former (**Fig 2.5A-C**). Signaling to bystander cells occurred with minimal detectable transfer of the labeled cytokine fusion to the bystander cells, suggesting prominent *in trans* signaling of the cytokine from pre-loaded to bystander T cells (**Fig 2.5A-C**). By contrast, non-targeted IgG-IL15 led to robust pSTAT5 signal in the preloaded population but failed to stimulate any bystander cells, likely due to its rapid internalization (**Fig 2.5A-C**). It's been hypothesized that inducing proximity between a membrane-associated phosphatase like CD45 and a cytokine receptor could hinder downstream signaling. Thus, we aimed to further confirm *cis* signaling through co-culture experiments with $CD45^-IL15R^-$ cells. Using an identical experimental set-up to the preloaded/bystander experiment, preloaded $CD8^+$ T cells were serially diluted into HEK bystanders (as $CD45^-IL15R^-$ cells) to increase the average distance between preloaded

cells. We confirmed pSTAT5 induction was unaffected by increasing dilution, as seen by steady percentage and MFI, confirming *cis* signaling by IL15 immunocytokines (**Fig 2.5D-E**).

To determine if cell surface retention and prolonged signaling was a general phenomenon for αCD45-cytokine fusions, we also generated αCD45-IL12, a fusion of a single chain IL12p70 with αCD45. This IL-12 immunocytokine was able to bind CD45 with no loss of cytokine bioactivity and led to increased surface retention as well as extended signaling, as measured by prolonged pSTAT4 levels (**Fig 2.6A-E**). To probe whether CD45 surface retention is a mouse-specific phenomenon, we performed internalization assays with human $CD8^+$ T cells and an anti-human CD45 antibody, and found, similar to the murine antibody, prolonged cell surface retention with a half of life of over 5 days (**Fig 2.7**).

Profiling the biodistribution of αCD45-cytokine fusions after local administration

We next assessed the *in vivo* biodistribution of these fusion proteins following intratumoral administration, reasoning that binding to leukocytes in the tumor and TDLN could allow for strong local immune stimulation without the toxicity observed with systemic cytokine administration. AlexaFluor-labeled IL-15 immunocytokines were injected into established MC38 flank tumors, and association of the constructs on cells in the tumor, TDLNs, and distribution into the blood 24 hours later was assessed by flow cytometry, microscopy, and fluorescence measurements (**Fig. 2.8A**). Injection of 10 μg αCD45-IL15 led to robust labeling of a majority of all $CD45^+$ cells in the tumor (**Fig. 2.8B-D**). By contrast, the non-targeted control cytokine only showed association with ~40% of intratumoral $CD45^+$ cells, and at much lower MFI levels than the αCD45 fusion (**Fig. 2.8B-D**). αCD45-IL15 bound effectively to all common intratumoral immune subsets while IgG-IL15 mostly associated with Natural Killer (NK) cells as the dominant target, likely due to high IL2Rβɣ expression by NK cells (**Fig 2.9A**). Confocal microscopy confirmed these results, showing broad distribution of αCD45-IL15 throughout the tumor (**Fig. 2.8E**). IgG-IL15 exposure was sparse and isolated to narrow sections of the tumor (**Fig. 2.8E**). This dose also led to

labeling of ~75% of CD45$^+$ cells in the TDLN by αCD45-IL15, whereas IgG-IL15 labeling was not statistically significant relative to untreated controls (**Fig. 2.8F, Fig. 2.9B**). Microscopy imaging revealed efficient drainage of labeled αCD45-IL15 throughout the TDLN and was readily apparent on CD8$^+$ T cells (**Fig. 2.8G, Fig. 2.9C**). Profiling of cytokine uptake by immune cell subsets in the TDLN again revealed NK cells as the only cellular subset with substantial uptake of IgG-IL15, while αCD45-IL15 was bound to T cells, B cells, macrophages and dendritic cells (**Fig. 2.9D**). Importantly, at this dose, no free αCD45-IL15 was detected in the serum and there was minimal association with peripheral blood mononuclear cells (PBMCs), while non-targeted IgG-IL15 was found accumulating in the blood (**Fig. 2.8H, Fig. 2.9E**). Intratumoral administration was required for simultaneous tumor and lymph node labeling, as peritumorally delivered αCD45-IL15 efficiently labeled the TDLN but failed to meaningfully accumulate in the tumor (**Fig. 2.9F**). Thus, CD45 targeting increased localization of the cytokine on immune cells in both tumors and TDLNs, while avoiding systemic exposure when doses were selected to not exceed the binding capacity of leukocyte surface CD45 in the tumor and TDLN.

To further understand the capacity of certain tissues for CD45 retention, we ran a small biodistribution experiment at a lower dose (1 μg) that we hypothesized would be high enough to coat the tumor, but not the TDLN. Mice bearing MC38 tumors were treated with 1 μg of AF647-labeled IL-15 immunocytokine for biodistribution analysis 24 hours later (**Figure 2.11**). For αCD45-IL15, this dose was enough to saturate CD8$^+$ T cells in the tumor while sparing the node and PBMCs. IgG-IL15 did not meaningfully accumulate in any tissues at this dose. Ultimately, these experiments served as references for understanding the CD45 capacity of a given tissue.

Optimizing therapeutic dosing schedule of CD45-targeted cytokines

Given this "goldilocks" biodistribution, we next sought to apply CD45 immunocytokines therapeutically. Motivated by dosing regimens presented in our previous collagen-binding work, we began by dosing IL-15 immunocytokines in combination with IL-12 immunocytokines every 6 days. We initially tested the efficacy of CD45 immunocytokines in syngeneic MC38 tumors, known for being checkpoint blockade responsive. Two doses of 10 μg of IL-15 and 2 μg of IL-12 led to complete responses in established MC38 tumors that were 30-35 mm^2 in size regardless of retention strategy (**Fig 2.12**). As we subsequently lowered the dose 10- or 100-fold, CD45-targeted cytokines retained their efficacy while IgG control cytokines lost their ability to control MC38 tumors (**Fig 2.12**). All survivors rejected a secondary re-challenged at d100 with 0.1M tumor cells in the opposite flank (**Fig 2.12**).

To understand if both doses were necessary, we next assessed the ability of a single medium dose (1 μg of IL-15 and 0.2 μg of IL-12) to elicit anti-tumor control in the same MC38 model (**Fig 2.13**). We found that this single-shot regimen was elicited complete responses in a majority of mice only when the cytokines were anchored to CD45. IgG control cytokines were only able to cure 20% of mice in this setting (**Fig 2.13**).

To further profile this combination therapy, we next wanted to understand the safety benefits of CD45 retention. Oftentimes, combination therapies are additive in both efficacy and toxicity(*17*, *20*, *57*). To probe this, we treated MC38-bearing mice with a higher dose of an IL-15 and IL-12 immunocytokine regimen that we hypothesized could be toxic (**Fig 2.14**). In this setting, 20 μg of unanchored IgG-IL15 in combination with 4 μg of unanchored IgG-IL12 led to stark weight loss, with 100% of mice having to be euthanized due to toxicity-related weight loss or poor body condition. In comparison, mice treated with the combination of αCD45-IL15 and αCD45-IL12 only suffered mild, transient weight loss. Additional studies confirmed this, where increasing the IL-12 dose from 4μg to 8μg worsened the toxicity profile even in the αCD45 treatment group (**Fig 2.15**). These initial

biodistribution and efficacy studies suggest a dose-dependent retention model for CD45-targeted proteins that is governed by the CD45 capacity of a given tissue.

To validate the ability of CD45-targeted cytokines to work in multiple tumors, we next evaluated the anti-tumor effects of this combination therapy in the B16F10 melanoma model. In comparison to MC38, B16F10 has far less immune infiltration and is unresponsive to immune checkpoint blockade. In an initial study, we treated d7 B16F10 tumors with a combination of 10 μg of IL-15 and 2 μg of IL-12 followed 7 days later by a second dose of 10 μg of IL-15 (**Fig 2.16**). In the more challenging B16F10 model, CD45-targeted cytokines elicited strong anti-tumor control leading to 80% complete response rate. IgG control cytokines were only able to delay tumor growth but did not lead to any long-term cures (**Fig 2.16**). However, at these doses, both αCD45 and IgG-targeted cytokines triggered toxicity-related weight loss. We hypothesized that due to B16F10's lower immune infiltrate, the "capacity" for CD45-targeted cytokines may be lower than in MC38 or more immune rich tumors. To test this, we once again lowered the dose to see if efficacy could be retained while minimizing toxicity. Mice bearing B16F10 tumors were treated on d7 and d14 with 5 μg of IL-15 and 1 μg of IL-12 cytokine, half of the dose that triggered toxicity in previous experiments (**Fig 2.17**). At this lower dose, mice treated with CD45-targeted cytokines did not elicit any weight loss while the mice treated with control cytokine displayed the same weight loss as had been seen previously. Efficacy remained at 80% complete response rate for the CD45-targeted group. Finally, we lowered the dose even further, to a dose-sparing regimen of 1μg of IL-15 immunocytokine and 0.2μg of IL-12 immunocytokine on d7 and d14 (**Fig 2.18**). At these lower doses, the control cytokines elicited no long-term survivors. CD45-targeted IL-15 + IL-12 still displayed stark anti-tumor control, curing 60% of mice in this study. This set of dose de-escalation studies in both MC38 and B16F10 demonstrate the ability of CD45 anchoring for cytokines to potently trigger efficacy even at low doses.

Developing a sequential CD45-targeted cytokine regimen

Because of the toxicity triggered by the combination therapy, we evaluated whether CD45-targeted cytokines could still be effective when dosed sequentially. To inform the spacing between two sequential doses, we aimed to understand the kinetics of CD45 turnover *in vivo.* We labeled IL-15 immunocytokines with different fluorophores, AF488 and AF647, and dosed these at 24 or 72 hour intervals, followed by flow cytometry analysis 24 hours after the last dose (**Fig 2.19A-B**). Interestingly, mice that were dosed with IL-15 24 hours apart displayed robust co-labeling of both fluorophores, suggesting meaningful CD45 turnover within a day (**Fig 2.19A**). When doses were spaced 72 hours, there was no presence of the initial dose and cells were entirely labeled by the most recent dose (**Fig 2.19A**). Overall, these turnover rates indicate faster *in vivo* receptor kinetics than is reported in *in vitro* experiments. As expected, IgG-IL15 fusions were not retained on cells at any time point (**Fig 2.19A-B**).

Taking biodistribution and kinetic experiments into account, we developed a finalized treatment regimen, which is referred to as αCD45-Cyt or IgG-Cyt therapy hereafter, that incorporates a single low dose of IL-12 immunocytokine that is isolated to the tumor followed a few days later by a higher dose of IL-15 immunocytokine that can reach the TDLN. Based on previous data, intratumoral IL-12 is highly effective at generating antigen and increasing presentation by APCs (*57*). Thus, dosing the IL-15 sequentially at a higher dose could help amplify newly primed CD8 T cells in the TDLN. In MC38 tumor bearing mice, this sequential αCD45-Cyt therapy was able to elicit 100% complete response rate while control IgG-Cyt therapy only led to 20% durable cures (**Fig. 2.20A**). While both cytokine therapies led to short-term tumor control, only αCD45-Cyt therapy was able to provide long-term control as seen by growth curves (**Fig. 2.20B**). In this sequential paradigm, neither treatment elicited weight loss (**Fig. 2.20C**). All surviving mice additionally rejected a secondary rechallenge 100 days after the initial inoculation, suggesting robust immune memory (**Fig. 2.20D**). In the following chapter, we further explore the efficacy and mechanism of αCD45-Cyt therapy.

Discussion

Redirecting cytokine signaling through immunocytokine fusions has been pursued extensively over the past decades. While most of those approaches solely aim to redirect specificity to a certain tissue, for example by TAA-targeting fusions, recent data suggests that targeting cytokines and other agonists to immune cells can elicit unique biology by engaging multiple cell-surface receptors. In this way, leukocyte targeted immunocytokines can alter not only biodistribution but also native cytokine signaling. In this chapter, we explore the development and optimization αCD45-cytokine fusions. The motivation for CD45 targeting of cytokines stems from 2 key properties of this universal leukocyte receptor. Primarily, CD45 displays a uniquely slow internalization rate, even upon binding. Previous work from the Irvine Lab suggested that minimizing cytokine internalization rate could extend downstream signaling (*90*); thus, we hypothesized that targeting cytokines to CD45 as a cell-surface "anchor" could enhance native signaling timescales. Second, CD45 is highly prevalent on the immune cell surface allowing for an increased target pool over that of the cytokine receptor alone.

To develop αCD45-cytokine fusions, we repurposed a publicly available pan-CD45 antibody clone (30-F11) and grafted its variable sequences onto a mouse IgG2c backbone with attenuated Fc effector function. Using IL-15/IL-15R as a prototypical payload, we generated an αCD45-IL15 fusion to probe the functionality and biology of these immunocytokines. Size-matched control IgG immunocytokines were also generated to match valency and molecular weight. Strikingly, αCD45-IL15 displayed a much longer surface half-life over the untargeted IgG-IL15 fusion as measured by fluorescence quenching experiments. This diminished internalization rate also led to extended and continuous pSTAT5 signaling over 24 hours. As will be discussed in more detail in Chapter 3, constitutive STAT5 signaling has been shown to antagonize exhaustion programs in T cells. Thus, our CD45-targeted IL-15 fusions may be able to elicit this effect therapeutically.

CD45-targeted IL-15 was shown to signal effectively in *cis* and *trans*, both of which have interesting implications. Likely due to the far larger pool of surface CD45 than IL-15R, cell-surface displayed IL-15 is able to effectively signal *in trans* to nearby cells, amplifying the signaling cascade. Despite this being how IL-15 naturally signals, the ability for a single "loaded" T cell to present IL-15 to neighboring cells may explain the profound efficacy described toward the end of this chapter and at length in Chapter 3. Demonstrating effective cis-signaling for CD45-targeted cytokines is also important to understand how inducing proximity between a phosphatase like CD45 and a cytokine receptor can impact relevant downstream JAK-STAT phosphorylation and signaling. Thus, although CD45's phosphatase properties have been previously employed to deactivate nearby tethered receptors(*88*), CD45-targeted antibody-cytokine fusions as designed here exhibit sustained and potent signaling. We believe this can be explained through two key differences between our system and others where CD45 proximity has been shown to hamper signaling(*88*, *89*). The first is that cytokines are soluble ligands for their cognate receptors as opposed to other immune regulatory receptors that signal through cell-cell synapses, such as PD-1 and CD40. In native cytokine signaling, CD45 is not sterically excluded, suggesting that inducing proximity between a cytokine receptor and CD45 may not affect signaling as in other cases where a synapse is formed. Secondly, one of the key kinases that triggers downstream cytokine signaling, JAK, is cytosolic and not membrane bound. Once again, other receptors where CD45 proximity has been shown to induce dephosphorylation rely on membrane associated kinases. Altogether, CD45-targeted cytokines as generated and tested in this work signal effectively and modulate downstream signaling by slowing internalization.

We also demonstrate broader applicability of CD45-targeting for cytokines by applying the same approach to IL-12, another immunostimulatory cytokine. αCD45-IL12 fusions similarly displayed longer surface retention and extended pSTAT4 signaling. To validate the translational aspect of this approach, we also show slow internalization of human CD45. We are actively making a fully human αCD45-IL15 (sequence in Table) and plan to test it on human CD8+ T cells to confirm consistent behavior with murine counterparts.

The in vitro assays in this chapter provide a framework for evaluating novel αCD45 fusions. Our current results suggest that this approach can be applied quite broadly across mouse and human for any immune agonist that does not require a synapse for native signaling. Key experiments to validate novel αCD45-agonist fusions include biofunctional assays such as proliferation or pSTAT readouts, internalization assays that demonstrate extended surface half-life, and pulse-chase experiments to probe signaling timescales.

Because of CD45's ubiquity, we explored these targeted immunocytokines in the context of local intratumoral administration. Flow cytometry based biodistribution experiments using fluorescent αCD45-cytokine proteins revealed a dose-dependent spatial model that was governed by the CD45 capacity of a given tissue. For these ~200 kDa fusion proteins, we found that ~1μg was enough to coat the tumor without reaching the TDLN and ~10μg was enough to saturate the tumor and the TDLN while sparing circulation. We didn't evaluate higher doses, but it's likely that >10μg doses would begin to saturate the PBMC compartment and likely stimulate bystander immune cells. This ability to dictate compartment-specific doses that include the TDLN is unique to CD45-based retention and is not seen with ECM-targeting or biomaterials retention.

To leverage CD45 retention therapeutically, we explored a variety of combination cytokine regimens that included IL-15 and IL-12 immunocytokines. These therapies were motivated by previous studies from our lab showing the highly synergistic effect of these cytokines in combination as well as the need to localize them to on-target tissues to prevent toxicity. CD45-targeted IL15 and IL12 in combination were shown to maintain their efficacy at very low doses in both MC38 and B16F10 models, far outperforming equivalent doses of size-matched untargeted IgG control cytokines. As has been reported with other localization strategies, CD45 retention of toxic cytokine combinations was shown to ablate toxicity-related weight loss. Finally, in this chapter, we present the final treatment regimen, referred to as αCD45-Cyt therapy, that we dissect in detail in Chapter 3.

Figures

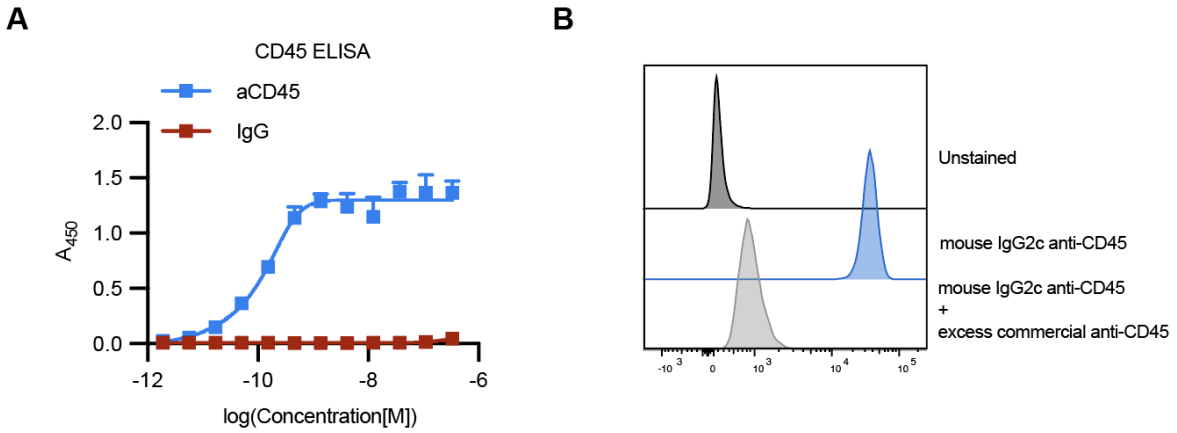

Figure 2.1. αCD45 clone 30-F11 binds plate-bound and cell surface mouse CD45 as a mIgG2c fusion.

A, ELISA absorbance measurement of αCD45 and IgG binding to plate-bound mouse CD45**. B,** Primary $CD8^+$ T cells were stained with in-house recombinantly produced αCD45 labeled with AF488 and in the presence of 10-fold molar excess of commercially purchased αCD45 of the same clone. Shown is representative AF488 signal. Data are mean ± s.d. from n = 3 biological replicates.

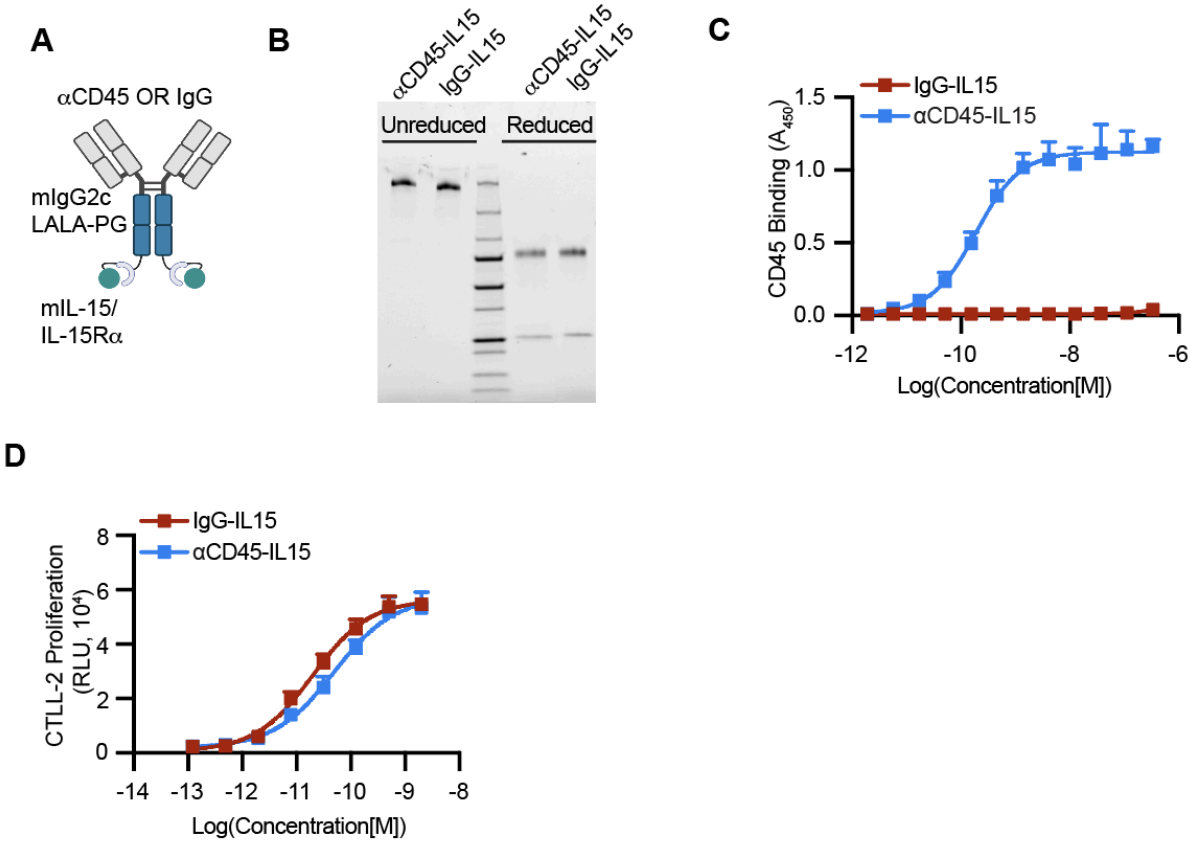

Figure 2.2. IL15 immunocytokines can be recombinantly expressed and are bioactive.

A, Schematic of IL-15 immunocytokine. **B,** SDS-PAGE of IL15 immunocytokines. **C,** ELISA absorbance measurement of αCD45-IL15 and IgG-IL15 binding to plate-bound mouse CD45. **D,** Luminescence measurement of CTLL-2 cell proliferation following 48 hr incubation with IgG-IL15 or αCD45-IL15 at indicated concentrations. Data are mean ± s.d. from n = 3 biological replicates

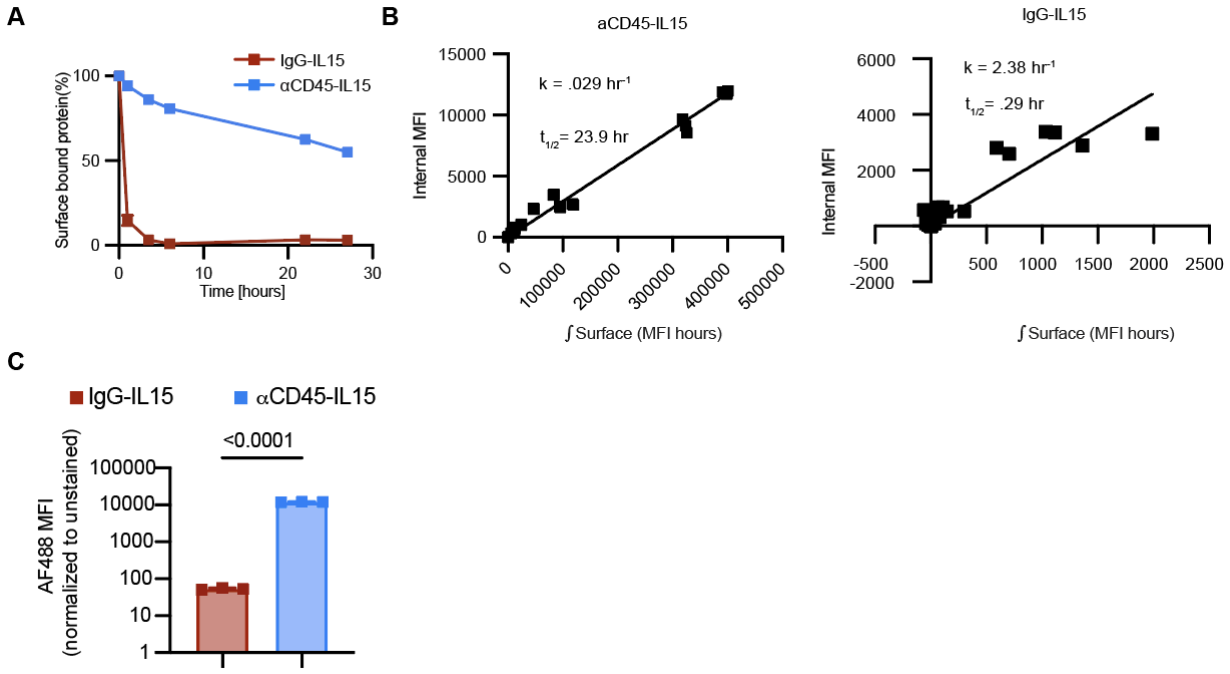

Figure 2.3. CD45 immunocytokines are retained on the cell surface.

A, Internalization kinetics of IgG-IL15 or αCD45-IL15 labeled with AF488 following binding to primary activated CD8⁺ T cells (n = 3 biological replicates per time point. Representative of n = 3 independent experiments). **B**, Derivation of internalization rate and half-life for αCD45-IL15 (left) and IgG-IL15 (right) on primary CD8 T cells. Surface signal was calculated by fluorescence quenching with an αAF488 antibody. **C,** AF488 signal of CD8⁺ T cells (n = 3 biological replicates) stained for 25 minutes with AF488-labeled αCD45-IL15 or IgG-IL15 for internalization experiment. Unstained background signal was subtracted for analysis.

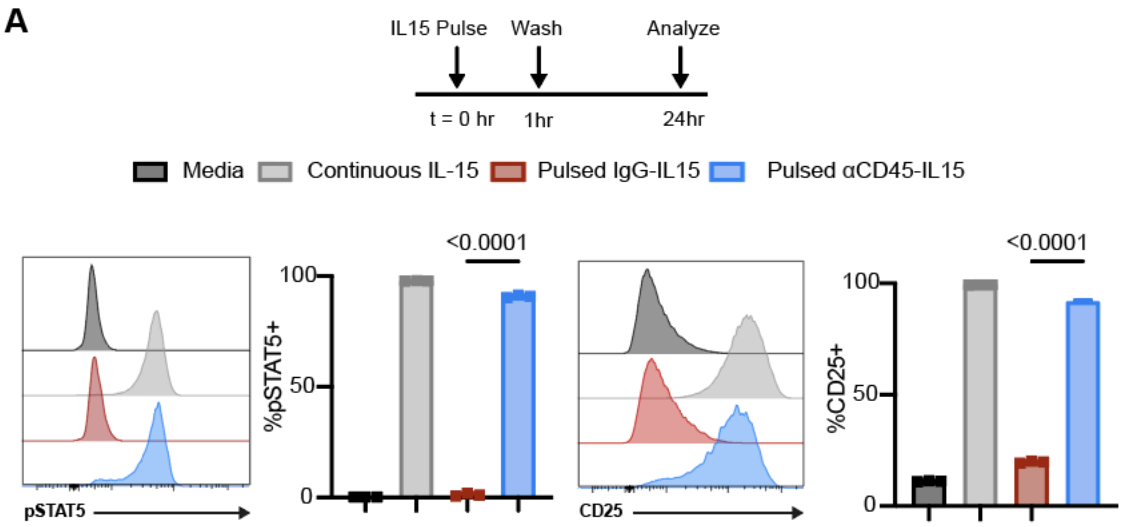

Figure 2.4. CD45 immunocytokines display extended signaling.

A, Primary CD8 T cells were pulsed for 1 hour with IL-15 immunocytokine fusions. Cells were washed to remove unbound cytokine, and 24 hours later fixed, permeabilized, and stained for flow cytometry analysis of pSTAT5 and CD25. Data are mean ± s.d. from n = 3 biological replicates. P values were determined by one-way ANOVA followed by Tukey's multiple comparison test.

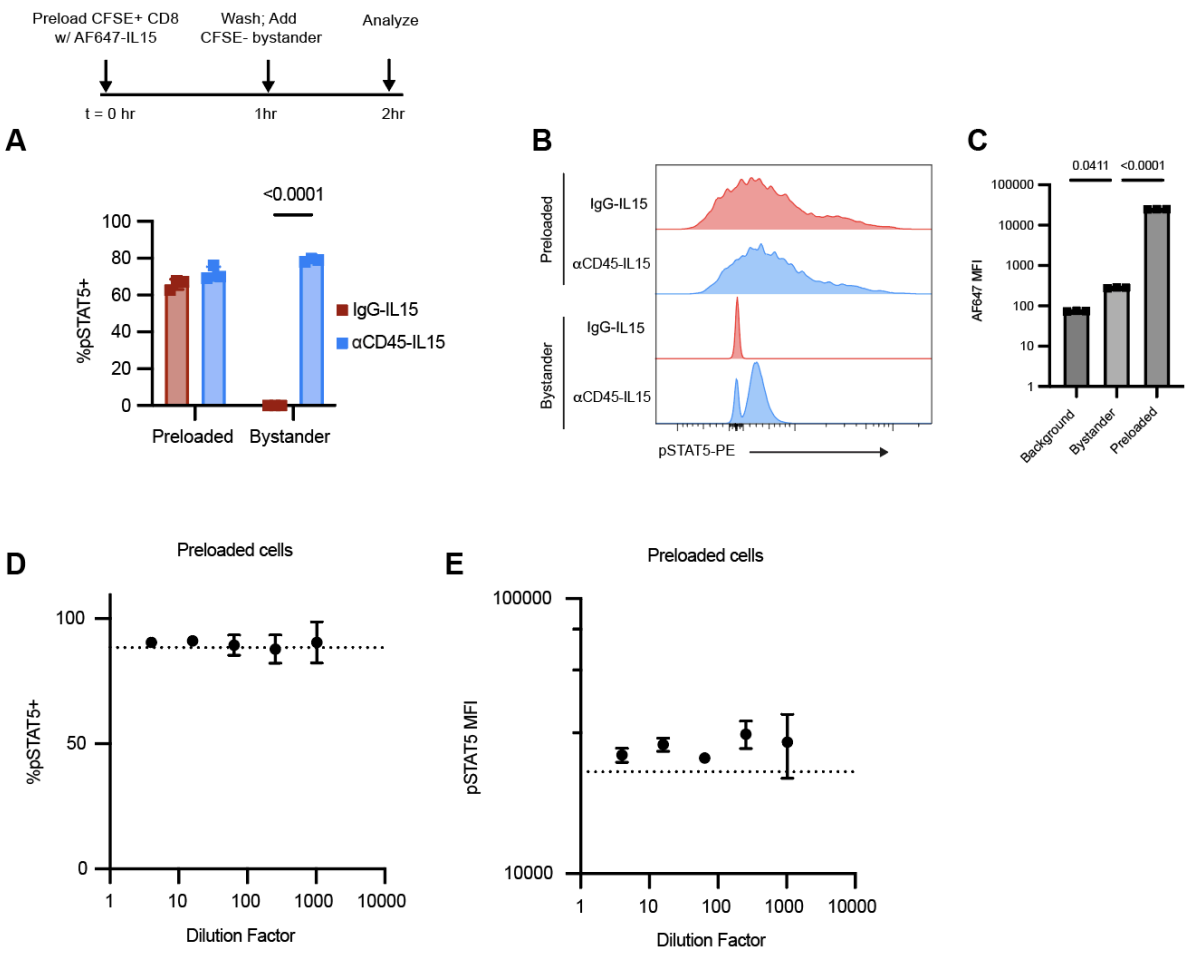

Figure 2.5. CD45 immunocytokines signal in cis and trans.

A-C, Primary CD8+ T cells were labeled with CFSE and incubated with AF647-labeled IL-15 immunocytokine fusions for 1 hr ("preloaded"), washed, and mixed into non-labeled "bystander" cells for 1 hr at a 1:20 preloaded: bystander ratio. Cells were then fixed, permeabilized, and stained for flow cytometry analysis of pSTAT5, shown in **A**. Bystander cells were defined as CFSE-AF647-. **B**, Representative pSTAT5 staining (n = 3) for the experimental set-up described in A. **C,** AF647 MFI signal of cells incubated with αCD45-IL15 (preloaded) and mixed with bystander cells. **D-E**, Primary CD8+ T cells were incubated with AF647-labeled αCD45-IL15 for 1 hr, washed, and diluted into HEK cells as CD45-IL15R- bystanders at the described dilution factors. Shown are pSTAT%+ (**D**) and pSTAT5 MFI (**E**). Data are mean ± s.d. from n = 3 biological replicates. P values were determined by one-way or two-way ANOVA followed by Tukey's multiple comparison test.

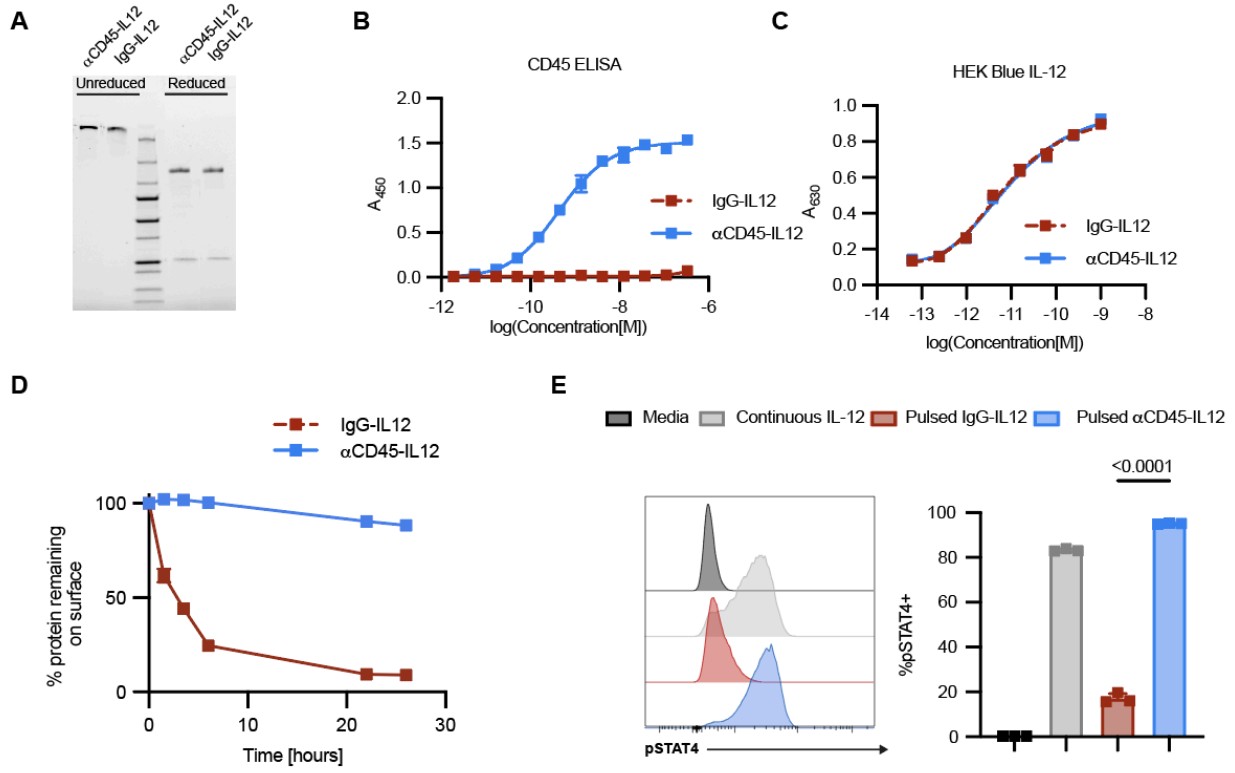

Figure 2.6. CD45-IL12 immunocytokines are retained on the cell surface and display extended signaling.

A, SDS-PAGE of IL12 immunocytokines. **B,** ELISA absorbance measurement of αCD45-IL12 and IgG-IL12 binding to plate-bound mouse CD45. **C,** Absorbance measurement of HEK-Blue-IL12 cells following 24 hr incubation with IgG-IL12 or αCD45-IL12 at indicated concentrations. **D,** Internalization kinetics of IgG-IL12 or αCD45-IL12 labeled with AF488 following binding to primary activated $CD8^+$ T cells. Surface signal was calculated by fluorescence quenching with an αAF488 antibody; **E**, Primary $CD8^+$ T cells were pulsed for with IL-12 immunocytokine fusions for 20 minutes. Cells were washed to remove unbound cytokine, and 24 hours later fixed, permeabilized, and stained for flow cytometry analysis of pSTAT4. In **B-E**, data are mean ± s.d. from n = 3 biological replicates. P values were determined by one-way ANOVA followed by Tukey's multiple comparison test.

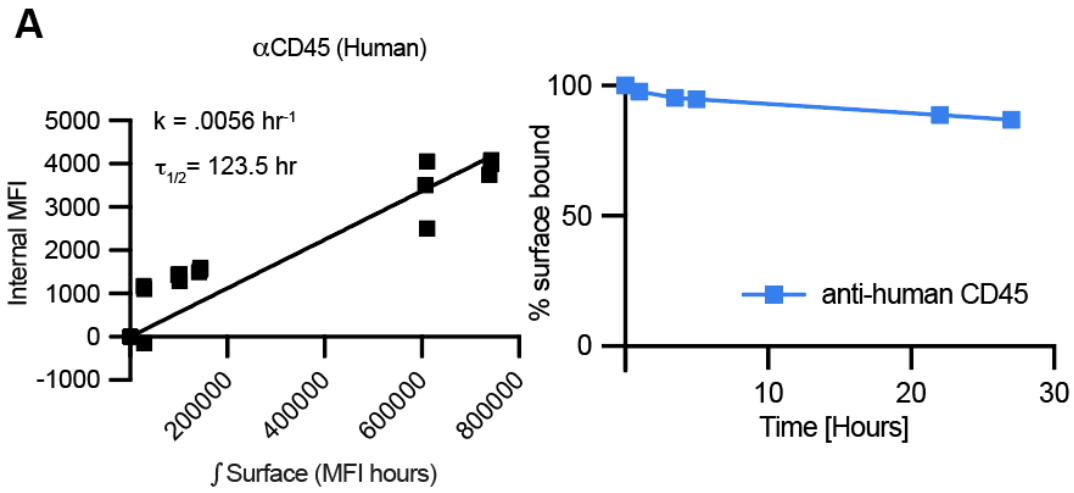

Figure 2.7. Human CD45 can be bound to without triggering internalization.

A, Derivation of internalization rate (left) and internalization kinetics (right) of primary human CD8+ T cells incubated with anti-human CD45 labeled with AF488 for stated time points. Surface signal was calculated by fluorescence quenching with an αAF488 antibody. Data are mean ± s.d. from n = 3 biological replicates.

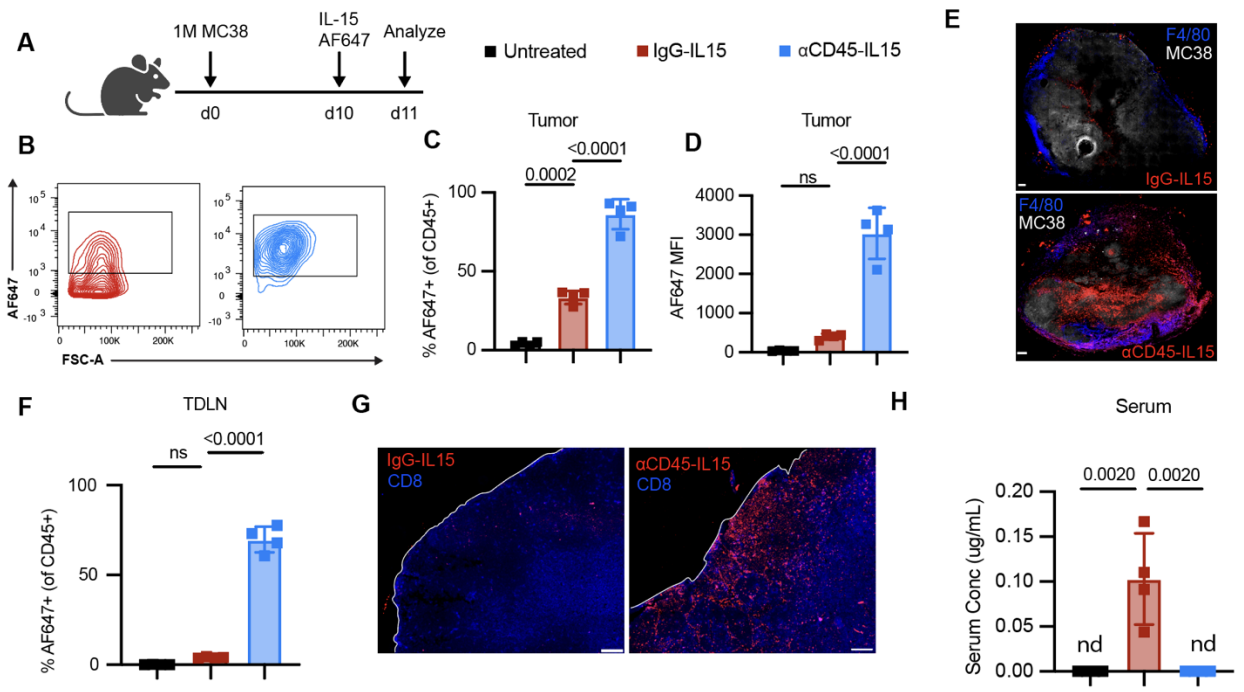

Figure 2.8. Intratumorally administered αCD45- IL15 is retained in the tumor and TDLN with negligible systemic exposure.

C57BL/6J mice (n = 4 mice/group) were inoculated with 1M MC38 (**B-D, F, H**) or MC38-ZsGreen (**E, G)** cells in the flank, and 10 days later administered AF647-labeled αCD45-IL15 or IgG-IL15 (10μg) intratumorally, followed by analysis of cytokine biodistribution 24 hr later. For microscopy experiments, MC38-ZsGreen tumors were used for easy detection of tumor cells. **A,** Study diagram. **B,** Representative histograms of antibody-cytokine fusion binding to $CD45^+$ tumor-infiltrating leukocytes. **C**, Frequencies of $AF647^+$ tumor-infiltrating leukocytes. **D**, AF647 MFI on TILs. **E**, Representative confocal images of tumors. Scale bar, 200μm . **F,** AF647 labeling on TDLN immune cells. **G,** Representative histological images of TDLN. Scale bar, 100 μm. **H**, Serum concentrations of dosed immunocytokines based on fluorescence spectroscopy measurements. nd = not detected. Shown are mean ± s.d. from n = 4 replicates/group. P values were determined by one-way ANOVA followed by Tukey's multiple comparison test.

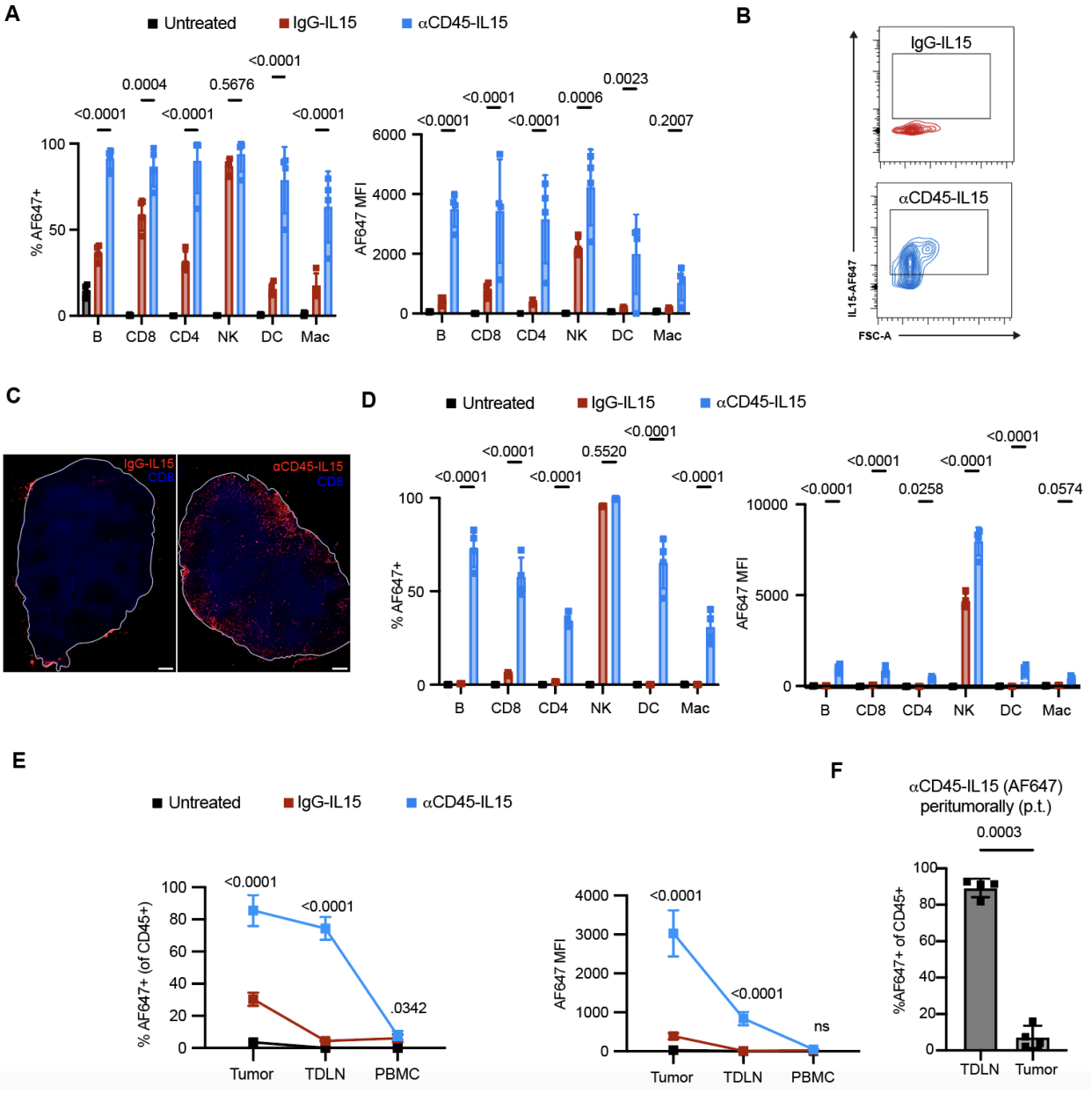
A
Untreated
IgG-IL15
αCD45-IL15
% AF647+
AF647 MFI
B
CD8
CD4
NK
DC
Mac
B
IgG-IL15
αCD45-IL15
IL15-AF647
FSC-A
C
IgG-IL15
CD8
αCD45-IL15
CD8
D
Untreated
IgG-IL15
αCD45-IL15
% AF647+
AF647 MFI
E
Untreated
IgG-IL15
αCD45-IL15
% AF647+ (of CD45+)
AF647 MFI
Tumor
TDLN
PBMC
F
αCD45-IL15 (AF647)
peritumorally (p.t.)
%AF647+ of CD45+
TDLN
Tumor

Figure 2.9. αCD45-IL15 displays altered biodistribution compared to IgG-IL15.

A-D, AF647-labeled αCD45-IL15 or IgG-IL15 was dosed (10μg) intratumorally in established MC38 tumors 24 hours prior to flow cytometry analysis (n = 4 mice/group). Shown are **A,** Tumor cell-type specific biodistribution by percentage (left) or MFI (right). **B,** Representative contour plot of AF647 signal on TDLN $CD45^+$ cells. **C**, Representative TDLN images from the experiment described in Fig. 2a. Scale bar, 200 μm. **D,** TDLN cell-type specific biodistribution by percentage (left) or MFI (right). **E,** Compartment specific biodistribution by MFI (left) or percentage (right). **F,** AF647-labeled αCD45-IL15 was dosed (10μg) peritumorally (s.c. at the tail-base) 24 hours prior to flow cytometry analysis (n = 4 mice/group). In **A,C,E** and **F**, data are mean +/- s.d. from n = 4 biological replicates. P values were determined by t-test, one-way, or two-way ANOVA followed by Tukey's multiple comparison test.

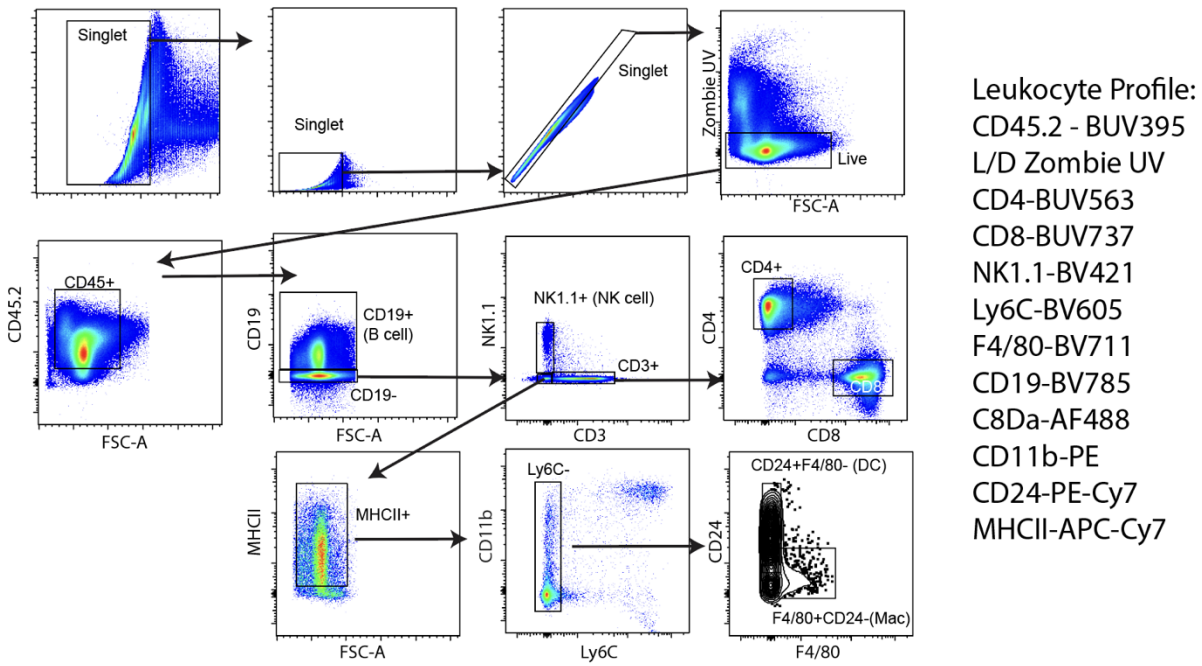

Figure 2.10. Leukocyte profiling gating strategy used in biodistribution experiments.

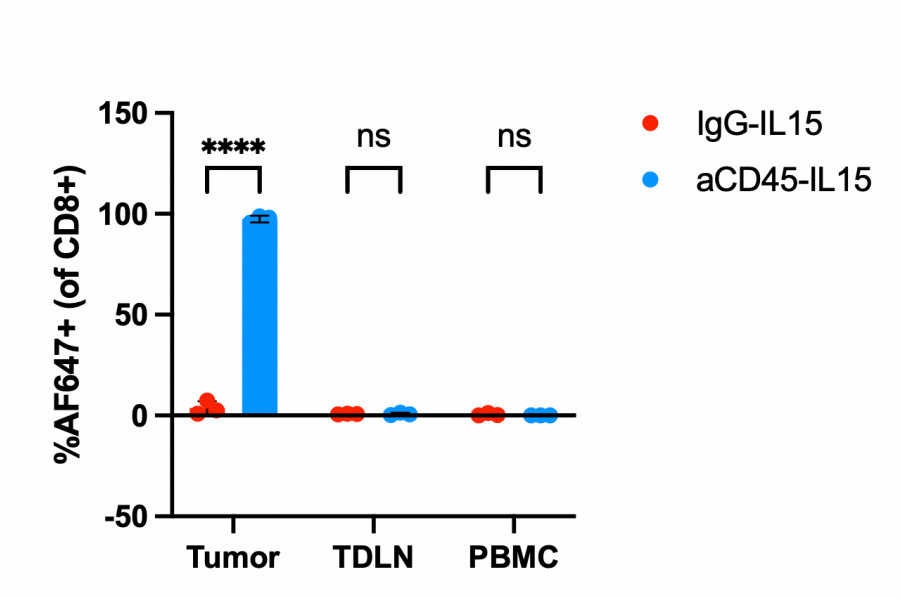

Figure 2.11. 1µg of αCD45-IL15 saturates intratumoral CD8+ T cells but spares the TDLN.

C57BL/6 mice were inoculated with 1M MC38 cells. On days 9, mice were treated with 1µg of AF647-labeled IL-15 immunocytokine. 24 hours later, AF647 signal on $CD8^+$ T cells was profiled by flow cytometry in various tissues. Data are mean +/- s.d. from n = 3 biological replicates. P values were determined by two-way ANOVA followed by Tukey's multiple comparison test.

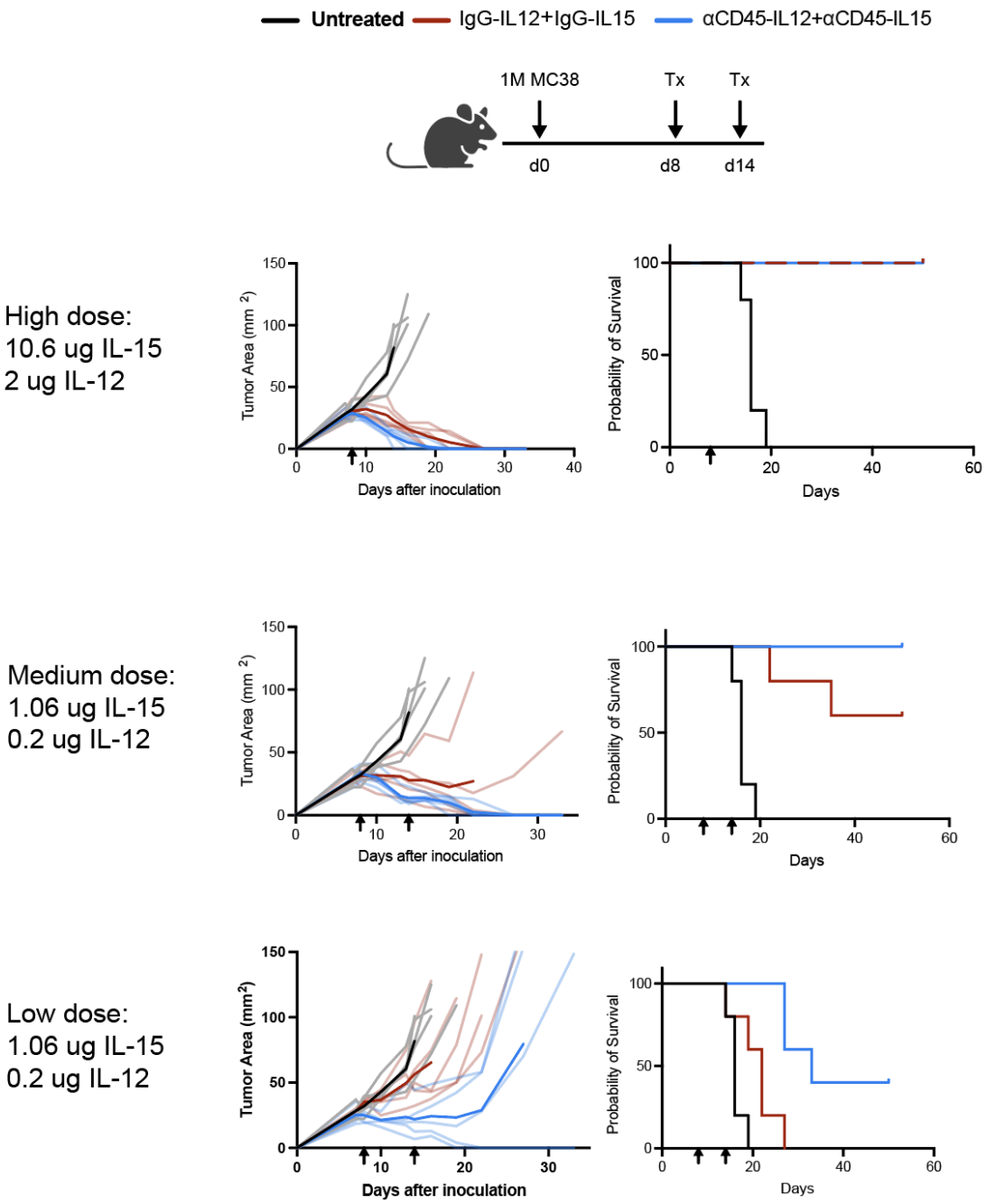

Figure 2.12. CD45-targeted IL-15 + IL-12 elicit efficacy in dose sparing regimens.

C57BL/6 mice were inoculated with 1M MC38 cells. On days 8 and 14, mice were treated with the specified doses of IgG or αCD45 immunocytokines. For each dose, shown are (left) tumor growth curves and (right) survival curves.

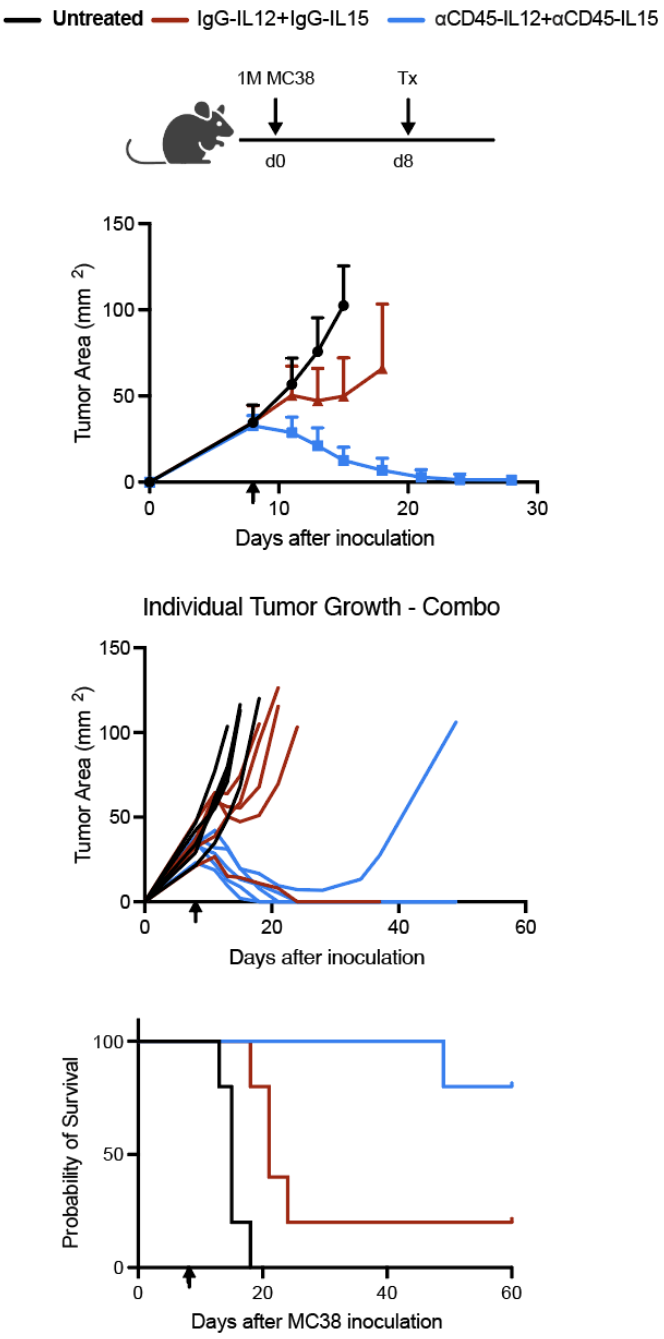

Figure 2.13. A single dose of αCD45-IL15 + αCD45-IL12 can cure MC38 tumors

C57BL/6 mice were inoculated with 1M MC38 cells. On day 8, mice were treated with the specified doses of IgG or αCD45 immunocytokines. Shown are (top) grouped tumor growth curves, (middle) individual tumor curves, and (bottom) survival curves.

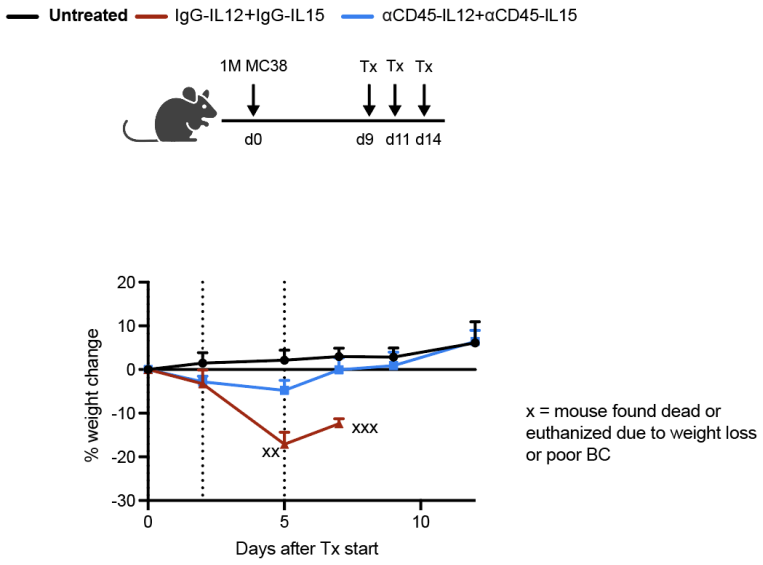

Figure 2.14. CD45 targeting retains proteins at the site of injection and minimizes toxicity for combination cytokine therapies.

C57BL/6 mice (n = 5) were inoculated with 1M MC38 tumors and treated as described in the figure with 20µg of IL-15 immunocytokine and 4µg of IL-12 immunocytokine. Shown is relative weight to pre-treatment. Vertical dashed lines indicate treatment. x on plot indicates euthanasia due to weight loss or poor body condition (BC).

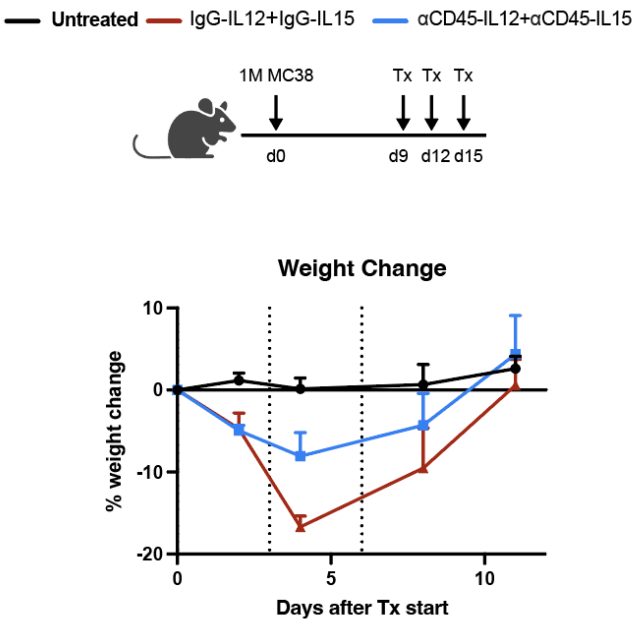

Figure 2.15. Local administration of CD45-retained cytokines can improve toxicity profiles.

C57BL/6 mice (n = 5) were inoculated with 1M MC38 tumors and treated as described in the figure with 20μg of IL-15 immunocytokine and 8μg of IL-12 immunocytokine. Shown is relative weight to pre-treatment. Vertical dashed lines indicate treatment.

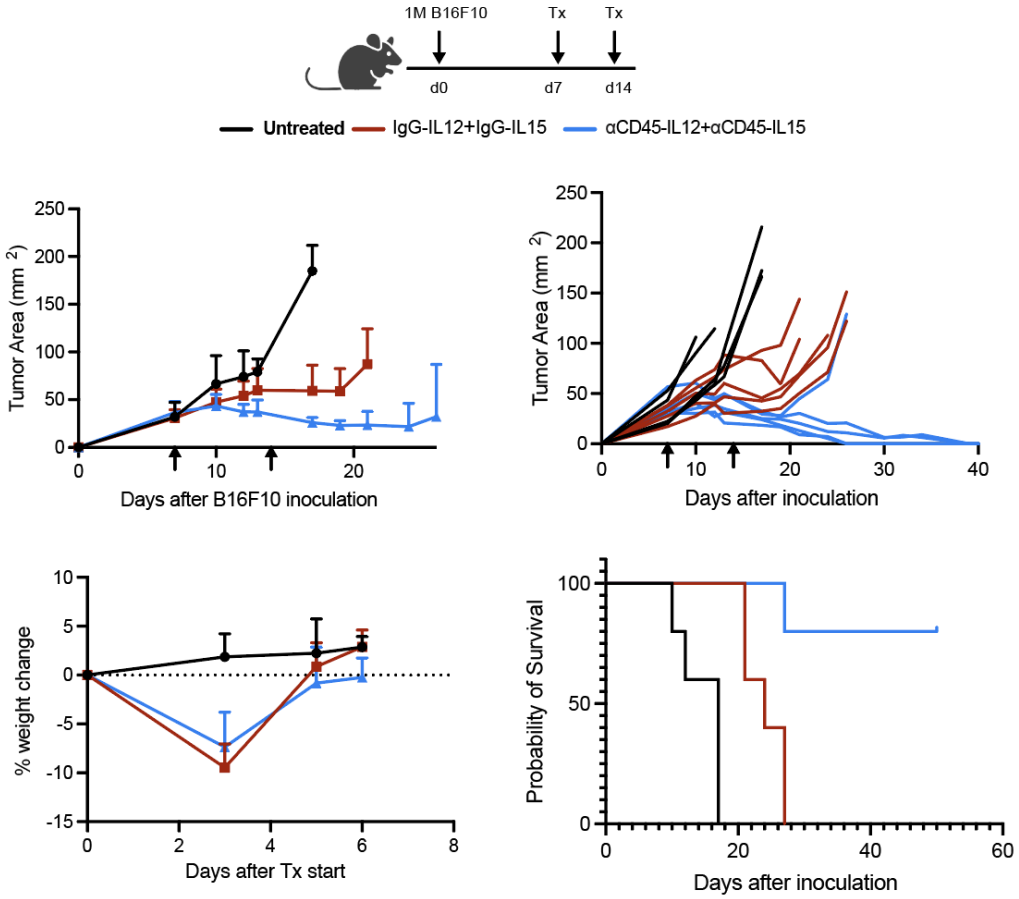

Figure 2.16. CD45-targeted cytokines are effective in B16F10.

C57BL/6 mice (n = 5) were inoculated with 1M B16F10 tumors and treated as described in the figure with 10µg of IL-15 immunocytokine and 2µg of IL-12 immunocytokine on d7 and 10µg of IL-15 immunocytokine on d14.

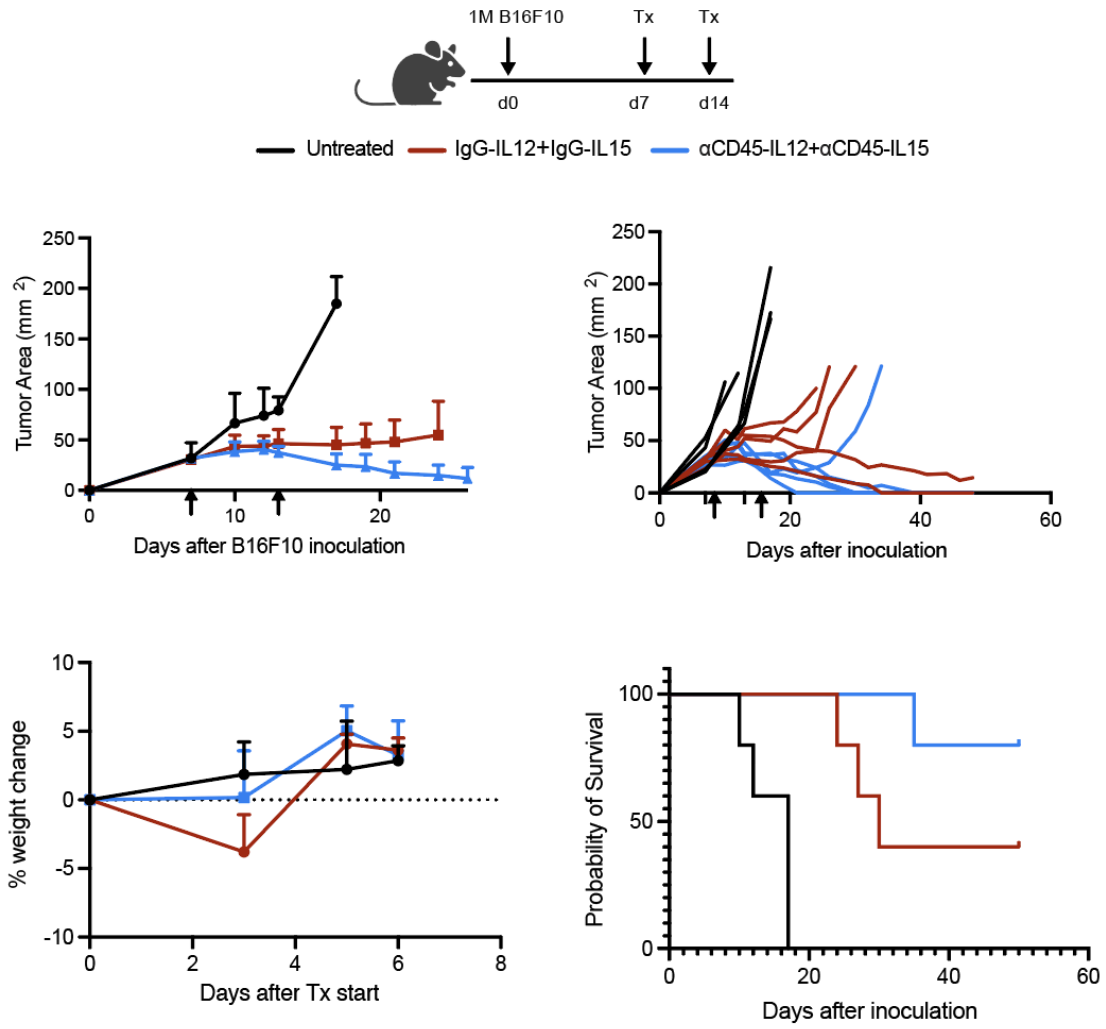

Figure 2.17. CD45-targeted IL-15 and IL-12 maintain efficacy at lower doses.

C57BL/6 mice (n = 5) were inoculated with 1M B16F10 tumors and treated as described in the figure with 5μg of IL-15 immunocytokine and 1μg of IL-12 immunocytokine on d7 and d14.

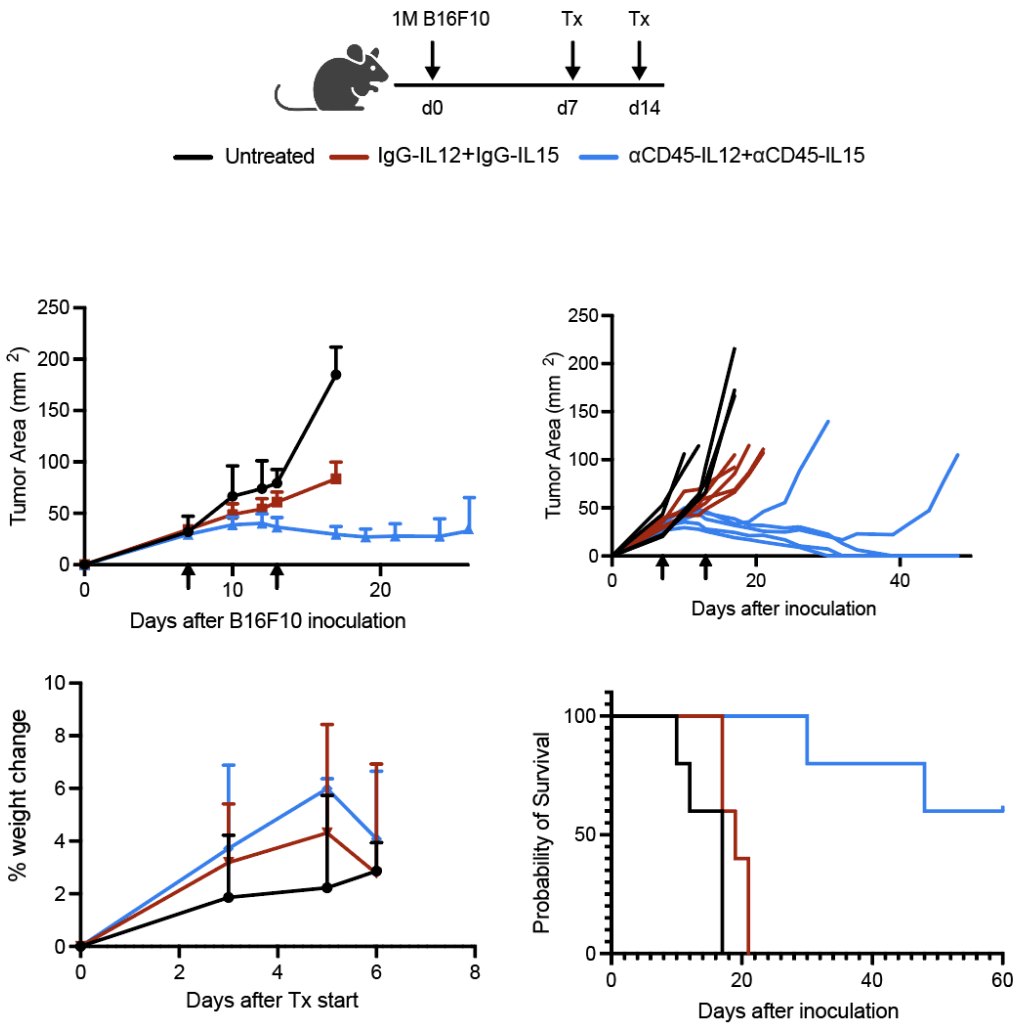

Figure 2.18.CD45-targeted IL-15 and IL-12 maintain efficacy at dose-sparing regimens.

C57BL/6 mice (n = 5) were inoculated with 1M B16F10 tumors and treated as described in the figure with 1µg of IL-15 immunocytokine and 0.2µg of IL-12 immunocytokine on d7 and d14.

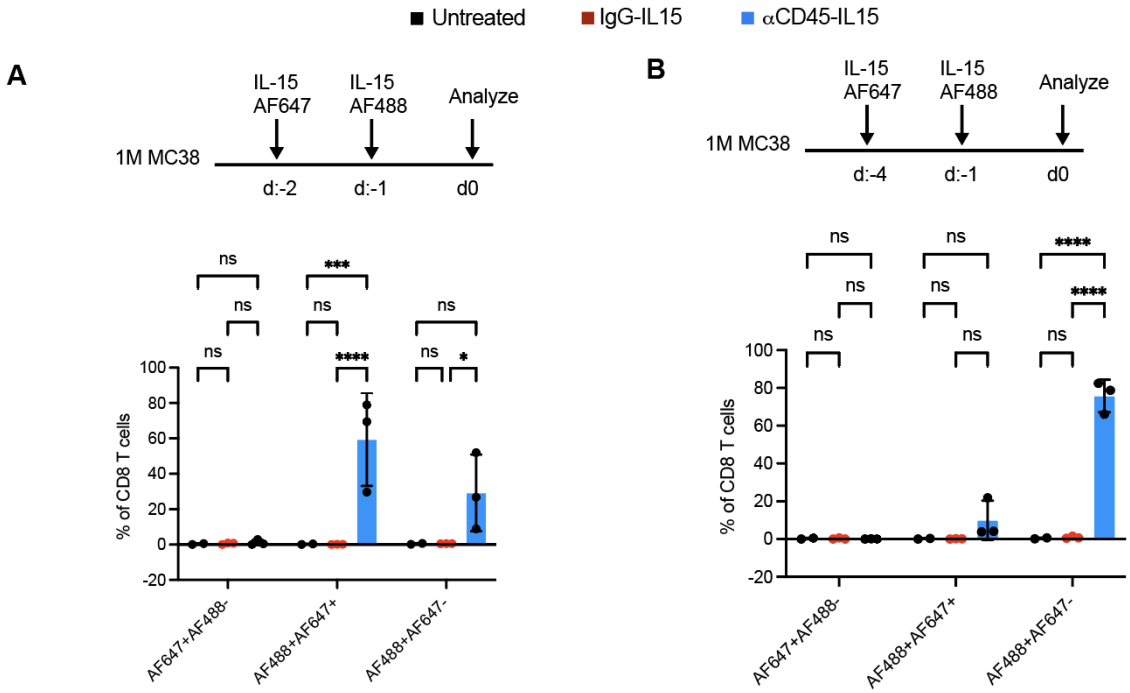

Figure 2.19. CD45 kinetic turnover in vivo.

A-B, C57BL/6 mice (n = 3) were inoculated with 1M MC38 tumors and treated as described in the figure with 1µg of IL-15 immunocytokine that was fluorescently labeled with AF488 or AF647. Cells were analyzed for fluorescence by flow cytometry 24 hours after the last dose. Cells were gated on live CD3+CD8+ for analysis. Data are mean +/- s.d. from n = 3 biological replicates. P values were determined by two-way ANOVA followed by Tukey's multiple comparison test.

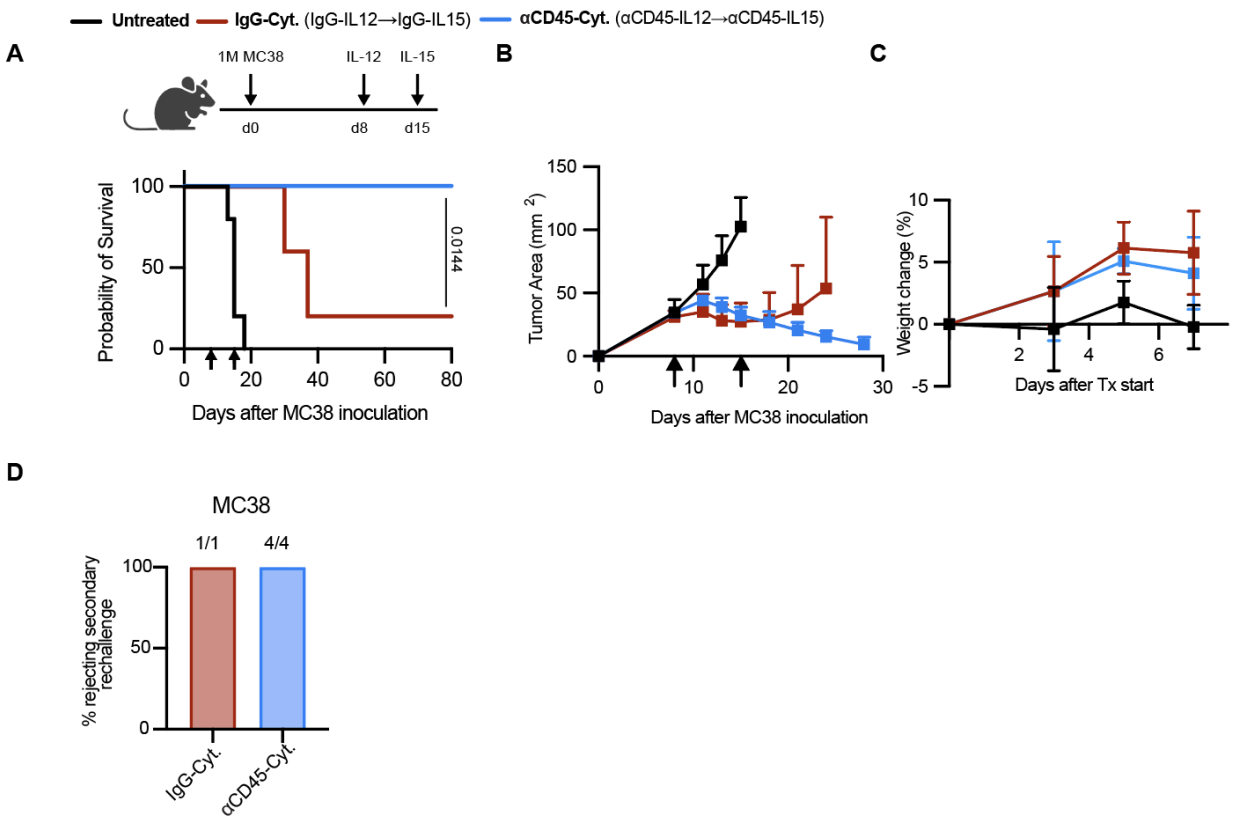

Figure 2.20. αCD45-Cyt therapy is safe and efficacious in MC38 tumors.

A-C, Mice (n = 5/group) inoculated with 1M tumor cells and treated with 1 µg of αCD45-IL12 and 10µg of αCD45-IL15 (referred to as αCD45-Cyt) or treated with 1 µg of IgG-IL12 and 10µg of IgG-IL15 (referred to as IgG-Cyt) as shown on the experimental timelines. **A,** Overall survival. Statistical comparison shown between IgG-Cyt and αCD45-Cyt groups. **B,** Grouped tumor growth curves. **C,** Weight change after beginning treatment. **D,** Surviving mice were rechallenged on d100 with 0.1M MC38 cells on the opposing flank to the primary challenge. P values were determined by log-rank (Mantel-Cox) test. For all plots, arrows indicate treatment.

Tables

Table 2.1. Amino acid sequences of various mouse αCD45-cytokine fusions.

Key: V_H, V_L, linker, constant region, cytokine

αCD45 (30-F11) V_H	QVQLLQSGGGLVQPGRSLKLSCLASGFIFSNYGMNWI RQAPGKGLEWVASISSTSSYIQYADTVKGRFTISRENA KNTLYLQMTSLISEDTALYYCARHGGYGYKGIWFAYW GQGTLVTVSS
αCD45 (30-F11) V_L	DIQLTQSPKSMSMSVGERVTLTCKASENVVTYVSWY QQKPEQSPKLLIYGASNRYTGVPDRFTGSGSATDFTL TISSVQAEDLADYHCGQGYSYPYTFGGGTKLEIK
IgG (4-4-20) V_H	DVKLDETGGGLVQPGRPMKLSCVASGFTFSDYWMN WVRQSPEKGLEWVAQIRNKPYNYETYYSDSVKGRFT ISRDDSKSSVYLQMNNLRVEDMGIYYCTGSYYGMDY WGQGTSVTVS
IgG (4-4-20) V_L	DVVMTQTPLSLPVSLGDQASISCRSSQSLVHSNGNT YLRWYLQKPGQSPKVLIYKVSNRFSGVPDRFSGSGS GTDFTLKISRVEAEDLGVYFCSQSTHVPWTFGGGTK LEIK
αCD45-IL15 Light Chain (mCκ)	DIQLTQSPKSMSMSVGERVTLTCKASENVVTYVSWY QQKPEQSPKLLIYGASNRYTGVPDRFTGSGSATDFTL TISSVQAEDLADYHCGQGYSYPYTFGGGTKLEIK RAD AAPTVSIFPPSSEQLTSGGASVVCFLNNFYPKDINVKW KIDGSERQNGVLNSWTDQDSKDSTYSMSSTLTLTKDE YERHNSYTCEATHKTSTSPIVKSFNRNEC
αCD45-IL15 Heavy Chain (mIgG2c LALA-PG)	QVQLLQSGGGLVQPGRSLKLSCLASGFIFSNYGMNWIR QAPGKGLEWVASISSTSSYIQYADTVKGRFTISRENAKN TLYLQMTSLISEDTALYYCARHGGYGYKGIWFAYWGQG TLVTVSS AKTTAPSVYPLAPVCGGTTGSSVTLGCLVKGY FPEPVTLTWNSGSLSSGVHTFPALLQSGLYTLSSSVTVT SNTWPSQTITCNVAHPASSTKVDKKIEPRVPITQNPCPP LKECPPCAAPDAAGGPSVFIFPPKIKDVLMISLSPMVTCV VVDVSEDDPDVQISWFVNNVEVHTAQTQTHREDYNSTL RVVSALPIQHQDWMSGKEFKCKVNNRALGSPIEKTISKP RGPVRAPQVYVLPPPAEEMTKKEFSLTCMITGFLPAEIA VDWTSNGRTEQNYKNTATVLDSDGSYFMYSKLRVQKS TWERGSLFACSVVHEGLHNHLTTKTISRSLGK GGGGS GTTCPPPVSIEHADIRVKNYSVNSRERYVCNSGFKRKAGT STLIECVINKNTNVAHWTTPSLKCIRDPSLAGGSGGSGG SGGSGGSGGSGGNWIDVRYDLEKIESLIQSIHIDTTLYTD SDFHPSCKVTAMNCFLLELQVILHEYSNMTLNETVRNVL

	YLANSTLSSNKNVAESGCKECEELEEKTFTEFLQSFIRIVQ MFINTS
IgG-IL15 Light Chain (mCκ)	DVVMTQTPLSLPVSLGDQASISCRSSQSLVHSNG NTYLRWYLQKPGQSPKVLIYKVSNRFSGVPDRFS GSGSGTDFTLKISRVEAEDLGVYFCSQSTHVPWT FGGGTKLEIK RADAAPTVSIFPPSSEQLTSGGASV VCFLNNFYPKDINVKWKIDGSERQNGVLNSWTDQ DSKDSTYSMSSTLTLTKDEYERHNSYTCEATHKTS TSPIVKSFNRNEC
IgG-IL15 Heavy Chain (mIgG2c LALA-PG)	DVKLDETGGGLVQPGRPMKLSCVASGFTFSDYWMN WVRQSPEKGLEWVAQIRNKPYNYETYYSDSVKGRFT ISRDDSKSSVYLQMNNLRVEDMGIYYCTGSYYGMDY WGQGTSVTVS AKTTAPSVYPLAPVCGGTTGSSVTLG CLVKGYFPEPVTLTWNSGSLSSGVHTFPALLQSGLYT LSSSVTVTSNTWPSQTITCNVAHPASSTKVDKKIEPRV PITQNPCPPLKECPPCAAPDAAGGPSVFIFPPKIKDVL MISLSPMVTCVVVDVSEDDPDVQISWFVNNVEVHTAQ TQTHREDYNSTLRVVSALPIQHQDWMSGKEFKCKVNN RALGSPIEKTISKPRGPVRAPQVYVLPPPAEEMTKKEFS LTCMITGFLPAEIAVDWTSNGRTEQNYKNTATVLDSDG SYFMYSKLRVQKSTWERGSLFACSVVHEGLHNHLTTK TISRSLGK GGGGS GTTCPPPVSIEHADIRVKNYSVNSR ERYVCNSGFKRKAGTSTLIECVINKNTNVAHWTTPSLK CIRDPSLAGGSGGSGGSGGSGGSGGSGGNWIDVRYD LEKIESLIQSIHIDTTLYTDSDFHPSCKVTAMNCFLLELQV ILHEYSNMTLNETVRNVLYLANSTLSSNKNVAESGCKEC EELEEKTFTEFLQSFIRIVQMFINTS
αCD45-IL12 Light Chain (mCκ)	DIQLTQSPKSMSMSVGERVTLTCKASENVVTYVSWY QQKPEQSPKLLIYGASNRYTGVPDRFTGSGSATDFTL TISSVQAEDLADYHCGQGYSYPYTFGGGTKLEIK RAD AAPTVSIFPPSSEQLTSGGASVVCFLNNFYPKDINVKW KIDGSERQNGVLNSWTDQDSKDSTYSMSSTLTLTKDE YERHNSYTCEATHKTSTSPIVKSFNRNEC
αCD45-IL12 Heavy Chain (mIgG2c LALA-PG)	MWELEKDVYVVEVDWTPDAPGETVNLTCDTPEEDDIT WTSDQRHGVIGSGKTLTITVKEFLDAGQYTCHKGGET LSHSHLLLHKKENGIWSTEILKNFKNKTFLKCEAPNYS GRFTCSWLVQRNMDLKFNIKSSSSSPDSRAVTCGMAS LSAEKVTLDQRDYEKYSVSCQEDVTCPTAEETLPIELAL EARQQNKYENYSTSFFIRDIIKPDPPKNLQMKPLKNSQV EVSWEYPDSWSTPHSYFSLKFFVRIQRKKEKMKETEEG CNQKGAFLVEKTSTEVQCKGGNVCVQAQDRYYNSSCS KWACVPCRVRSGGSGGGSGGGSGGGSRVIPVSGPAR CLSQSRNLLKTTDDMVKTAREKLKHYSCTAEDIDHEDITR DQTSTLKTCLPLELHKNESCLATRETSSTTRGSCLPPQK

	TSLMMTLCLGSIYEDLKMYQTEFQAINAALQNHNHQQIILD KGMLVAIDELMQSLNHNGETLRQKPPVGEADPYRVKMKL CILLHAFSTRVVTINRVMGYLSSA GGGGSGGGGSGGGGS QVQLLQSGGGLVQPGRSLKLSCLASGFIFSNYGMNWIRQ APGKGLEWVASISSTSSYIQYADTVKGRFTISRENAKNTLY LQMTSLISEDTALYYCARHGGYGYKGIWFAYWGQGTLV TVSS AKTTAPSVYPLAPVCGGTTGSSVTLGCLVKGYFPE PVTLTWNSGSLSSGVHTFPALLQSGLYTLSSSVTVTSNT WPSQTITCNVAHPASSTKVDKKIEPRVPITQNPCPPLKEC PPCAAPDAAGGPSVFIFPPKIKDVLMISLSPMVTCVVVDVS EDDPDVQISWFVNNVEVHTAQTQTHREDYNSTLRVVSALP IQHQDWMSGKEFKCKVNNRALGSPIEKTISKPRGPVRAP QVYVLPPPAEEMTKKEFSLTCMITGFLPAEIAVDWTSNGRT EQNYKNTATVLDSDGSYFMYSKLRVQKSTWERGSLFACSV VHEGLHNHLTTKTISRSLGK
IgG-IL12 Light Chain (mCκ)	DVVMTQTPLSLPVSLGDQASISCRSSQSLVHSNG NTYLRWYLQKPGQSPKVLIYKVSNRFSGVPDRFS GSGSGTDFTLKISRVEAEDLGVYFCSQSTHVPWT FGGGTKLEIK RADAAPTVSIFPPSSEQLTSGGASV VCFLNNFYPKDINVKWKIDGSERQNGVLNSWTDQ DSKDSTYSMSSTLTLTKDEYERHNSYTCEATHKTS TSPIVKSFNRNEC
IgG-IL12 Heavy Chain (mIgG2c LALA-PG)	MWELEKDVYVVEVDWTPDAPGETVNLTCDTPEED DITWTSDQRHGVIGSGKTLTITVKEFLDAGQYTCHK GGETLSHSHLLLHKKENGIWSTEILKNFKNKTFLKC EAPNYSGRFTCSWLVQRNMDLKFNIKSSSSSPDSR AVTCGMASLSAEKVTLDQRDYEKYSVSCQEDVTCP TAEETLPIELALEARQQNKYENYSTSFFIRDIIKPDPP KNLQMKPLKNSQVEVSWEYPDSWSTPHSYFSLKFF VRIQRKKEKMKETEEGCNQKGAFLVEKTSTEVQCK GGNVCVQAQDRYYNSSCSKWACVPCRVRSGGSG GGSGGGSGGGSRVIPVSGPARCLSQSRNLLKTTDD MVKTAREKLKHYSCTAEDIDHEDITRDQTSTLKTCLP LELHKNESCLATRETSSTTRGSCLPPQKTSLMMTLC LGSIYEDLKMYQTEFQAINAALQNHNHQQIILDKGML VAIDELMQSLNHNGETLRQKPPVGEADPYRVKMKL CILLHAFSTRVVTINRVMGYLSSA GGGGSGGGGSG GGGS DVKLDETGGGLVQPGRPMKLSCVASGFTFS DYWMNWVRQSPEKGLEWVAQIRNKPYNYETYYSD SVKGRFTISRDDSKSSVYLQMNNLRVEDMGIYYCTG SYYGMDYWGQGTSVTVS AKTTAPSVYPLAPVCGGT TGSSVTLGCLVKGYFPEPVTLTWNSGSLSSGVHTFP ALLQSGLYTLSSSVTVTSNTWPSQTITCNVAHPASST KVDKKIEPRVPITQNPCPPLKECPPCAAPDAAGGPSV

	FIFPPKIKDVLMISLSPMVTCVVVDVSEDDPDVQISWF VNNVEVHTAQTQTHREDYNSTLRVVSALPIQHQDWM SGKEFKCKVNNRALGSPIEKTISKPRGPVRAPQVYVLP PPAEEMTKKEFSLTCMITGFLPAEIAVDWTSNGRTEQN YKNTATVLDSDGSYFMYSKLRVQKSTWERGSLFACSV VHEGLHNHLTTKTISRSLGK

Table 2.2. Amino acid sequences of human αCD45-IL15 fusions

Key: V_H/V_L, linker, constant region, cytokine

Human αCD45 (BC8) V_L	DIALTQSPASLAVSLGQRATISCRASKSVSTSGYSYLHW YQQKPGQPPKLLIYLASNLESGVPARFSGSGSGTDFTLN IHPVEEEDAATYYCQHSRELPFTFGSGTKLEIK
Human αCD45 (BC8) V_H	EVKLLESGGGLVQPGGSLKLSCAASGFDFSRYWMSWVR QAPGKGLEWIGEINPTSSTINFTPSLKDKVFISRDNAKNTL YLQMSKVRSEDTALYYCARGNYYRYGDAMDYWGQGTSVTVSS
Human αCD45-IL15 Light Chain (hCκ)	DIALTQSPASLAVSLGQRATISCRASKSVSTSGYSYLHW YQQKPGQPPKLLIYLASNLESGVPARFSGSGSGTDFTLN IHPVEEEDAATYYCQHSRELPFTFGSGTKLEIK RTVAAPS VFIFPPSDEQLKSGTASVVCLLNNFYPREAKVQWKVDNA LQSGNSQESVTEQDSKDSTYSLSSTLTLSKADYEKHKVY ACEVTHQGLSSPVTKSFNRGEC
Human αCD45-IL15 Heavy Chain (hIgG1 LALA-PG)	EVKLLESGGGLVQPGGSLKLSCAASGFDFSRYWMSWVR QAPGKGLEWIGEINPTSSTINFTPSLKDKVFISRDNAKNTL YLQMSKVRSEDTALYYCARGNYYRYGDAMDYWGQGTSV TVSS ASTKGPSVFPLAPSSKSTSGGTAALGCLVKDYFPEP VTVSWNSGALTSGVHTFPAVLQSSGLYSLSSVVTVPSSSL GTQTYICNVNHKPSNTKVDKKVEPKSCDKTHTCPPCPAPE AAGGPSVFLFPPKPKDTLMISRTPEVTCVVVDVSHEDPEV KFNWYVDGVEVHNAKTKPREEQYNSTYRVVSVLTVLHQD WLNGKEYKCKVSNKALGAPIEKTISKAKGQPREPQVYTLPP SRDELTKNQVSLTCLVKGFYPSDIAVEWESNGQPENNYKT TPPVLDSDGSFFLYSKLTVDKSRWQQGNVFSCSVMHEALH NHYTQKSLSLSPGK GGGS ITCPPPMSVEHADIWVKSYSLYS RERYICNSGFKRKAGTSSLTECVLNKATNVAHWTTPSLKCIR GGSGGSGGSGGSGGSGGSGGNWVNVISDLKKIEDLIQSMHI DATLYTESDVHPSCKVTAMKCFLLELQVISLESGDASIHDTVE NLIILANDSLSSNGNVTESGCKECEELEEKNIKEFLQSFVHIVQ MFINTSHHHHHH

Methods

Cell lines and animals

Cell lines CTLL-2 (ATCC), Expi293F (Gibco), HEK-Blue IL-12 (Invivogen) were cultured according to vendor instructions. MC38 (Kerafast), MC38-ZsGreen (developed in the lab as described previously(*96*)), and B16F10 (ATCC) cells were cultured in Dulbecco's Modified Eagle's Medium (DMEM) supplemented with 10% fetal bovine serum (FBS), 100 units ml^{-1} penicillin and 100 µg ml^{-1} streptomycin. All cells were maintained at 37 °C and 5% CO_2, and all confirmed to be negative for mycoplasma.

All animal studies and procedures were carried out following federal, state and local guidelines under an institutional animal care and use committee-approved animal protocol by the Committee of Animal Care at MIT. Female C57BL/6J (The Jackson Laboratory, 000664) and *Batf3–/–* (The Jackson Laboratory, 013755) mice at 6-8 weeks age were purchased and maintained in the animal facility at MIT.

Cloning and protein purification

Gene blocks (gBlock, IDT) encoding for the light and heavy chain variable regions of anti-CD45 (clone: 30-F11(*97*)) or untargeted isotype control (anti-FITC, clone: 4-4-20) were cloned into a mouse kappa light chain and IgG2c backbone with LALA-PG(*23*) mutations, respectively, in the mammalian expression vector gWiz (Genlantis). For αCD45-IL15, murine IL-15/IL-15$Rα_{sushi}$, as described previously(*57*), was then cloned at the C terminus of the anti-CD45 (or anti-FITC control) heavy chain. To generate αCD45-IL12, murine single chain IL-12 (scIL-12), as described previously(*57*), was cloned at the N terminus of the anti-CD45 (or anti-FITC control) heavy chain. For both IL-15 and IL-12 immunocytokines, a $(Gly_4Ser)_3$ linker was used between the cytokine and antibody. A gBlock encoding for the extracellular domain of mouse CD45RO (used for ELISAs; sequence obtained from Uniprot) was cloned into gWiz with a His_6 tag. Plasmid sequences confirmed by Sanger sequencing (Quintara Biosciences) were transformed into Stellar Competent Cells (Takara Bio) and purified using the NucleoBond Xtra Midi

endotoxin-free midi-prep kit (Takara Bio). For immunocytokines, equal mass of heavy and light chain plasmids were transfected into Expi293F cells (Gibco) per manufacturer's instructions and harvested 6 days after transfection. All immunocytokines were purified using rProteinA Sepharose Fast Flow resin (Cytiva Life Sciences) and validated for size by SDS-PAGE. His-tagged CD45RO was purified by TALON affinity resin (Takara) according to the manufacturer's instructions. Purified proteins were confirmed to be endotoxin-free (<0.1 EU per dose) using the Endosafe Nexgen-PTS system (Charles River). Purified proteins were flash-frozen in liquid nitrogen and stored at -80C until use.

ELISA and bioactivity assays

For ELISA assays, Maxisorp 96-well flat bottom plates (ThermoFisher) were coated with recombinant CD45RO at 0.2µg/mL in PBS (Corning) overnight at 4C. Subsequent washes were performed with PBST (PBS supplemented with 0.05% v/v Tween-20 (Millipore-Sigma)). Blocking was performed in PBSTA (PBS supplemented with 1% w/v BSA (Sigma Aldrich) and 0.05% v/v Tween-20) overnight. Immunocytokines were diluted to relevant concentrations in PBSTA and detected via an HRP-conjugated anti-mouse IgG secondary diluted 1:3000 (Abcam). 1-Step Ultra TMB-ELISA substrate solution (ThermoFisher) was added to develop for 5 minutes and quenched with 2N sulfuric acid (VWR). Absorbance at 450 nm with reference at 570nm was measured on an Infinite M200 microplate reader (Tecan).

For IL-15 bioactivity, 10,000 CTLL-2 cells were seeded in a 96-well U-bottom plate in incomplete media per manufacturer's instructions with stated IL-15 immunocytokine dilutions for 48hrs at 37C. Proliferation was measured via CellTiter-Glo 2.0 Assay (Promega) following manufacturer's instructions. Luminescence was measured on a microplate reader (Tecan) with an integration time of 0.25 seconds. IL-12 bioactivity was

measured with HEK-Blue IL-12 reporter cells according to manufacturer's instructions (Invivogen).

Primary CD8$^+$ T cell preparation

Spleens from 6-8 week old C57BL/6J female mice were harvested and processed into single-cell suspensions. CD8$^+$ T cells were isolated using the EasySep Mouse CD8$^+$ T cell isolation kit (StemCell Technologies) and resuspended at a concentration of 10^6 cells/mL in complete RPMI supplemented with 1X sodium pyruvate (ThermoFisher), 1X non-essential amino acids (ThermoFisher), and 1X beta-mercaptoethanol (ThermoFisher). Media was additionally supplemented with 10 ng/mL murine IL-2 (BioLegend) prior to resuspension and subsequent passaging. Isolated CD8+ T cells were activated for 48 hours on 6-well non-tissue culture (non-TC) treated plate that was precoated with 0.5 µg/mL anti-CD3 (BioXCell, Clone 2C11) and 5 µg/mL anti-CD28 (BioXCell, Clone 37.51) overnight at 4C. The plate was washed twice prior to activation. Following activation, T cells were cultured for 48 hours before use in downstream experiments.

Fluorescence-quenching internalization assay

Internalization assays were performed and analyzed as described previously(*98*). Briefly, immunocytokines were conjugated with AlexaFluor 488 (AF488) using NHS ester chemistry (Invitrogen). Free dye was removed by Zeba spin desalting column purification (ThermoFisher). 100,000 primary CD8 T cells were seeded in 96-well plate and incubated with AF488-labeled immunocytokines at 10 µg/mL staggered at desired time points. Wells were then split such that one set was incubated with 25 µg/mL anti-AF488 quenching antibody (ThermoFisher, A-11094) for 25 minutes. For human CD8$^+$ T cell internalization assay, anti-human CD45 (clone: MEM-28) conjugated to AF488 (ThermoFisher) was used. Human CD8+ T cells were purchased from StemCell Technologies. Viability was

assessed via DAPI staining. AF488 signal was measured using a BD LSR Fortessa and data were analyzed in Flowjo.

Analysis of STAT phosphorylation by flow cytometry

For *in vitro* STAT5 experiments, primary $CD8^+$ T cells cultured as described above were starved of IL-2 for 24 hours and seeded into 96-well plates at 100k cells/well. IL-15 immunocytokines were added at 10 µg/mL for 1 hour and subsequently washed with incomplete T cell media (no IL-2) twice prior to resting for 24 hours. IgG-IL15 added at the same molar concentration (without washing) was used as a continuous control. Cells were immediately fixed in media with equal volumes of BD Phosflow Fixation Buffer I at 37C for 10 minutes. When required, cells were stained with Zombie Aqua viability stain for 5 minutes in PBS (1:1000 dilution) prior to fixation. Cells were permeabilized for 30 minutes on ice with BD Phosflow Perm Buffer III that had been pre-chilled to -20C. Staining with anti-pSTAT5 antibodies (clone 47, BD) conjugated to AF647 or PE was carried out at room temperature for 1 hour. STAT4 experiments were performed identically, but used complete media supplemented with IL-2 and immunocytokine incubation was performed at 2 µg/mL for 20 minutes. pSTAT4 signal was detected with anti-pSTAT4 (clone 38, BD). For trans-signaling experiments, immunocytokines were conjugated with AF647 using NHS-ester chemistry. Preloaded cells were labeled with CFSE per manufacturer's instructions.

Measurement of STAT5 levels *in vivo* was carried out as previously described(*99*). Briefly, TDLN were processed into single cell suspensions directly in BD Fixation Buffer I and samples were incubated at 37C for 10 minutes. Downstream permeabilization and staining was performed as described above. In all cases, pSTAT signal was measured using a BD LSR Fortessa and data were analyzed in Flowjo.

Tumor inoculation and treatment preparation

For all single-tumor experiments, mice aged 6-8 weeks old were injected subcutaneously in the shaved right flank with 1M tumor cells (MC38, MC38-ZsGreen, or B16F10) in a

volume of 50 µL PBS. For two-tumor experiments, the contralateral tumor was inoculated on the left flank 3 days after the primary tumor, as stated in study schematics. Prior to treatment, mice were randomized to ensure equal mean initial tumor size across groups. Immunocytokines were prepared at their stated doses (1µg for IL-12 immunocytokines, 10µg for IL-15 immunocytokines, where the mass indicated is the mass of the entire fusion protein) and dosed intratumorally in 20 µL PBS unless otherwise stated. Doses were informed by our biodistribution experiments as well as previous intratumoral cytokine work from our lab(*17*). Peritumoral administration was performed in 50 µL PBS injected s.c. at the tail-base. Intraperitoneal administration was performed in 100 µL PBS. Tumor area was calculated as the product of tumor length and width. For single-tumor studies, mice were euthanized when tumor area exceeded 100 mm^2; for two-tumor studies, mice were euthanized when cumulative tumor area exceeded 200 mm^2. Immune memory rechallenge experiments were carried out 100 days after initial challenge with 10^5 tumor cells on the left flank. Age-matched naïve mice were used as controls for these studies. For the lung metastasis model used in Extended Data Fig. 6, 0.2M B16F10 cells in 100 µL PBS were inoculated retro-orbitally on the same day as the standard 1M tumor cell flank inoculation.

Tissue processing for flow cytometry

B16F10 or MC38 tumors were harvested, weighed, and subsequently minced using dissection scissors in gentleMACS mouse tumor dissociation buffer (Miltenyi) prepared per manufacturer's instructions. As noted in the Miltenyi protocol, Enzyme R was reduced to 20% of the stated amount to preserve surface epitope integrity. Minced tumors were processed on a gentleMACS Octo-dissociator with heaters (Miltenyi) using program mTDK_1 for B16F10 and mTDK_2 for MC38. Dissociated tumors were then filtered through a 70-micron strainer and 25 mg tumor was plated for downstream staining. TDLN were harvested, weighed, and subsequently dissociated and filtered through a 5 mL round-bottom tube with cell-strainer cap (Falcon) using the blunt rubber end of a 1mL syringe plunger (Falcon). 5 mg of TDLN was used for downstream staining. Blood was collected by sub-mandibular bleeding into MiniCollect K2-EDTA tubes (Greiner) and red

blood cells were lysed using ACK Lysis Buffer (Gibco). When intracellular cytokine staining (ICS) was performed, as in Fig. 5, samples were resuspended and plated in complete RPMI supplemented with 1X sodium pyruvate (ThermoFisher), 1X non-essential amino acids (ThermoFisher), 1X beta-mercaptoethanol (ThermoFisher), and 1X brefeldin A (BioLegend) and allowed to incubate at 37C for 3 hours prior to staining. Precision counting beads (50uL, BioLegend) were added after initial resuspension and used for downstream data analysis. Viability was assessed with Zombie UV or Zombie NIR dyes (BioLegend, 1:1000) in PBS for 20 minutes at room temperature. Subsequent washes and surface staining was performed in PBS supplemented with 1% bovine serum albumin and 2mM EDTA (ThermoFisher). Samples were resuspended in Mouse Fc block Plus (BioLegend) prior to surface staining for 15 minutes. Antibodies against surface targets used as following: CD3 (17A3, BD, 1:100), CD4 (GK1.5, BD, 1:100), CD8 (53-6.7, BD, 1:200), CD19 (6D5, BioLegend, 1:100), CD24 (M1/69, BioLegend, 1:100), CD25 (PC61, BioLegend, 1:100), CD44 (IM7, BD, 1:100), CD45.2 (BD, clone: 104, 1:100), NK1.1 (PK136, BioLegend, 1:100), MHCII (M5/114.15.2, BioLegend, 1:100), Ly6C (HK1.4, BioLegend, 1:100), F4/80 (BM8, BioLegend, 1:100), PD1 (29F.1A12, BioLegend, 1:100), TIM3 (RMT3-23, BioLegend, 1:100). P15E tetramer (MBL) staining was performed in the presence of 50 nM dasatinib at a 1:75 dilution and anti-CD8 antibody clone KT15 (ThermoFisher) was used to minimize background signal. Dasatinib incubation was not included in the staining mixture for the RNAseq experiment. When performing intracellular staining, cells were fixed and permeabilized using the Foxp3 transcription buffer set (eBioscience). Samples against intracellular antigens used as following: TCF1 (C63D9, Cell Signaling Technologies, 1:250), IFNg (XMG1.2, BioLegend, 1:200), Granzyme B (QA16A02, BioLegend, 1:200). Intracellular staining was performed overnight at 4C. Cells were collected using a BD FACSymphony A3 and data were analyzed in FlowJo.

Biodistribution serum measurements

IL-15 immunocytokines were labeled with AF647 using NHS-ester chemistry per the manufacturer's instructions. Free dye was removed with Zeba desalting columns. Molar

amounts of dye for each immunocytokine were matched prior to dosing. Serum concentrations were calculated based on a standard curve prepared using known amounts of serially diluted AF647-labeled immunocytokine.

Immunofluorescence Staining

Inguinal LNs and tumors were harvested 24 h post injection as described in Fig. 2a, embedded in O.C.T. buffer (Fischer Scientific) and fresh frozen. 10 µm tissue sections were then post-fixed with 4% paraformaldehyde for 10 minutes, followed by three washes with PBS. Sections were incubated with Fc receptor blocker (Innovex) for 30 minutes and blocked for 1 hour with 5% goat serum, 2.5% BSA in PBS. Staining with primary antibodies was performed overnight at 4°C in blocking buffer (LN: IgD (Biolegend, 405705), and CD8 (Abcam, ab217344). Tumors: CD8, and F4/80 (Abcam, ab105156)). After 3 washes with PBS, the sections were incubated with fluorochrome-conjugated secondary antibody (ThermoFisher, 35551) in blocking buffer for 30 minutes at room temperature. After three washes with PBS, the sections were mounted onto glass slides using mounting media (ProLong Diamond Antifade Mountant, Thermo Fisher Scientific). High magnification images were acquired using a Leica SP8 laser-scanning confocal microscope equipped with a white light laser, a 405 solid state laser line, and selective emission filters. Images were collected using a 25x water immersion lens and a 63x oil immersion lens.

Chapter 3 : Efficacy and mechanism of action of locally delivered CD45-targeted cytokine therapy

Parts of this chapter appear as described in Santollani et al., *bioRxiv* (2024).

Introduction

In the previous chapter, we developed CD45-targeted immunocytokines and optimized a treatment regimen, called αCD45-Cyt therapy, which uses a single low dose of αCD45-IL12 followed a few days later by a higher dose of αCD45-IL15. In this chapter, we focus on applying this therapy across a variety of tumor models, including models to test the abscopal effects of this localized therapy. While previous local immunotherapy approaches have elicited profound regressions of directly treated lesions, they typically elicit modest responses at distal untreated sites, often requiring an additional systemically administered agent such as checkpoint blockade immunotherapy (CBI) to drive abscopal effects. Limited abscopal responses are consistent with the findings of many other groups employing diverse therapeutic approaches in both preclinical models and early-stage clinical trials(*51*, *92*). Collectively, these data raise the question of whether localized immunotherapies are capable of eliciting robust systemic responses against metastatic disease.

Here, we characterize the response and mechanism of action of αCD45-Cyt therapy to show that CD45-targeted immunocytokines are retained on the cell-surface and trigger enhanced and prolonged signaling relative to their native cytokine counterparts. Leveraging this altered biology, we found that a single dose of CD45-targeted IL-12 concentrated in the tumor followed by a single dose of CD45-targeted IL-15 accumulated in both tumor and the tumor-draining lymph node dramatically altered T cell programming in the TDLN. When compared to untargeted control IgG-Cyt therapy, αCD45-Cyt therapy elicited complete responses in a majority of B16F10 tumors. Antibody depletion and knock-out mice revealed a CD8 and *batf3* dependency indicative of *de novo* priming. We also characterize various routes of administration – intratumoral, peritumoral,

intraperitoneal – to demonstrate that intratumoral delivery of these anchored cytokines exclusively unlocks their efficacy. We then move to test αCD45-Cytokine therapy in more challenging settings that probe its ability to elicit systemic immunity beyond curing a single tumor. In two-tumor flank models as well as i.v.-seeded metastatic B16F10 models, αCD45-Cyt therapy demonstrates systemic anti-tumor responses. Finally, we probe the phenotypic effect on tumor-specific CD8+ T cells through paired RNAseq and flow cytometry studies. αCD45-Cyt therapy expanded tumor-specific $CD8^+$ T cells with potent effector phenotypes displaying a transcriptional signature mirroring effective responses to acute viral infection, while maintaining a pool of stem-like T cells. Dissemination of this potent effector T cell pool led to strong systemic anti-tumor immunity characterized by complete responses in both treated and untreated tumors.

Results

αCD45-Cyt therapy eradicates single tumors

We evaluated the impact of this altered signaling and biodistribution on the therapeutic potential of a cytokine therapy employing both αCD45-IL15 and αCD45-IL12. We first treated established tumors 30-35 mm^2 in size with a single i.t. injection of 1 μg αCD45-IL12 followed by one injection of 10 μg αCD45-IL15 several days later. Our rationale for this sequencing was to use the IL-12 immunocytokine to inflame the tumor and promote an initial wave of tumor immunogenic cell death and tumor antigen release by pre-existing or newly recruited TILs(*57*), followed by amplification of newly primed tumor-specific T cells in the TDLN by the IL-15 immunocytokine several days later(*76*, *77*). The selected doses were informed by findings from the biodistribution experiments and aimed to retain IL-12 at the tumor but deliver IL-15 to both the tumor and TDLN. On a cytokine mass basis, these doses did not surpass 2 μg of total cytokine. Hereafter, we refer to this sequential αCD45-IL12/αCD45-IL15 regimen as αCD45-Cyt; the untargeted cytokine control therapy consisting of IgG-IL12 followed by IgG-IL15 is referred to as IgG-Cyt.

We tested this therapeutic regimen in the B16F10, an aggressive and poorly ICB responsive syngeneic melanoma model (**Fig. 3.1A**). Injection of control IgG-Cyt elicited an extension in survival, but no animals were long-term survivors (**Fig 3.1A-B**). By contrast, >90% of tumors treated with αCD45-Cyt therapy were rejected, and animals exhibited no signs of cytokine toxicity, as assessed via weight loss (**Fig 3.1C**). Mice cured B16F10 tumors by αCD45-Cyt therapy displayed robust immune memory upon secondary tumor rechallenge (**Fig 3.1D**).

We performed a variety of mechanistic studies to isolate the importance of each part contributing to the efficacy of αCD45-Cyt therapy. Potential modulation of the immune response by CD45 engagement did not contribute to efficacy, as treatment with αCD45 in the absence of cytokines provided no tumor control (**Fig 3.2A**). We assessed the mechanism of tumor rejection by αCD45-Cyt therapy through antibody depletions and

knockout mice: αCD45-Cyt therapy entirely depended on $CD8^+$ T cells and *batf3*$^+$ dendritic cells, consistent with a critical role for tumor antigen cross-presentation (**Fig. 3.2B**). NK cells, neutrophils, and macrophages were each dispensable for anti-tumor efficacy (**Fig. 3.2B**). Use of both cytokines in the treatment was required, as αCD45-IL15 or αCD45-IL12 monotherapy using the same treatment schedule elicited no long-term survivors (**Fig 3.2C**).

To study the importance of cytokine localization to the tumor and TDLN, we varied the route of administration of αCD45-Cyt therapy. Dosing the same αCD45-Cyt treatment paradigm systemically (i.p.) led to a complete loss of efficacy, confirming the importance of intratumoral exposure and efficient TDLN drainage for activity (**Fig. 3.3A-C**). Next, to determine the relevant contributions to efficacy from tumor vs TDLN leukocytes, we administered αCD45-Cyt therapy peritumorally, which predominantly acts on the TDLN while sparing the tumor (**Fig 2.9F**). While dosing both cytokines peritumorally completely ablated efficacy, we found that intratumoral αCD45-IL12 followed by peritumorally delivered αCD45-IL15 displayed comparable early tumor control to the full intratumoral paradigm (**Fig. 3.4A**). However, a majority of these mice (3/5) eventually succumbed to tumor burden, suggesting that optimal long-term tumor control and rejection required both doses to be administered intratumorally (**Fig 3.4B**).

αCD45-Cyt therapy elicits a systemic response

The successful translation of intratumorally administered immunotherapies will depend on their ability to drive a systemic anti-tumor immune response that can eliminate lesions that are not directly treated. To evaluate abscopal immune responses elicited by this localized therapy, MC38 tumors were inoculated on opposite flanks of mice followed by treatment of only the right-flank tumor with αCD45-Cyt therapy. Strikingly, this led to 90% of mice rejecting both the treated and untreated tumors and becoming long-term survivors, while only 20% of animals receiving IgG-Cyt therapy eliminated both tumors (**Fig. 3.5A-B**). These results were obtained despite the fact that tracking of fluorescently-

labeled constructs showed that locally delivered IgG-Cyt readily diffused out of the treated lesion and accumulated in the distal site, while no statistically significant accumulation of αCD45-Cyt was measured at the untreated tumor (**Fig. 3.5C**). To determine whether regression of distal tumors relied on lymphocyte trafficking, we tested αCD45-Cyt in the same two-tumor MC38 model but in the presence of FTY720 to block lymphocyte exit from lymphoid tissue (**Fig. 3.5D**). The addition of FTY720 ablated the ability of αCD45-Cyt to control the untreated left-flank tumor and led to no long-term survivors, suggesting that rejection of untreated lesions is driven by lymphocyte migration (**Fig. 3.5E-F**). αCD45-Cyt therapy still triggered regression of the treated tumor in the presence of FTY720, but no tumors had been cured at the time of euthanasia due to outgrowth of the untreated distal lesion (**Fig 3.5G**). To further stress test this treatment, we tested abscopal responses in the aggressive B16F10 model. While IgG-Cyt treatment led to some delay of treated tumors, all untreated tumors progressed (**Fig 3.6A-C**). By contrast αCD45-Cyt therapy led to primary tumor regression in all mice and only 2 of 5 untreated tumors escaped (**Fig 3.6A-C**). Finally, to assess the ability of αCD45-Cyt therapy to eliminate metastases, we treated mice that had been injected with 0.2M B16F10 cells intravenously in addition to flank tumor inoculation, giving rise to lung metastases. Once untreated mice had reached euthanasia criteria due to flank tumor outgrowth (day 15), we analyzed lung metastasis control across groups. In line with our previous experiments, regression of the treated primary tumor was in progress for αCD45-Cyt therapy at this time point (**Fig 3.7A**). We also found significant control of lung metastases by αCD45-Cyt therapy, as measured by a dramatic reduction in total metastatic tumor burden and average metastasis size (**Figure 3.7B-D**). Altogether, we find that αCD45-Cyt therapy is able to prime a robust systemic immune response after localized treatment that is able to control both treated and distal untreated lesions.

αCD45-Cyt therapy triggers an acute anti-viral gene signature in responding TDLNs

We next sought to understand how localized αCD45-Cyt treatment elicited such potent systemic immunity, focusing on the $CD8^+$ T cells required for efficacy. Recent reports

demonstrating the spatial segregation of T cell priming and activation between the TDLN and tumor(*100*), respectively, motivated us to profile the TDLN CD8$^+$ phenotypes after treatment. To assess effects of αCD45-Cyt therapy on tumor-specific T cells, we treated B16F10 tumors with αCD45-Cyt or IgG-Cyt therapy, and 1 day after dosing of the IL-15 immunocytokine, sorted CD8$^+$ T cells specific for the immunodominant p15E endogenous retroviral antigen expressed by B16F10 tumors(*101*) via peptide-MHC tetramer staining for downstream RNA sequencing (RNA-seq). αCD45-Cyt therapy dramatically reprogrammed the CD8$^+$ T cell response, leading to significant upregulation of 1726 genes and downregulation of 1279 genes in comparison to the untreated condition (Fig. 4a). Many upregulated genes were associated with effector function (*IL2ra, Gzmb, Klrg1, Prf1*) as well as interferon signaling (*Ifng*, *Ifngr1*, *Ifitm1*), suggesting an ability of αCD45-Cyt therapy to promote activation and effector differentiation of T cells within the TDLN (**Fig. 3.8A**). Concurrently, genes related to lymph node trafficking (*Cxcr3, Cxcr5*) as well as stemness (*Tcf7*) were downregulated (**Fig. 3.8A**).

Recent reports have demonstrated that, unlike the endogenous anti-tumor response, effective virus-specific T cell responses, such as following acute lymphocytic choriomeningitis virus Armstrong (LCMV Arm) infection, are accompanied by high expression of inflammatory cytokines and differentiation markers in responding lymph nodes(*100*). We thus performed gene set enrichment analysis (GSEA) to probe whether αCD45-Cyt therapy induces an anti “viral-like” signature within the tumor-reactive TDLN CD8$^+$ compartment. We compared the untreated and αCD45-Cyt treated transcriptomes of tumor-specific CD8$^+$ T cells for enrichment of a previously reported tumor (“TDLN”) or acute viral (“LCMV Arm”) transcriptional response (**Fig. 3.8B**). Transcriptional profiles of CD8$^+$ T cells from untreated TDLNs closely matched the previously reported endogenous anti-tumor response, broadly characterized by a lack of effector molecules and activation markers (**Fig 3.8B, 3.9A**). In contrast, αCD45-Cyt therapy elicited a signature highly enriched for the canonical anti-viral response, suggesting that the prolonged cytokine exposure within TDLNs induced by αCD45-Cyt triggers an immune response mirroring effective anti-viral T cell priming (**Fig 3.8B, 3.9A**). We next characterized differences in

the transcriptional response of αCD45-Cyt treatment vs. control IgG-Cyt therapy. Principal-component analysis (PCA) showed that IgG-Cyt and αCD45-Cyt transcriptomes clustered separately (**Fig. 3.8C**). Pathway analysis comparing the two treatment conditions revealed a striking upregulation of hallmark STAT5 signaling triggered by αCD45-Cyt therapy, likely driven by the extended signaling of CD45-bound IL-15, as shown in Fig. 1e (**Fig. 3.8D**). Other upregulated genes belonged to pathways involving inflammatory responses, cytokine signaling, and cell-cycle metabolism (**Fig. 3.8D**). Finally, we examined the top 20 differentially expressed genes (DEGs) between αCD45-Cyt and IgG-Cyt therapy and found *Ifng* expression as the most differentially upregulated, along with other metabolism and inflammation genes (**Fig. 3.8E, 3.9B**). Altogether, these data are indicative of a highly activated and proliferative TDLN compartment following αCD45-Cyt therapy.

αCD45-Cyt generates optimal effectors

Recently, genetically-induced sustained STAT5 activation has been shown to rewire exhausted T cells into a unique effector profile that enables control of chronic infection or tumors(*102*). Based on our pathway analysis and *in vitro* data, we hypothesized that αCD45-IL15 stimulation may therapeutically elicit similar sustained STAT5 induction and downstream generation of tumor-specific effectors, which could then traffic to distal lesions and promote tumor rejection. Probing the signaling dynamics of CD45 immunocytokines in the TDLN 24 hours after intratumoral dosing with αCD45-IL15 alone revealed robust STAT5 phosphorylation induced in 80% of $CD8^+$ T cells in the TDLN (**Fig. 3.10A-B**). By contrast, injection of IgG-IL15 led to a dim $pSTAT5^+$ population, closely mirroring the *in vitro* and RNA-seq results shown in Figs. 1e and 4d (**Fig. 3.10A-B**).

Next, using an identical experimental set-up to that used in the RNA-seq analysis, we treated B16F10 tumors with αCD45-Cyt or IgG-Cyt therapy and profiled $p15E^+CD8^+$ T cells in the tumor and TDLN 24 hours after IL15 dosing by flow cytometry. Only αCD45-Cyt treatment led to a statistically significant expansion of tetramer positive $CD8^+$ T cells

in the TDLN relative to untreated tumors (**Fig. 3.11A-B**). In agreement with the RNA-seq results, in addition to expanded numbers, TDLN tumor-specific cells primed by αCD45-Cyt exhibited a profound increase in IFNγ expression as measured by MFI and the number of IFNγ^{+}p15E^{+} cells (**Fig. 3.11C-E**). IgG-Cyt therapy was unable to elicit IFNγ production within the TDLN (**Fig. 3.11C-E**). Tumor-reactive cells in the TDLN additionally displayed high levels of Granzyme B expression after treatment with either cytokine therapy (**Fig. 3.11F**). Both cytokine therapies also significantly increased CD25 expression over untreated control, but αCD45-Cyt treatment induced this upregulation on a larger fraction of the CD8^{+} compartment (**Fig. 3.11G**).

Recent studies have suggested that antigen-specific TCF1^{+} stem-like T cells in disease-site-draining lymph nodes (in models of tumors, chronic infections, or autoimmune disease) play a critical role as a source of effector cell generation(*100*, *102–107*). Given the robust effector response exhibited in treated TDLNs, we evaluated the impact of αCD45-Cyt therapy on the magnitude of the stem-like (T_{SL}, TCF1^{+}TIM3^{-}) compartment. Though both cytokine therapies led to the expected drop in the relative proportion of TCF1^{+} T cells, the absolute number of tumor-specific stem-like cells expressing PD1^{+} and TCF1^{+} increased, with αCD45-Cyt therapy eliciting a 6-fold higher count of stem-like cells in the TDLN over untreated mice (**Fig. 3.12A-B**). Conversely, cytokine therapy skewed CD8^{+} T cells towards a terminally differentiated (TD, TCF1^{-}TIM3^{+}) phenotype as seen by high TIM3 expression in both treatment groups (**Fig. 3.12C**). However, αCD45-Cyt therapy triggered a significantly larger expansion of the TD compartment by absolute count over IgG-Cyt therapy (**Fig 3.12D**).

Analysis of intratumoral p15E^{+}CD8^{+} T cells revealed similar patterns as in the TDLN. αCD45-Cyt therapy led to increased numbers of tumor-reactive CD8^{+} T cells not seen after IgG-Cyt therapy (**Fig. 3.13A**). Phenotypic profiling once again highlighted the unique ability of αCD45-Cyt, but not IgG-Cyt, therapy to induce significantly higher levels of IFNγ within p15E-specific cells (**Fig. 3.13B-C**). This led to significantly higher numbers of intratumoral IFNγ^{+}CD8^{+}cells (**Fig. 3.13B-C**). Mice treated with αCD45-Cyt also displayed

higher levels of CD25 expression, both by percentage and magnitude (**Fig 3.13D-E**). Finally, intratumoral Granzyme B expression was high across all groups, but only αCD45-Cyt therapy was able to generate a significant increase in the compartment size (**Fig 3.13F-G**). Taken together, these immunophenotyping results show that local αCD45-Cyt therapy is not only able to dramatically alter the treated TME, as other local therapies have accomplished, but also reprogram the tumor-specific $CD8^+$ population in the TDLN, correlating with stronger abscopal responses.

Discussion

Antibody-targeted cytokines have been pursued for many years with modest impact, driven in part by the focus on targeting cancer cells lacking truly disease-specific antigens and the problem that their biodistribution is often governed by the cognate cytokine receptor and not the antibody target(*1*, *33*). Recent approaches, focusing on targeting immune cells through lineage markers or phenotype have shown promising preclinical data(*43*, *47*). A report of a PD-1 targeted IL-2 immunocytokine demonstrated unique internalization and signaling behavior relative to the parental cytokine, highlighting the potential of multi-receptor targeting to elicit novel cell signaling biology(*43*). Here we focused on targeting host immune cells, using the unique biology of CD45 to develop αCD45-cytokine fusions capable of modulating tumor-specific T cells within the TME and TDLN. We leveraged CD45 as a unique cell-based "anchor" for cytokines in two key ways: 1) its ability to be bound without triggering internalization, and 2) its abundant expression on the immune cell surface, with reported measurements upwards of 100,000 molecules per cell(*108*). We find evidence that these two characteristics allow for both *cis* and *trans* signaling of CD45-tethered cytokines, as shown by the ability of CD8 T cells preloaded with αCD45-IL15 to efficiently signal to multiple unloaded, bystander cells. Thus, by decorating leukocytes *in vivo* with CD45-targeted immunocytokines, bystander cells lacking the cognate receptor can serve as cellular depots that "present" the cytokine to nearby cells, extending the cytokine's residence time. We show that specified intratumoral doses of CD45-targeted IL-15 and IL-12 are retained at the tumor and TDLN for prolonged periods of time, leading to extended pSTAT5 signaling and acquisition of a potent effector program by tumor-reactive $CD8^+$ T cells. When we applied this strategy in a therapeutic context, this led to a reprogramming of the anti-tumor $CD8^+$ T cell response at the TDLN and robust systemic anti-tumor immunity. On a cytokine basis, the doses given in the αCD45-Cyt paradigm did not exceed 2 μg, a highly dose-sparing regimen highlighting the benefit of administration at the right time and place.

Recent studies have suggested the endogenous cancer response is a two-step priming and activation process that is confined to TDLN and tumors, respectively(*100*). However, treatment with αCD45-Cyt therapy was able to alter this endogenous response and triggered a striking expansion of activated cytotoxic effector cells within the TDLN characterized by high expression of CD25, IFN-γ, granzyme B, and TIM3. In striking contrast to the endogenous unmanipulated anti-tumor response, T cells within the αCD45-Cyt-treated TDLN had transcriptional signature resembling an acute viral response. These changes in T cell activation in the TDLN also have many similarities with effects recently reported for antigen-specific T cells transduced to express constitutively active STAT5 (STAT5CA) in the setting of chronic LCMV infection(*102*). In that case, splenic STAT5CA T cells were found to transition to a polyfunctional effector state, with depletion of the exhausted precursor TCF1$^+$ subset, and persist in the face of chronic infection. Interestingly, prolonged signaling from cell-bound αCD45-IL15 may represent a pharmacologically feasible approach to achieve similar effects in native T cells. Importantly however, αCD45-Cyt therapy does not appear to deplete the tumor-specific stem-like TCF1$^+$PD1$^+$ subset that is thought to be the critical self-renewing precursor to produce effector cells.

The ability to generate these potent effectors at the TDLN, in addition to the tumor, may explain the systemic response primed by αCD45-Cyt therapy. We hypothesize that tumor-reactive CD8$^+$ T cells in TDLNs acted on by αCD45-Cyt therapy migrate into the systemic circulation and disseminate agnostically to distal lesions. In our treatment paradigm, we found evidence for a robust systemic response in two-tumor models of both MC38 colon carcinoma and B16F10 melanoma, as well as in a metastasis model using B16F10 lung metastases in combination with a flank tumor. These abscopal responses were not driven by drug leakage into the contralateral tumor, but were dependent on immune cell trafficking, as FTY720 ablated tumor control at the untreated lesion. These results suggest that nodal cytokine retention following administration can prime potent anti-tumor immunity capable of systemic tumor control.

This approach is uniquely enabled by direct intratumoral administration as a conduit for lymph node exposure. Current interventional radiology and surgery techniques allow access to almost any surface or visceral lesion, bolstering intratumoral immunotherapies in human cancer as a viable approach. Notably, the FDA-approved oncolytic therapy talimogene laherparapvec (TVEC) is administered intratumorally. In addition, intranodal or s.c. peritumoral administration, which we explore in our αCD45-Cyt paradigm, can be considered as alternative administration routes for TDLN exposure. Finally, while we explored some facets of CD45 biology, there are other potential aspects to consider. Differential splicing of human CD45 can correspond to distinct cell states, with shorter CD45 isoforms upregulated upon CD8 T cell activation(*80*, *83*, *84*). A CD45RO specific antibody might therefore enable more targeted delivery of cytokines to activated T cells. In summary, our results highlight CD45 anchoring as a potent modular platform for enhancing the retention and response of immune agonists and provide rationale for further development of CD45 immunocytokines.

Figures

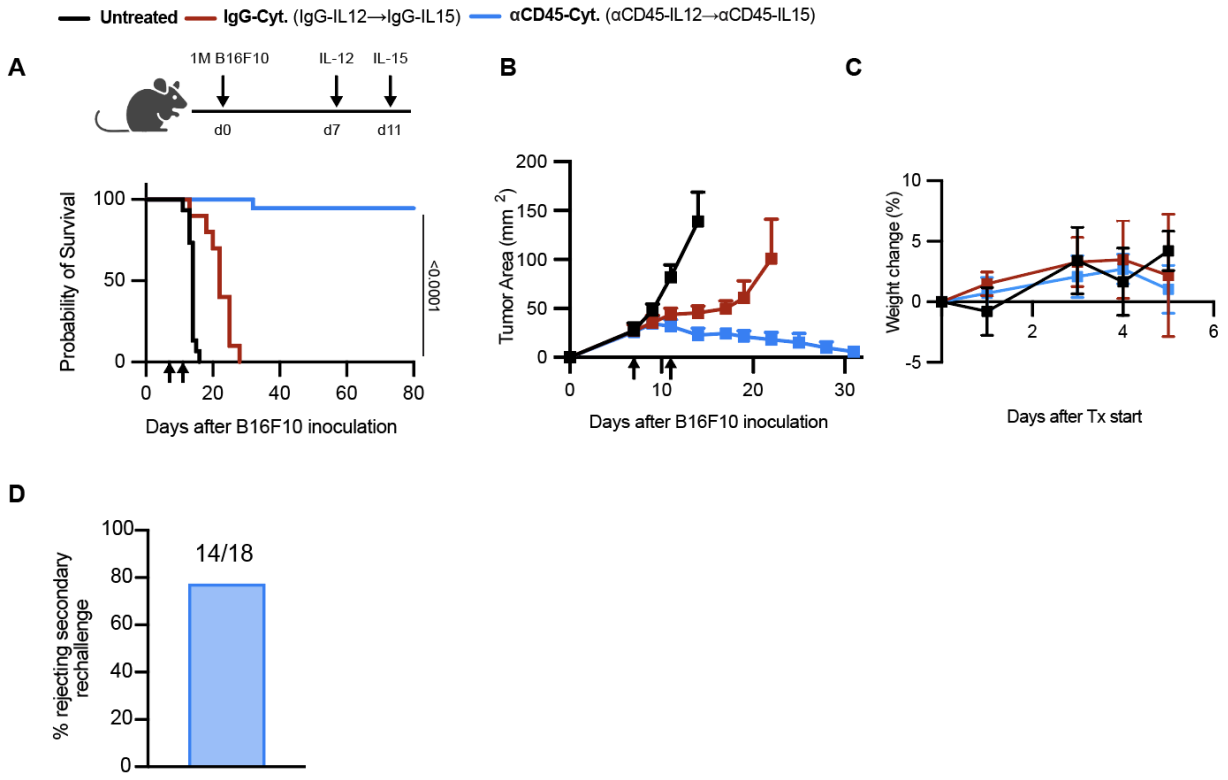

Figure 3.1. αCD45-Cyt therapy is safe and efficacious in B16F10.

A-C, Mice (n = 10-19/group) inoculated with 1M tumor cells and treated with 1 µg of αCD45-IL12 and 10µg of αCD45-IL15 (referred to as αCD45-Cyt) or treated with 1 µg of IgG-IL12 and 10µg of IgG-IL15 (referred to as IgG-Cyt) as shown on the experimental timelines. **A,** Overall survival. Statistical comparison shown between IgG-Cyt and αCD45-Cyt groups. **B,** Grouped tumor growth curves. **C,** Weight change after beginning treatment. **D,** Surviving mice were rechallenged on d100 with 0.1M B16F10 cells on the opposing flank to the primary challenge. P values were determined by log-rank (Mantel-Cox) test. For all plots, arrows indicate treatment.

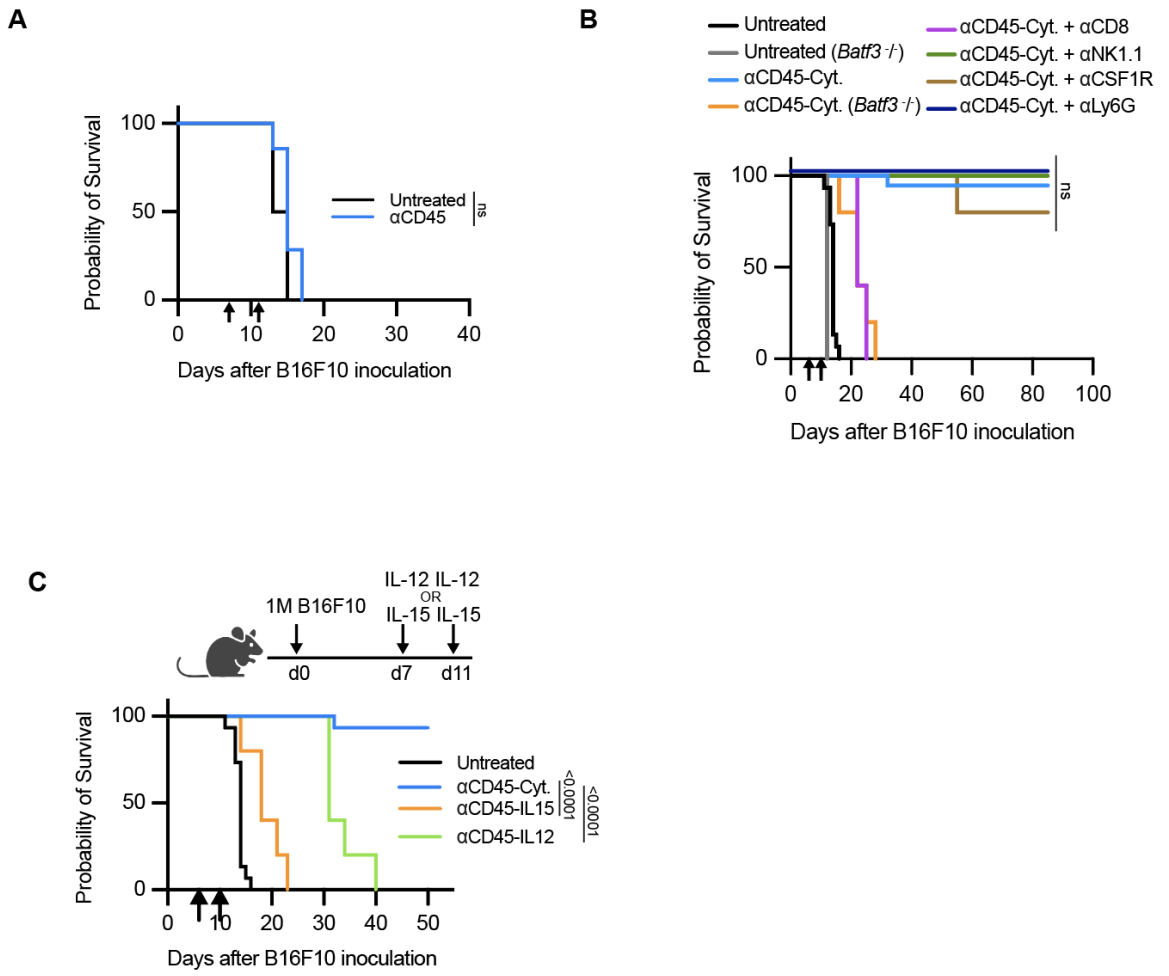

Figure 3.2. αCD45-Cyt efficacy is driven through CD8⁺ and *batf*3⁺ DCs.

A, Overall survival of mice (n = 6 *in PBS cohort, n = 7 in* αCD45 *group*) bearing B16F10 tumors treated with αCD45 (in the absence of cytokine) on an identical regimen and molar matched dose to that described in Fig. 3.2A. **B,** Kaplan Meier survival of mice (n = 5/group) bearing B16F10 tumors treated with αCD45-Cyt therapy in combination with depleting antibodies or performed in knockout mice as shown. **C,** Kaplan Meier survival plot of mice (n = 5/group) inoculated with 1M B16F10 tumor cells and treated with IL-12 immunocytokine monotherapy (1 µg dose) or IL-15 immunocytokine monotherapy (10 µg dose) as shown on the diagram. P values were determined by log-rank (Mantel-Cox) test. For all plots, arrows indicate treatment.

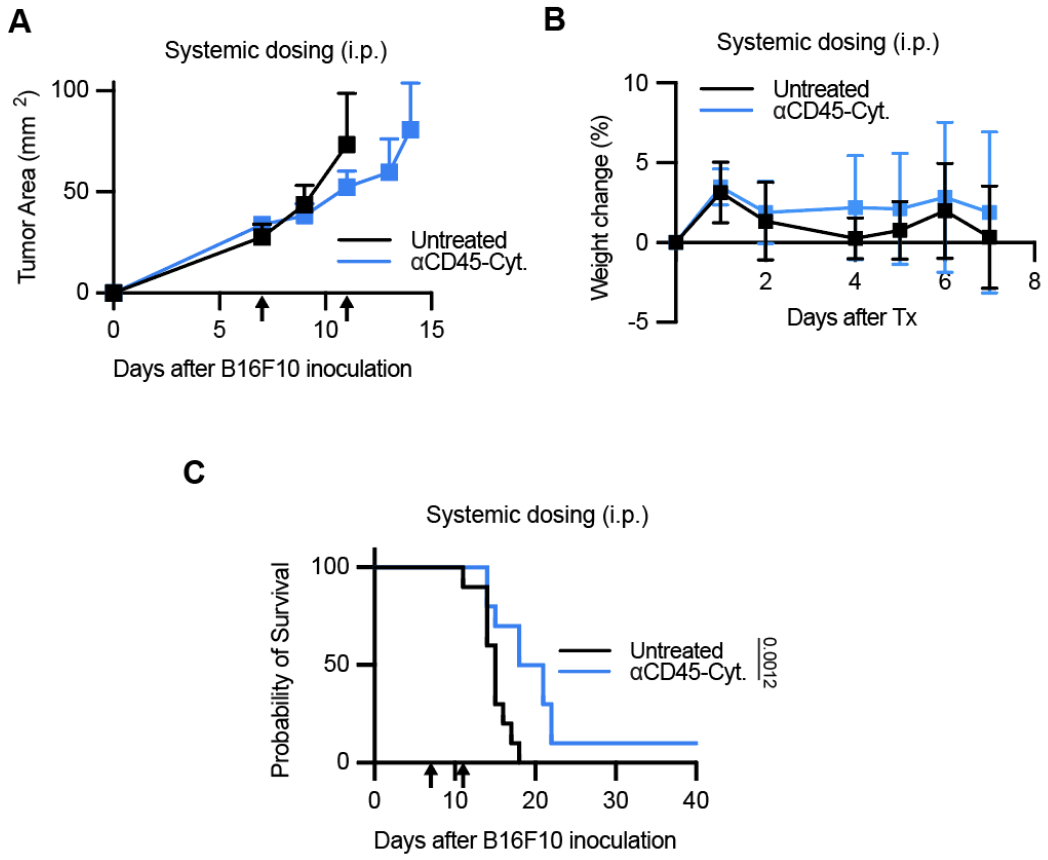

Figure 3.3. Systemic dosing of αCD45-Cyt is not efficacious.

A, Tumor growth curves of mice (n = 5/group representative of 2 independent experiments) inoculated with 1M B16F10 cells and treated systemically (i.p.) with αCD45-Cyt therapy with the same doses and schedule as in Fig. 3.1A. **B**, Weights of mice shown in A. **C**, Overall survival of mice shown in A. P values were determined by log-rank (Mantel-Cox) test. For all plots, arrows indicate treatment.

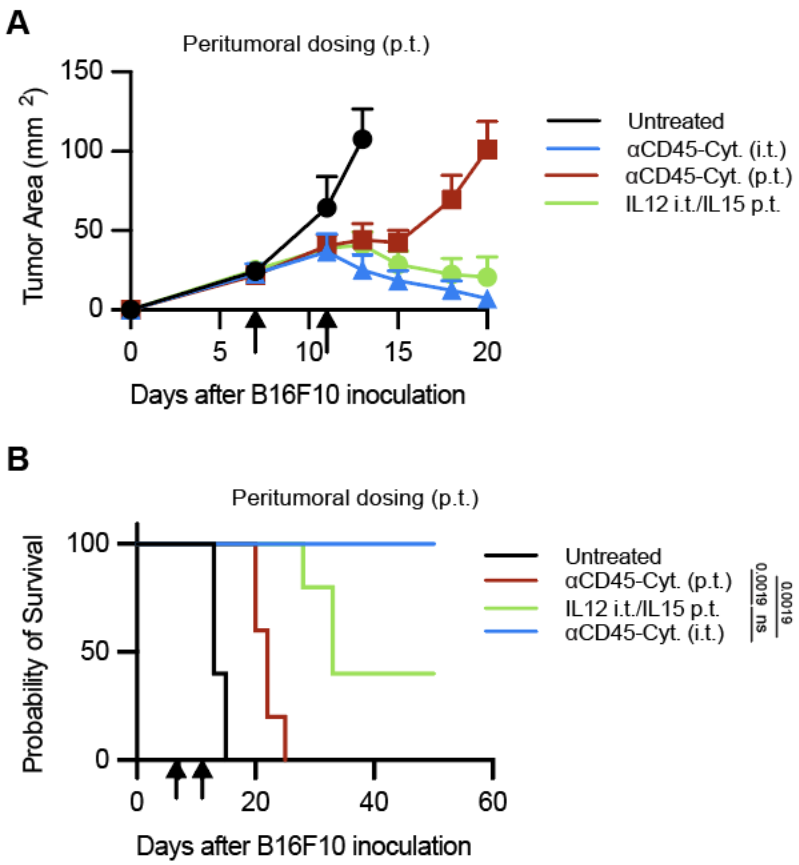

Figure 3.4. Peritumoral delivery of αCD45-Cyt therapy elicits tumor control

A, Tumor growth curves of mice inoculated with 1M B16F10 cells and treated with the full αCD45-Cyt intratumorally, peritumorally, or the IL-12 immunocytokine given intratumorally and the IL-15 immunocytokine given peritumorally, as described in the text. **B**, Overall survival of the mice shown in A. P values were determined by log-rank (Mantel-Cox) test. For all plots, arrows indicate treatment.

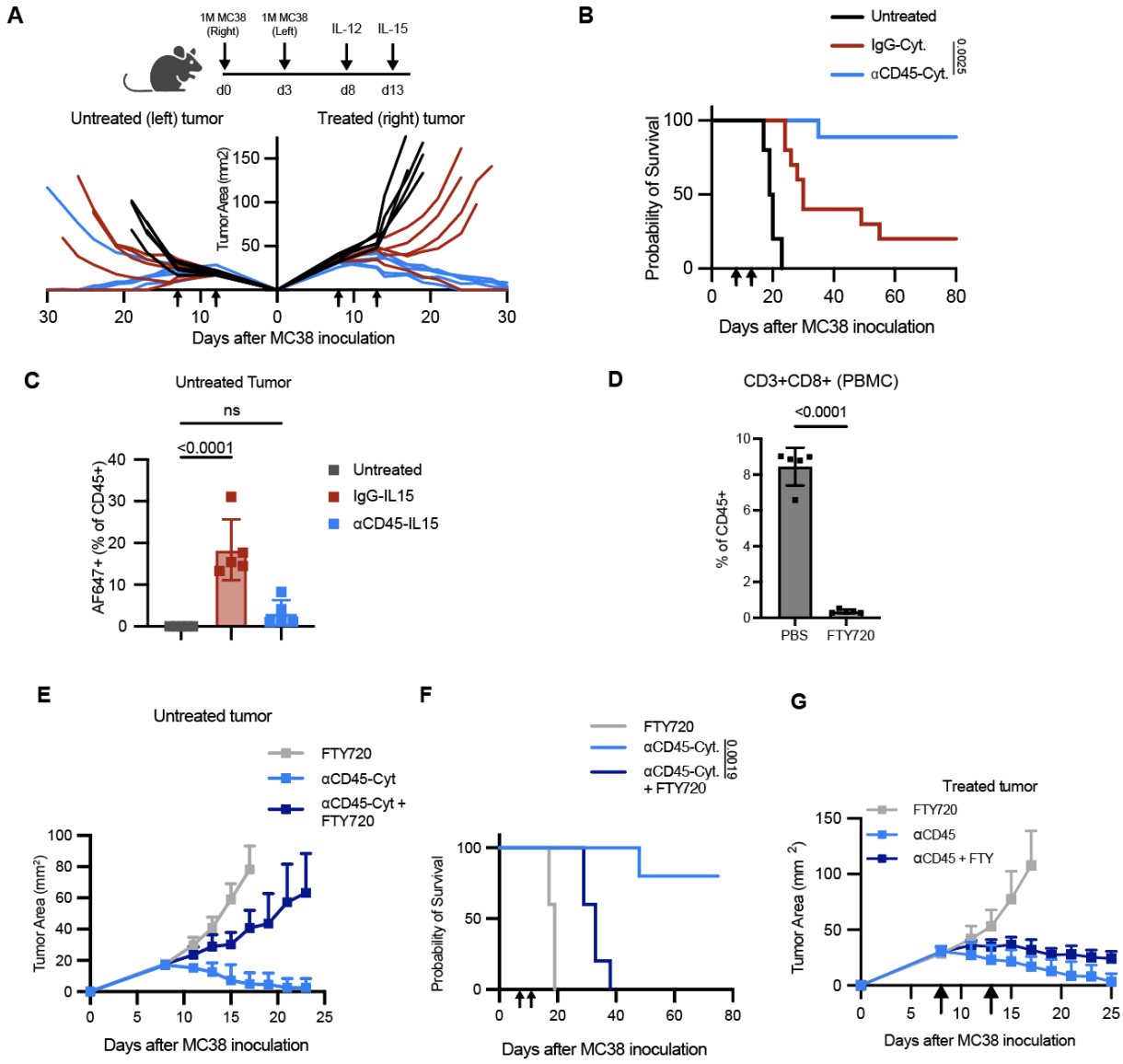
A
1M MC38 (Right)
1M MC38 (Left)
IL-12
IL-15
d0
d3
d8
d13
Untreated (left) tumor
Treated (right) tumor
Tumor Area (mm2)
Days after MC38 inoculation
B
Untreated
IgG-Cyt.
αCD45-Cyt.
0.0025
Probability of Survival
Days after MC38 inoculation
C
Untreated Tumor
ns
<0.0001
AF647+ (% of CD45+)
Untreated
IgG-IL15
αCD45-IL15
D
CD3+CD8+ (PBMC)
<0.0001
% of CD45+
PBS
FTY720
E
Untreated tumor
FTY720
αCD45-Cyt
αCD45-Cyt + FTY720
Tumor Area (mm²)
Days after MC38 inoculation
F
FTY720
αCD45-Cyt.
αCD45-Cyt. + FTY720
0.0019
Probability of Survival
Days after MC38 inoculation
G
Treated tumor
FTY720
αCD45
αCD45 + FTY
Tumor Area (mm 2)
Days after MC38 inoculation

Figure 3.5. αCD45-Cytokine therapy drives abscopal effects in MC38.

Mice bearing MC38 tumors on both flanks were treated with 1μg IL-12 and 10μg of IL-15 in the right tumor only at indicated times (n = 10 in untreated cohort, n = 10 in IgG-Cyt cohort, n = 9 in αCD45-Cyt cohort across 2 independent experiments). Shown are **A,** individual tumor growth curves from one representative experiment. **B,** Kaplan Meier survival from experiment shown in A. **C,** Mice (n = 5/group) were inoculated with bilateral MC38 tumors as described and dosed with 10μg of AF647-labeled IL-15 immunocytokine. Shown are AF647 levels on immune cells at the contralateral tumor 24 hours after administration of IL-15. **D**, Mice (n = 5/group) were dosed i.p. with 1.5mg/kg FTY720. Two days later, PBMCs were collected and shown is the CD8+ T cell frequency. **E-G**, Mice bearing bilateral MC38 tumors were treated with αCD45-Cyt therapy in the presence of FTY720 starting on d5. Shown is **E,** the average tumor growth curve for the untreated tumor, the **F,** overall survival from experiment, and **G,** the average tumor growth curve for the treated tumor. P values were determined by log-rank (Mantel-Cox) test. For all plots, arrows indicate treatment. Shown are mean ± s.d. P values were determined by t-test or one-way ANOVA followed by Tukey's multiple comparison test.

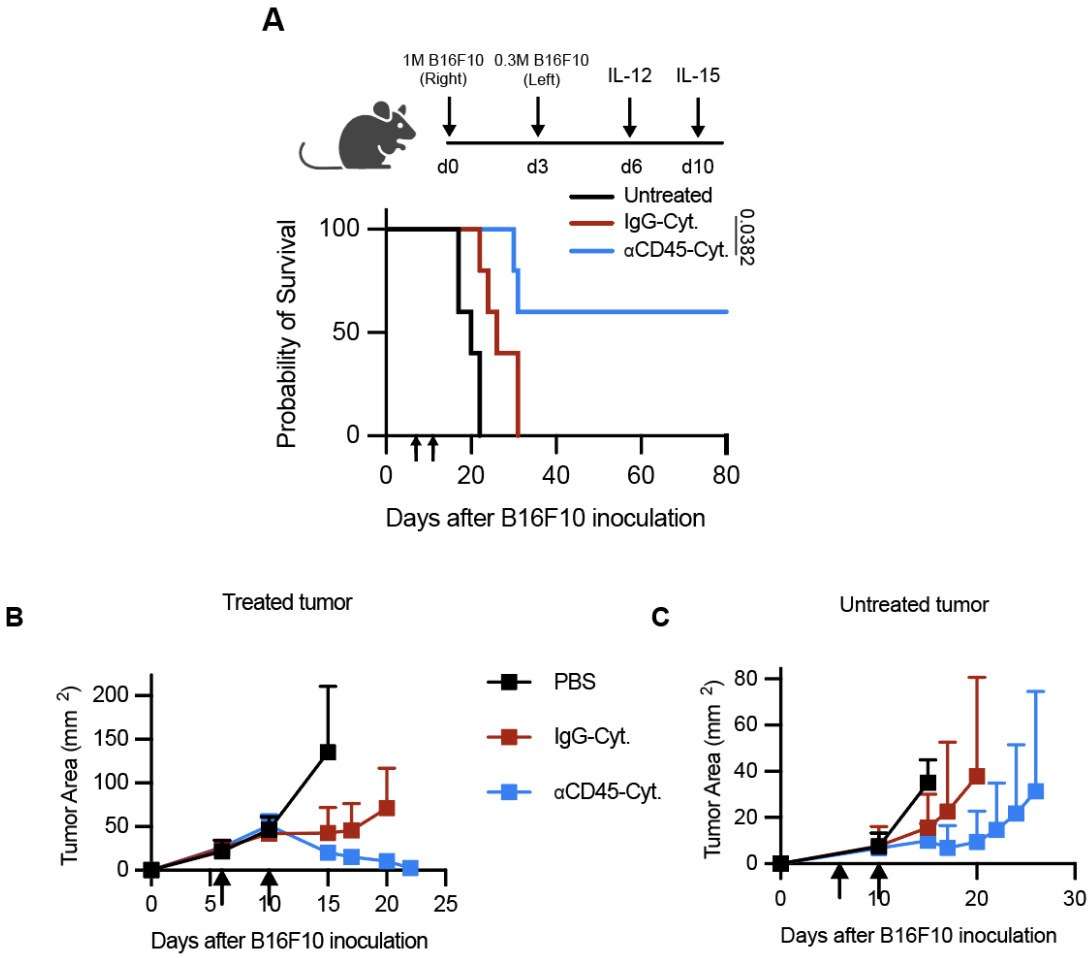

Figure 3.6. αCD45-Cyt therapy drives abscopal effects in B16F10.

Mice bearing bilateral B16F10 tumors (n = 5) were treated with IgG-Cyt or αCD45-Cyt therapy as described. Shown are **A**, overall survival, **B**, tumor growth curves for the treated tumor, and **C**, untreated tumor.

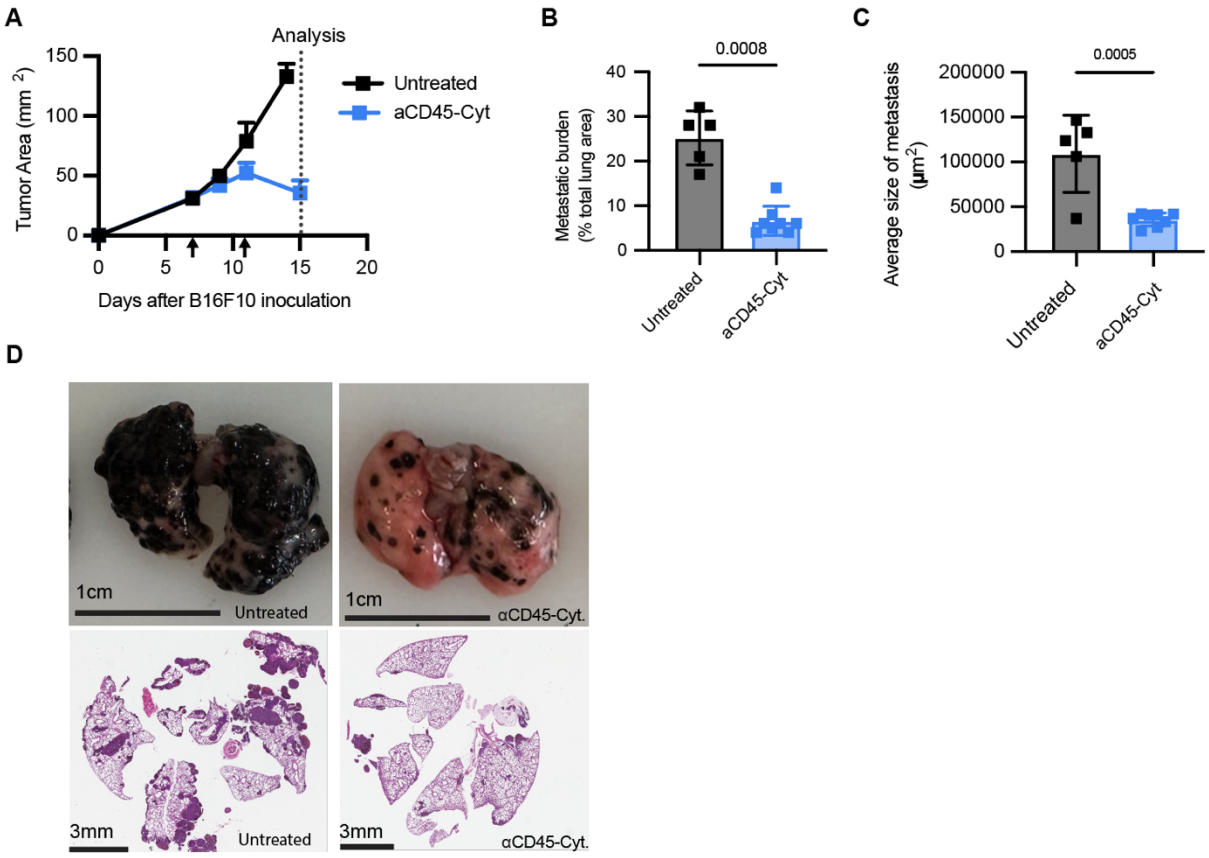

Figure 3.7. αCD45-Cyt therapy triggers systemic anti-tumor immunity.

C57BL/6J (n=5 in untreated cohort, n = 8 in αCD45-Cyt cohort) were simultaneously inoculated with 1M B16F10 cells s.c. and 0.2M cells retro-orbitally (r.o.) to develop lung metastases. Mice were treated with 1µg αCD45-IL12 immunocytokine on day 7 and 10µg αCD45-IL15 on day 11 (αCD45-Cyt). On d15, animals were euthanized and tumor burden was analyzed. **A,** Tumor growth curves with arrows denoting treatment. Dashed line denotes analysis timeline. **B,** Metastatic lung burden shown as percentage of lung tissue after αCD45-Cyt treatment. **C,** Average metastasis size after αCD45-Cyt treatment. **D,** Representative images of untreated (top left) or αCD45-Cyt treated (top right) lungs. Representative histology of untreated (bottom left) or αCD45-Cyt treated (bottom right) lungs. Shown are mean ± s.d. For metastatic burden, P values were determined by Mann-Whitney non-parametric test. For average metastasis size, P values were determined by *t*-test.

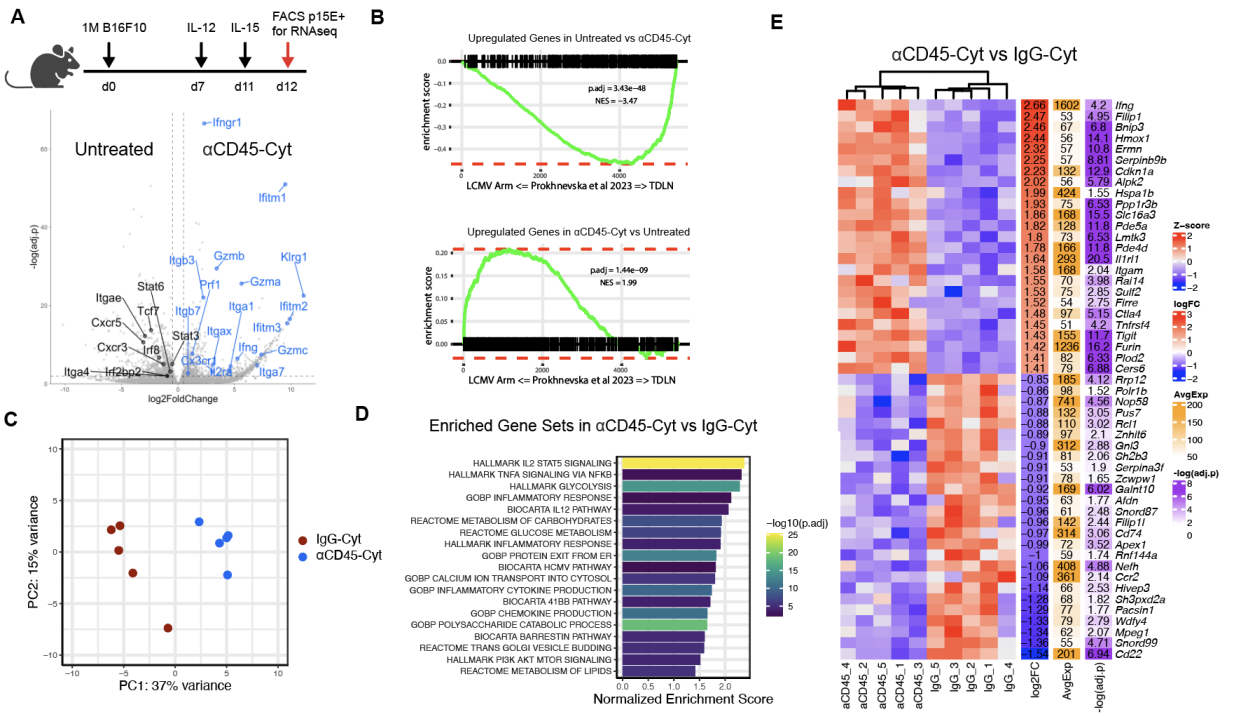

Figure 3.8. αCD45-Cyt therapy induces an anti-viral signature in the tumor-specific TDLN compartment.

B16F10 tumors (*n* = 4 in PBS cohort) treated with αCD45-Cyt (n = 5) or IgG-Cyt (n = 5) therapy were sorted for CD8⁺ T cells specific for the immunodominant p15E retroviral antigen for downstream RNA-seq. **A**, Volcano plot of differentially expressed genes between untreated and αCD45-Cyt with selected genes labeled. **B**, GSEA using the differentially expressed genes between untreated and αCD45-Cyt, compared with T cell gene signatures from LCMV-Arm infection or TDLN from Prokhnevska et al. 2023 (GSE216731). Enrichment score is plotted. Adjusted p values and normalized enrichment scores (NES) are labeled. **C**, PCA of IgG-Cyt and αCD45-Cyt treated samples. **D**, Enriched pathways in αCD45-Cyt samples compared to IgG-Cyt samples. **E**, Top 25 differentially expressed genes between αCD45-Cyt samples and IgG-Cyt samples. Statistical significance was determined using the Wald test with Benjamini-Hochberg post hoc correction.

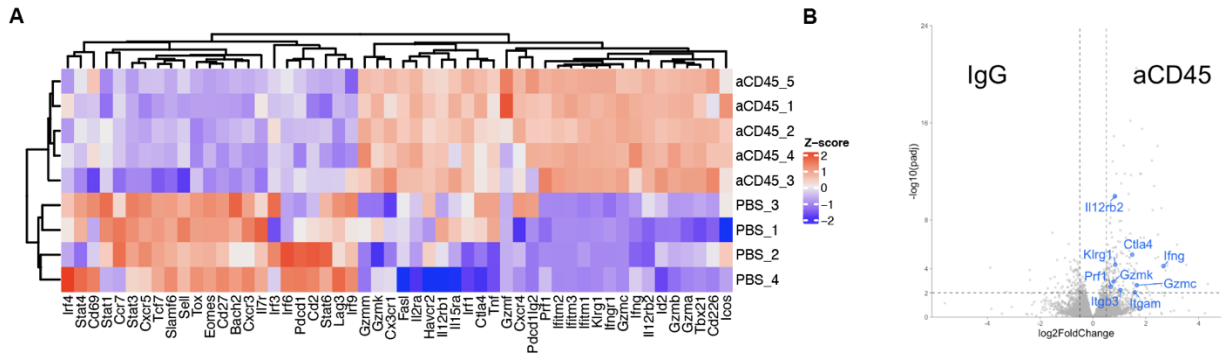

Figure 3.9. αCD45-Cyt therapy enhances activation of the tumor-specific TDLN compartment.

B16F10 tumors (*n* = 4 in untreated group) treated with αCD45-Cyt (n = 5) or IgG-Cyt (n = 5) therapy were sorted for $CD8^+$ T cells specific for the immunodominant p15E retroviral antigen for downstream RNA-seq. **A,** Differential gene expression of select inflammatory and activation markers between untreated and αCD45-Cyt treated mice. **B,** Volcano plot of differentially expressed genes between IgG-Cyt and αCD45-Cyt with selected genes labeled.

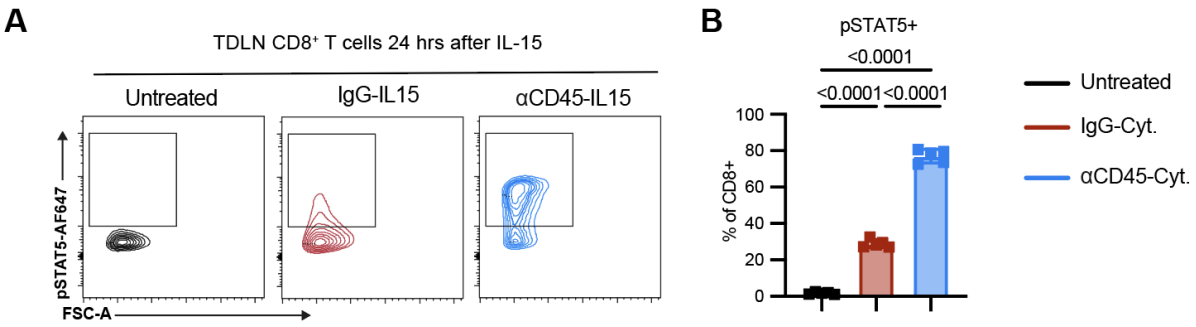

Figure 3.10. αCD45-IL15 triggers extended pSTAT5 in vivo.

C57BL/6J mice (n=5/group) inoculated with B16F10 tumors were treated on d7 with 10 µg IL-15 immunocytokine. 24 hours later, lymph nodes were fixed, permeabilized, and stained for pSTAT5. **A**, Representative pSTAT5 contour plots after IL-15 treatment, previously gated on live CD3+CD8+ cells. **B**, Summary data for pSTAT5 induction shown in A.

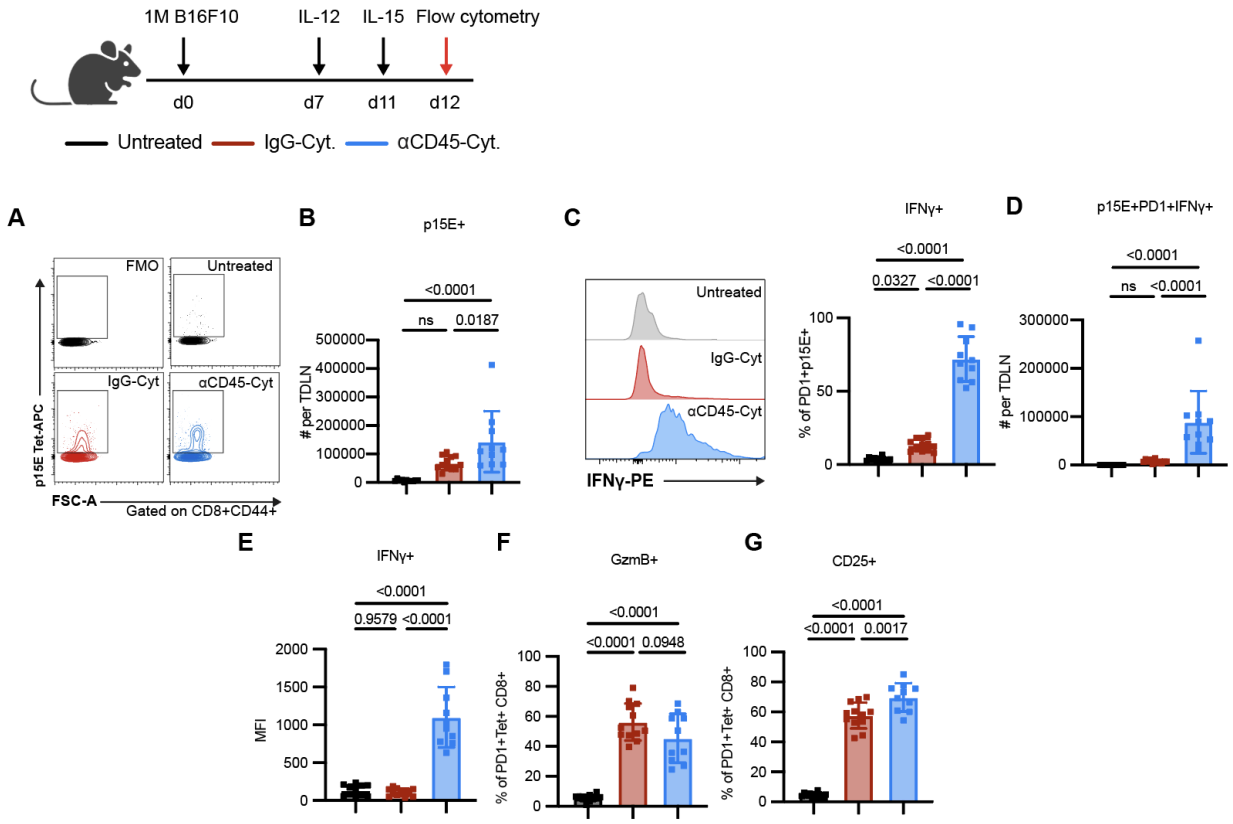

Figure 3.11. αCD45-cytokine therapy reprograms the TDLN leading to an optimal IFNg-producing tumor-specific CD8+ T cell effector subset.

Mice (n = 11 in untreated cohort, n = 12 in IgG-Cyt cohort, n = 10 in αCD45-Cyt cohort across two independent studies) inoculated with 1M B16F10 tumor cells were treated with IgG-Cyt or αCD45-Cyt therapy starting on d7. Lymph nodes were harvested 24 hours after completion of therapy. **A**, Representative contour plots and gating for p15E tetramer+ cells in the TDLN, previously gated on live CD8+CD44+ cells. **B**, Treatment effects on p15E+ tumor-reactive cells in TDLN. **C**, (Left) sample histogram of IFNγ expression and (right) TDLN frequency of tumor-specific cells expressing IFNγ+. **D**, TDLN counts of IFNγ+PD-1+p15E+ T cells. **E**, IFNg MFI levels. **F**, Granzyme B expression. **G**, CD25 expression. Shown are mean ± s.d. P values were determined by one-way ANOVA followed by Tukey's multiple comparison test.

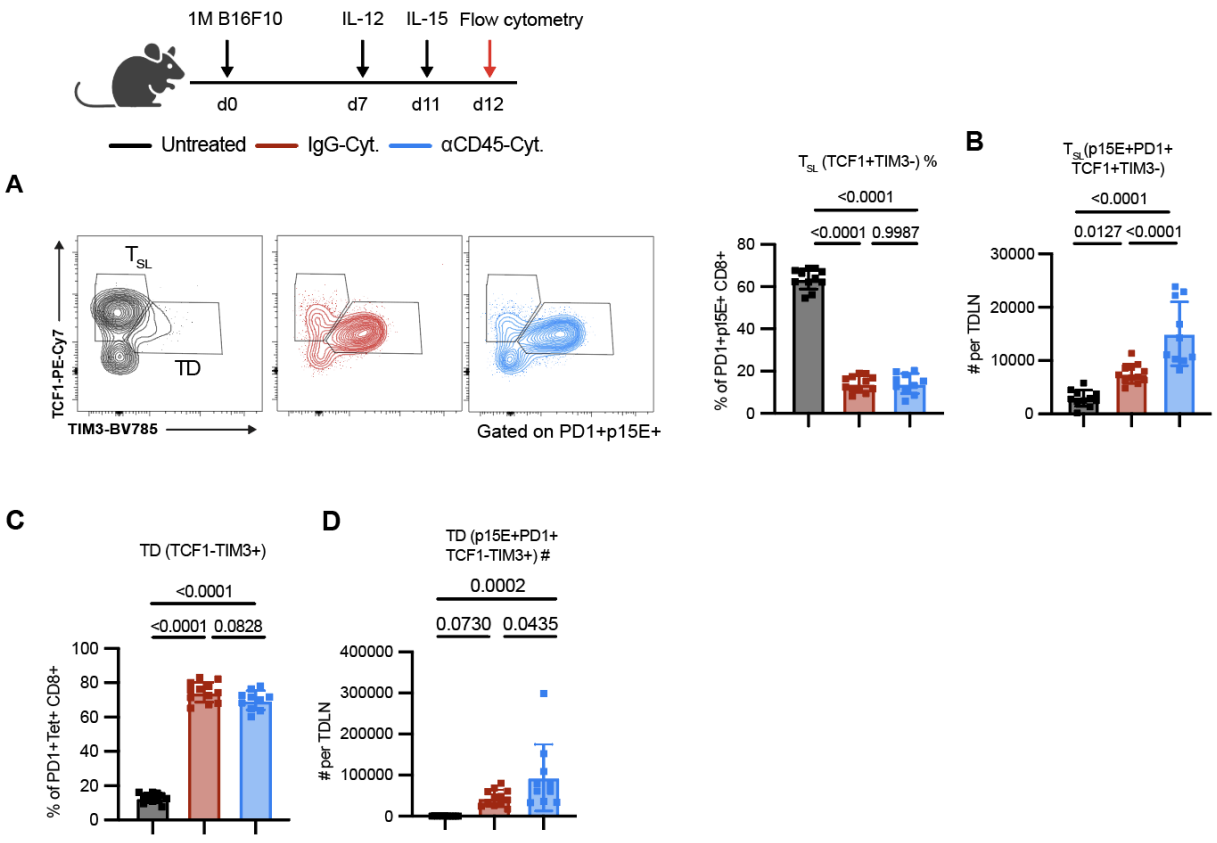

Figure 3.12. αCD45-cytokine therapy differentiates TDLN tumor-specific CD8 T cells without depleting the stem-like progenitor exhausted pool.

Mice (n = 11 in untreated cohort, n = 12 in IgG-Cyt cohort, n = 10 in αCD45-Cyt cohort across two independent studies) inoculated with 1M B16F10 tumor cells were treated with IgG-Cyt or αCD45-Cyt therapy starting on d7. Lymph nodes were harvested 24 hours after completion of therapy. **A**, (Left) stem-like (T_{SL}) vs. terminally differentiated (TD) sample gating and (right) TDLN frequency of stem-like $PD1^{+}TCF1^{+}CD8^{+}$ T cells. **B,** TDLN counts of stem-like $PD1^{+}TCF1^{+}CD8^{+}$ T cells. **D**, Expression of terminally differentiated phenotype ($TCF1^{-}TIM3^{+}$) **E,** Absolute TDLN counts of terminally differentiated cells. Shown are mean ± s.d. P values were determined by one-way ANOVA followed by Tukey's multiple comparison test.

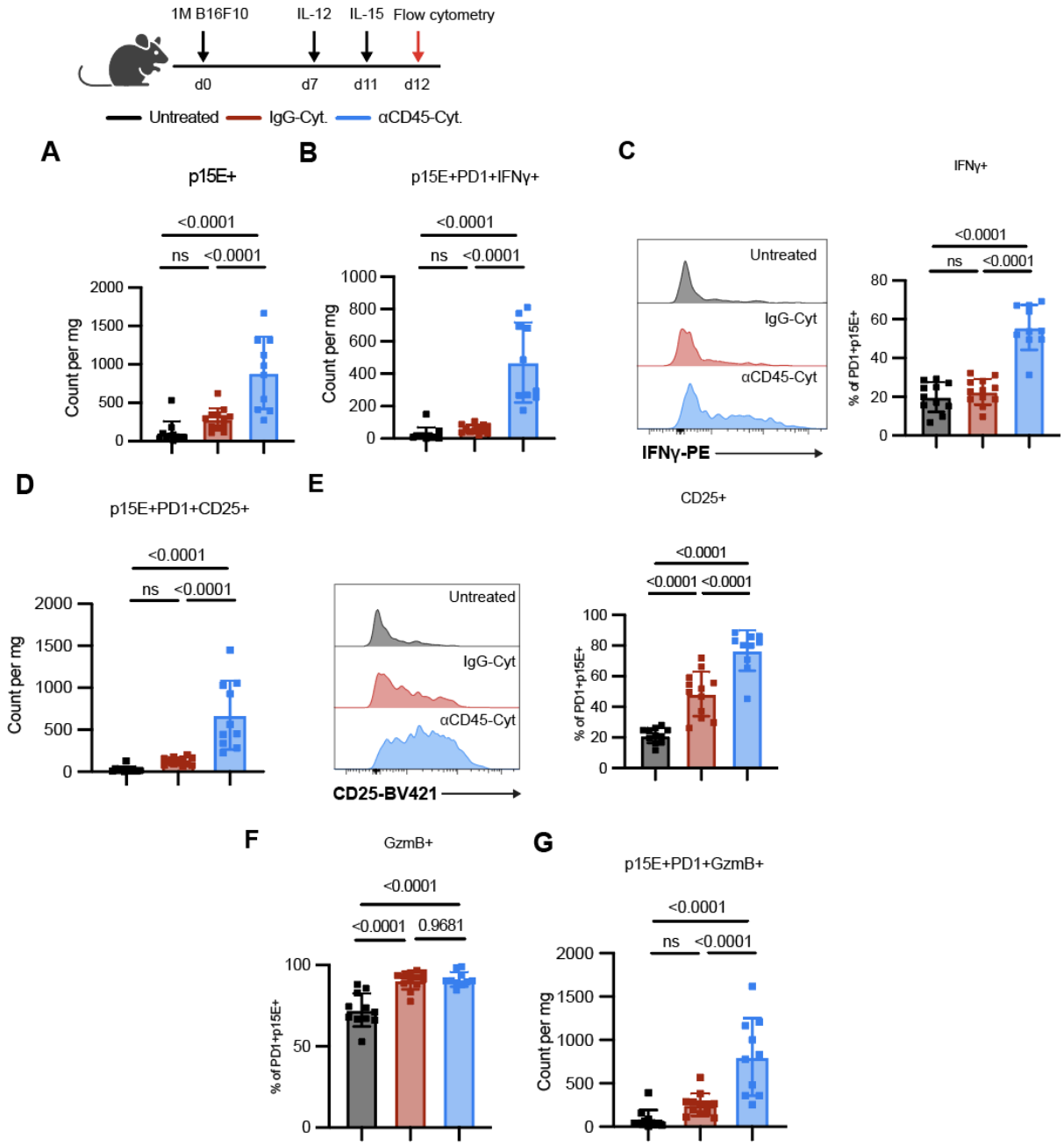
1M B16F10
IL-12
IL-15
Flow cytometry
d0
d7
d11
d12
Untreated
IgG-Cyt.
αCD45-Cyt.
A
p15E+
B
p15E+PD1+IFNγ+
C
IFNγ+
Untreated
IgG-Cyt
αCD45-Cyt
IFNγ-PE
D
p15E+PD1+CD25+
E
CD25+
CD25-BV421
F
GzmB+
G
p15E+PD1+GzmB+
Count per mg
% of PD1+p15E+
<0.0001
ns
0.9681

Figure 3.13. αCD45-cytokine therapy triggers increased infiltration of highly cytotoxic tumor-specific CD8+ T cells.

Mice (n = 11 in untreated cohort, n = 12 in IgG-Cyt cohort, n = 10 in αCD45-Cyt cohort across two independent studies) inoculated with 1M B16F10 tumor cells were treated with IgG-Cyt or αCD45-Cyt therapy starting on d7. Tumors were harvested 24 hours after completion of therapy. A-G demonstrate the effects of αCD45-Cyt therapy on intratumoral $p15E^{+}CD8^{+}$ T cells. **A**, Counts of p15E $tetramer^{+}CD8^{+}$ TILs. **B,** Counts of p15E $tetramer^{+}CD8^{+}$ TILs expressing IFNγ. **C**, Sample histogram of IFNg staining (left) and expression data (right). **D,** Counts of p15E $tetramer^{+}CD8^{+}$ TILs expressing CD25. **E**, Sample histogram of CD25 staining (left) and expression data (right). **F**, Granzyme B expression. **G,** Counts of p15E $tetramer^{+}CD8^{+}$ TILs expressing Granzyme B. Shown are mean ± s.d. P values were determined by one-way ANOVA followed by Tukey's multiple comparison test.

Methods

In vivo pSTAT measurement

Measurement of STAT5 levels *in vivo* was carried out as previously described(*99*). Briefly, TDLN were processed into single cell suspensions directly in BD Fixation Buffer I and samples were incubated at 37C for 10 minutes. Downstream permeabilization and staining was performed as described above. In all cases, pSTAT signal was measured using a BD LSR Fortessa and data were analyzed in Flowjo.

Tumor inoculation and treatment preparation

For all single-tumor experiments, mice aged 6-8 weeks old were injected subcutaneously in the shaved right flank with 1M tumor cells (MC38, MC38-ZsGreen, or B16F10) in a volume of 50 µL PBS. For two-tumor experiments, the contralateral tumor was inoculated on the left flank 3 days after the primary tumor, as stated in study schematics. Prior to treatment, mice were randomized to ensure equal mean initial tumor size across groups. Immunocytokines were prepared at their stated doses (1µg for IL-12 immunocytokines, 10µg for IL-15 immunocytokines, where the mass indicated is the mass of the entire fusion protein) and dosed intratumorally in 20 µL PBS unless otherwise stated. Doses were informed by our biodistribution experiments as well as previous intratumoral cytokine work from our lab(*17*). Peritumoral administration was performed in 50 µL PBS injected s.c. at the tail-base. Intraperitoneal administration was performed in 100 µL PBS. Tumor area was calculated as the product of tumor length and width. For single-tumor studies, mice were euthanized when tumor area exceeded 100 mm^2; for two-tumor studies, mice were euthanized when cumulative tumor area exceeded 200 mm^2. Immune memory rechallenge experiments were carried out 100 days after initial challenge with 10^5 tumor cells on the left flank. Age-matched naïve mice were used as controls for these studies. For the lung metastasis model used in Extended Data Fig. 6, 0.2M B16F10 cells in 100 µL PBS were inoculated retro-orbitally on the same day as the standard 1M tumor cell flank inoculation.

Tissue processing for flow cytometry

B16F10 or MC38 tumors were harvested, weighed, and subsequently minced using dissection scissors in gentleMACS mouse tumor dissociation buffer (Miltenyi) prepared per manufacturer's instructions. As noted in the Miltenyi protocol, Enzyme R was reduced to 20% of the stated amount to preserve surface epitope integrity. Minced tumors were processed on a gentleMACS Octo-dissociator with heaters (Miltenyi) using program mTDK_1 for B16F10 and mTDK_2 for MC38. Dissociated tumors were then filtered through a 70-micron strainer and 25 mg tumor was plated for downstream staining. TDLN were harvested, weighed, and subsequently dissociated and filtered through a 5 mL round-bottom tube with cell-strainer cap (Falcon) using the blunt rubber end of a 1mL syringe plunger (Falcon). 5 mg of TDLN was used for downstream staining. Blood was collected by sub-mandibular bleeding into MiniCollect K2-EDTA tubes (Greiner) and red blood cells were lysed using ACK Lysis Buffer (Gibco). When intracellular cytokine staining (ICS) was performed, as in Fig. 5, samples were resuspended and plated in complete RPMI supplemented with 1X sodium pyruvate (ThermoFisher), 1X non-essential amino acids (ThermoFisher), 1X beta-mercaptoethanol (ThermoFisher), and 1X brefeldin A (BioLegend) and allowed to incubate at 37C for 3 hours prior to staining. Precision counting beads (50uL, BioLegend) were added after initial resuspension and used for downstream data analysis. Viability was assessed with Zombie UV or Zombie NIR dyes (BioLegend, 1:1000) in PBS for 20 minutes at room temperature. Subsequent washes and surface staining was performed in PBS supplemented with 1% bovine serum albumin and 2mM EDTA (ThermoFisher). Samples were resuspended in Mouse Fc block Plus (BioLegend) prior to surface staining for 15 minutes. Antibodies against surface targets used as following: CD3 (17A3, BD, 1:100), CD4 (GK1.5, BD, 1:100), CD8 (53-6.7, BD, 1:200), CD19 (6D5, BioLegend, 1:100), CD24 (M1/69, BioLegend, 1:100), CD25 (PC61, BioLegend, 1:100), CD44 (IM7, BD, 1:100), CD45.2 (BD, clone: 104, 1:100), NK1.1 (PK136, BioLegend, 1:100), MHCII (M5/114.15.2, BioLegend, 1:100), Ly6C (HK1.4, BioLegend, 1:100), F4/80 (BM8, BioLegend, 1:100), PD1 (29F.1A12, BioLegend, 1:100), TIM3 (RMT3-23, BioLegend, 1:100). P15E tetramer (MBL) staining was performed in the presence of 50 nM dasatinib at a 1:75 dilution and anti-CD8 antibody

clone KT15 (ThermoFisher) was used to minimize background signal. Dasatinib incubation was not included in the staining mixture for the RNAseq experiment. When performing intracellular staining, cells were fixed and permeabilized using the Foxp3 transcription buffer set (eBioscience). Samples against intracellular antigens used as following: TCF1 (C63D9, Cell Signaling Technologies, 1:250), IFNg (XMG1.2, BioLegend, 1:200), Granzyme B (QA16A02, BioLegend, 1:200). Intracellular staining was performed overnight at 4C. Cells were collected using a BD FACSymphony A3 and data were analyzed in FlowJo.

Antibody-mediated cellular depletion

Immune cell depletions were carried out with antibodies targeting CD8a (BioXcell, Clone 2.43, 400 µg twice weekly), NK1.1 (BioXCell, clone PK136, 400 µg twice weekly), CSF1R (BioXCell, clone AFS98, 300 µg every other day) as previously described(*57*). All depletions were given i.p. in 100 µL of PBS. Depletions were initiated 1 day prior to treatment and carried out for four weeks. Depletions were carried out in C57BL/6J mice unless otherwise noted.

FTY720 Preparation and dosing

FTY720 hydrochloride (Sigma Aldrich) was stored in stock solutions at 10 mg/mL in DMSO. Prior to treatment, stock solutions were diluted to a dose of 30µg in 150 µL in PBS. In 2-tumor MC38 studies, FTY720 was dosed every other day i.p. starting on day 5 after tumor inoculation.

Immunohistochemistry staining of lung sections

Animals were euthanized and transcardially perfused with PBS before harvesting the lungs. Tissues were fixed overnight in 4% paraformaldehyde (PFA) at 4°C, processed using conventional methods, embedded in paraffin, and sectioned at 10 µm. Sections were then stained with hematoxylin and eosin and scanned using the Aperio Brightfield

(Leica Biosystems) Slide Scanning System. The lung tissue and metastatic lesions were automatically detected via distinct pixel classifiers using QuPath v0.4.3.

CD8 T cell RNA sequencing, mapping, and analysis

For RNA-seq experiments, 2-40k live $CD3^+CD8^+$ $CD44^+p15E^+$ cells processed from TDLN were sorted using a Sony MA900. RNA extraction was performed using the Qiagen RNEasy Micro kit per manufacturer's instructions. RNA libraries were prepared using the Clontech SMARTer Stranded Total RNA-Seq Kit - Pico Input Mammalian and sequenced using the Illumina NextSeq500 75nt kit. RNAseq reads were aligned to the mouse genome with STAR (v2.7.9a) using ensembl GRCm39 primary assembly as the reference. Aligned reads were quantified using RSEM (v1.3.1) with ensembl GRCm39 (release 110) transcript annotations. The resulting counts were analyzed in R using DESeq2 for differential expression analysis, fgsea for gene set enrichment analysis (GSEA), and msigDB for the gene set database. Data visualization was done with ggplot2 and ComplexHeatmap. GSEA was utilized for the correlative analysis between our RNAseq data and the gene expression signatures from Prokhnevska et al. 2023. The gene expression count matrix was obtained from NCBI Gene Expression Omnibus with accession No. GSE216731. Differential gene expression analysis was performed on the LCMV Arm and TDLN groups, and the genes were ranked by Wald test statistics. The ranked genes were compared to gene signatures from our data, specifically, the upregulated genes in αCD45-Cyt vs. untreated mice and the upregulated genes in untreated vs αCD45-Cyt mice. The enrichment score suggests the degree of correlation with T cells from either LCMV Arm or TDLN.

Statistical Methods

Statistics were computed in GraphPhad Prism v9 as denoted in the figure captions. For *in vitro*, biodistribution, and flow cytometry immunophenotyping experiments, comparisons were made by *t*-test or one- or two-way analysis of variance (ANOVA) followed by Tukey's multiple comparison test. Survival comparisons were made by log-rank (Mantel-Cox) tests. Differential gene expression analysis in the RNA-seq data was

performed by Wald tests. In all RNA-seq analysis, P values are corrected by Benjamini-Hochberg to account for multiple hypothesis testing. Exact P values are denoted in figures.

Chapter 4 : Next steps and outlook of αCD45-Cytokine therapy

Parts of this chapter appear as published in Santollani and Wittrup, *Immunological Reviews* (2023)(*1*).

Introduction

As demonstrated in the last 2 chapters, in this work we designed, tested, and optimized a modular cytokine engineering platform through antibody-mediated targeting to the universal leukocyte phosphatase CD45. CD45's abundance on intratumoral leukocytes paired with its long surface half-life translated into a promising anchor that allowed for improved payload retention at a macro level as well as enhanced signaling biology at a cellular level. Optimization of dose and sequencing yielded a powerful sequential cytokine treatment that was highly efficacious across various syngeneic tumor models and did not trigger toxicity-related weight loss.

In this chapter, we focus on preliminary data and discussion on the future translational potential of CD45 targeted cytokines. To facilitate the ease of translation of αCD45-Cyt therapy, we design and develop a single αCD45/IL15/IL12 single fusion chimera, referred to as αCD45-dual-IL. As opposed to having to make two separate proteins, a single dual-IL molecule allows for an all-in-one approach. In preliminary in vitro and in vivo tests, the initial αCD45-dual-IL prototype behaves consistently with its individual counterparts. We contextualize this data in upcoming plans to pilot αCD45-Cyt therapy in canine patients.

Additionally, we look to combine αCD45-IL15's lymph-node retention capabilities with another localized therapy developed in our lab, a materials-anchored IL-12. In a two-tumor MC38 model, a single dose of alum/IL-12 followed by a single dose of αCD45-IL15 leads to complete responses in a subset of mice. In the discussion, we highlight how the unique capabilities of these two localized approaches may synergize to provide a robust anti-tumor response.To conclude, we present a final discussion and outlook on the future of engineered cytokine therapies.

Preliminary results and discussion on future work

A single molecule approach and plans for canine translation

Given the promising efficacy and mechanism results in syngeneic tumors, we have most recently spent time laying the groundwork for effective translation of αCD45-Cytokine therapy. One potential hurdle in translation the current treatment paradigm is the need for two separate immunocytokines (IL-15 and IL-12). For recombinant protein therapeutics like immunocytokines, where clinical grade good manufacturing practice (GMP) material for a small Phase I trial can cost upwards of $5M per asset, having to produce two independent molecules could be gating.

Based on this, we wondered whether a single fusion protein that incorporates both cytokines could be equally effective. This all-in-one approach has been validated for another localized cytokine therapy from our lab. In translating Momin et al's collagen-binding cytokines, Cullinan Oncology developed a single protein incorporating IL-2, IL-12, human serum albumin (HSA, for half-life extension), and the collagen binding domain. This IL-2/IL-12 fusion, termed CLN-617, demonstrated impressive preclinical responses and was recently dosed in a first-in-human study.

We hypothesized that a similar single fusion approach could be used to simplify αCD45-Cyt therapy. Using the same αCD45 antibody scaffold, we generated a bivalent IL-15/IL-12 fusion, referred to as αCD45-dual-IL hereafter (**Fig 4.1A**). αCD45-dual-IL was able to dose-dependently proliferate $CD8^+$ T cells to the same extent as IgG-IL15 or αCD45-IL15 (**Fig 4.1B**). αCD45-dual-IL was retained on the cell surface to a far greater degree than IgG fusions but was internalized more rapidly than αCD45-IL15 (**Fig. 4.1C**). As discussed in Chapter 2, this suggests that there is a balance between CD45's slow turnover and cytokine receptor's rapid internalization rate. Increasing the valency of cytokine payloads (four cytokines in αCD45-dual-IL vs two cytokines in individual αCD45/IL15 or αCD45/IL12) seems to increase internalization of the molecule.

With promising in vitro validation of the αCD45-dual-IL construct, we tested its ability to induce anti-tumor immunity in vivo. Mice bearing B16F10 tumors that were ~35mm^2 in size were treated with αCD45-dual-IL on d8 and d12 at doses that were molar matched to the original αCD45-Cyt paradigm. For the larger αCD45-dual-IL molecule, this corresponds to 1.6 and 16 μg for the d8 and d12 doses, respectively. Treatment with αCD45-dual-IL did not trigger any weight loss despite the toxicity often associated with combination of IL-15 and IL-12 (**Fig 4.2**). The two doses led to complete responses in the entire cohort (**Fig 4.2**).

Despite these encouraging initial results, there needs to be additional testing with the αCD45-dual-IL molecule to ensure it is triggering a similar immune response to the original sequential αCD45-Cyt therapy. Most importantly, αCD45-dual-IL needs to display comparable abscopal effects to αCD45-Cyt therapy to justify its translation. Furthermore, there should be further optimization of the cytokine valency before nominating a final construct for future translation.

The next planned step in translation for αCD45-Cyt therapy will be a small pilot trial in canine patients carried out through the lab's standing collaboration with Dr. Tim Fan at UIUC. Dogs with spontaneously occurring malignancies can serve as an interesting bridge model between mouse and human. Namely, 1) pet dogs are exposed to the same environmental factors that we are, and 2) the timescale of canine tumorigenesis is commensurate with that of human cancer. The lab has previously translated collagen-anchored cytokines where they have shown signal in both melanoma and sarcoma patients (*64*, *109*).

To translate CD45-targeted cytokines into canine patients, we aimed to generate canine surrogates of our mouse αCD45 immunocytokine molecules. Because we were not able to find an anti-dog CD45 antibody sequence in the patent literature or in publications, we recently began a yeast surface display campaign using a VHH library(*110*). Once a selective binder is discovered and affinity matured, we will generate bivalent VHH-Fc-

cytokine or monovalent VHH-cytokine fusions (**Fig. 4.3**). The final format of this molecule will be guided by any final experiments exploring alternative mouse αCD45-dual-IL constructs.

Future experiments will be focused on validating canine surrogate molecules to ensure consistent behavior with their murine counterparts. Due to the more limited set of dog reagents, we plan to test the surface retention and extended signaling of dog CD45-targeted cytokines by performing a pulse-chase proliferation experiment. Canine PBMCs labeled with Cell Trace Violet will be incubated with canine surrogate molecules for 1 hour, washed of unbound cytokine, and allowed to proliferate for 48 hours. CTV dilution will be measured by flow cytometry and compared to untargeted control cytokines. We expect only CD45-targeted cytokines to induce proliferation of canine PBMCs after a 1 hour pulse. A positive result in this experiment would validate 1) binding to CD45, 2) cytokine bioactivity, and 3) consistent construct behavior (i.e. signal extension by CD45 surface retention).

αCD45-IL15 can drive abscopal responses in combination with alum-IL12

In the αCD45-Cyt treatment regimen, the IL-12 immunocytokine dose was designed to be isolated to the tumor and spare the TDLN. The rationale was to use IL-12 as an antigen-generation compound that would initiate an immune response that would later be amplified by the IL-15 dose. We specifically dosed IL-12 at 1 μg to prevent any direct TDLN exposure to avoid terminal differentiation of the nodal stem-like progenitor exhausted pool which could lead to poor immune memory. We thus hypothesized that other tumor-localized IL-12 therapies could serve the same purpose as αCD45-IL12 and synergize well with αCD45-IL15. As a proof of concept for this idea, we replaced the initial αCD45-IL12 dose in αCD45-Cyt therapy with a locally delivered alum-IL12 dose. Alum anchoring, another localization strategy previously developed by our labs, relies on phosphoserine affinity tags that are fused to therapeutic proteins and enable long-term

linkages on the traditional vaccine adjuvant alum. For more background on alum-anchoring, refer to previous thesis work from our labs or relevant publications(*20*, *57*).

To test whether a single dose of alum/IL-12 would combine well with αCD45-IL15, we tested this sequential regimen in a two-tumor MC38 model. Mice treated with alum/IL-12 monotherapy rejected the treated tumor but were unable to control the distal tumor. Mice treated with alum/IL-12 followed by αCD45-IL15 successfully controlled the primary tumor and about 40% of mice additionally rejected the contralateral tumor (**Fig 4.4**). While this abscopal effect is not as pronounced as that seen by αCD45-Cyt therapy, it may be due to differences in experimental set-up. In comparison to the two-tumor experiments shown in Chapter 3, this experiment involved simultaneous inoculation of both tumors on either flank, allowing for 3 additional days of tumor establishment on the contralateral flank. Future study of this combination therapy should focus on mechanistic and phenotypic comparison of alum/IL12 and αCD45-IL12 to truly understand whether they are interchangeable.

This combination therapy highlights the key differences and strengths of different localization strategies developed in the lab. For example, alum anchoring enables retention on timescale of weeks to months, far longer than αCD45 anchoring. However, due to the micron-sized depots that alum forms, it does not allow for efficient lymph node drainage. In contrast, as we have shown throughout the thesis, CD45 targeting elicits day-long lymph node retention when dosed appropriately. Future combinations of engineered cytokines that each address key aspects of the anti-tumor response could prove promising.

Final words

Since the initial excitement around the potential of cytokines in cancer immunotherapy, the field has matured and evolved tremendously. Our growth in understanding of T cell immunology, structural biology, and protein engineering tools have sustained an engineering campaign over the last two decades attempting to unlock the potential of cytokine therapies. After initial half-life engineering, the next generation of cytokines was mostly defined by simple tumor-targeting immunocytokines and not-alpha IL2 candidates. Today, a majority of cytokine engineering falls into conditional activation, cis-targeting immunocytokines, and intratumoral anchoring. Furthermore, each of these strategies can be paired with additional engineering endeavors in cellular therapies (e.g. cytokine armored CAR-Ts) and gene therapies (e.g. gene delivery of engineered cytokines). Because endogenous cytokines are exquisitely regulated by the immune system, it's likely that engineering them as therapies will not be a one-size-fits-all approach. Depending on the specific payload, a given intensity and duration of signaling may be productive or harmful. Just like their endogenous counterparts, cytokine therapies will need to be fine-tuned in space and time to maximize patient benefit.

In this work, we engineered and optimized a potent cytokine therapy through targeting of the universal immune cell receptor CD45. Multi-receptor engagement between CD45 and the cognate cytokine receptor led to extended surface half-life and enhanced signaling for IL-15 and IL-12. Preliminary data suggests that this behavior will be consistent for other cytokines and for human CD45 as well, highlighting the potential and broad applications of CD45 targeting for certain immune agonists. As the immunotherapy field moves into cis-targeting on immune cells, emerging properties related to engaging multiple cell surface receptors simultaneously will likely be discovered.

For most of this thesis, we applied CD45-targeting therapeutically in a regimen referred to as αCD45-Cyt therapy. At its crux, αCD45-Cyt therapy is modeled after a “prime and boost” strategy that used an initial intratumoral dose of IL-12 to kickstart the anti-tumor response and a sequential dose of IL-15 a few days later to amplify newly primed $CD8^+$ T cells. The relevant IL-12 and IL-15 doses were informed by the biodistribution experiments highlighted in Chapter 2. These results revealed a “fountain” model for intratumorally delivered CD45 targeted proteins in which protein subsequently drains from tumor to TDLN to systemic circulation in a dose-dependent manner. This allowed us to select doses for controlled compartment-specific exposure and most consequently enabled sustained TDLN retention by αCD45-cytokines. Ultimately, we attribute this lymph-node retention as the key differentiator that unlocked the profound systemic anti-tumor immunity that was seen with αCD45-Cyt therapy. Our FTY-720 experiments suggest that effector cells generated at the treated TDLN then disseminate and agnostically infiltrate distal tissues. Rather than focusing solely on intratumoral targeting and retention, as the field often has, this work clearly demonstrates the importance of lymph node biology and lymph node exposure for effective systemic immunity. Regardless of administration route or engineering approach, future cytokine therapies should be developed with lymph node exposure and biology in mind. This is likely even more important in clinical settings, where it is becoming increasingly appreciated that the key immune cell subsets responding to immunotherapy such as progenitor exhausted cells largely reside in lymph nodes (*111*, *112*).

Systemic toxicities have always been a key part of the conversation around cytokines. Though many strategies have been developed to tackle this problem, including the strategy developed in this thesis, gauging toxicity from novel cytokine therapies is difficult because preclinical models are often not as sensitive to cytokine toxicity as humans. For example, antibody IL-2 fusions that appeared safe in mice have resulted in dose-limiting toxicities when tested in humans(*113*). Shockingly, IL-12 toxicity has been reported for intratumoral doses as low as 100ng/kg (*91*, *114*). This would correspond to

single digit nanogram doses for an average sized mouse, far lower than what we and others traditionally dose in preclinical models. Certain mouse models have been reported to be more sensitive to cytokine toxicity. For IL-12, the C3H/HeJ background has been shown to be sensitive to low-dose recombinant IL-12 and is a good tool for probing the toxicity of engineered constructs(*67*, *115*). For other cytokines, weight loss and liver enzymes are key metrics for predicting toxicity in new engineering approaches. Finally, as discussed earlier in this chapter, spontaneous canine malignancies may serve as an emerging intermediate translational model for cytokine development. In comparison to syngeneic mouse tumors, which often grow and vascularize much more rapidly than human tumors, canine tumors mirror human cancers more faithfully(*64*, *109*, *116*). Thus, they may serve as an effective bridge between murine preclinical studies and first-in-human studies.

While we were able to probe many aspects of the biology and mechanism that underpin αCD45-Cyt therapy's effects, there are still outstanding questions. Because the majority of our analysis occurred after completion of the entire regimen (that is, after the IL-15 dose), we do not yet fully understand the individual contributions of each dose of therapy. For example, based on our understanding of each component – IL-12 for cell death and antigen release and IL-15 for proliferation – the therapy should not be as effective if the doses were reversed (i.e. IL-15 first followed by IL-12). A related question is whether the αCD45-IL12 uniquely enabled the therapy's activity or if other antigen-generating agents could replace this first dose. Preliminary experiments replacing αCD45-IL12 with alum/IL-12 suggest that at least other engineered IL-12 molecules could be effective, but it would be interesting to probe more traditional agents like radiation or immunogenic cell death(ICD)-inducing chemotherapy.

A paradoxical aspect of this approach has always been that it involves inducing proximity between CD45, a potent phosphatase, and domains that require phosphorylation for downstream signaling (i.e. cytokine receptors). As shown

throughout the entire work, in the format we designed our immunocytokines, they were unaffected by CD45 proximity – if anything, they displayed enhanced signaling. Ultimately, we hypothesize that CD45's phosphatase properties did not hinder this approach for 3 key reasons: 1) cytokines are soluble ligands as opposed to membrane-bound ligands that form the type of cell-cell synapses that naturally exclude CD45 (e.g. many co-stimulatory receptors like CD40), 2) downstream signaling is dependent on a cytosolic, not membrane-bound, kinase (i.e. JAK), and 3) the distance between the CD45 and cytokine receptor was large enough in this immunocytokine format as to not allow for dephosphorylation. Future experiments could be focused on proving or disproving these hypotheses by applying CD45 anchoring to membrane-bound agonists (e.g. CD28, CD40, 4-1BB) and varying construct architecture to increase or decrease distance between CD45 engagement and the signaling domain. Another related aspect that could play role in understanding how binding CD45 impacts cytokine signaling is the epitope of the CD45 antibody. Based on its ability to bind all isoforms of murine CD45, the clone used in this work (30-F11) likely binds in a membrane-proximal region of CD45. Future experiments probing the importance of CD45 epitope on this approach may be hugely valuable in ensuring effective translation.

Finally, a few thoughts on the prospects of translating αCD45-Cyt therapy. While the IL15/IL12 paradigm we applied this approach was particularly effective, it is unclear that these are the optimal cytokines for eliciting an anti-tumor response and moving forward with. For example, there is compelling data demonstrating IL-21 as another common gamma chain cytokine that can elicit anti-tumor immunity. Additionally, for intratumoral T cells, which are likely much further on their differentiation and exhaustion trajectory, pSTAT3 signaling cytokines like IL-10 may be the optimal payload to metabolically re-invigorate them. Depending on the dose and objective, different payloads should be explored and optimized.

In thinking of future translation of this work, it's also crucial to consider key differences between our preclinical mouse models and spontaneous malignancies in canine, or potentially human, patients. As described previously, the order of administration of αCD45-Cyt therapy was motivated by using the IL-12 dose to prime a T cell response and expand it using the IL-15. For syngeneic mouse tumors that are treated within a week of inoculation and have not had time to generate an endogenous T cell response, this reasoning makes sense. However, in established human tumors that have been interfacing with the immune systems for months to years, there is already an existing T cell response. Thus, the premise for staging IL-12 followed by IL-15 is likely not as important as in our preclinical mouse work. One could even rationalize the inverse treatment, using IL-15 to expand existing T cells and then IL-12 to reprogram them into an activated cytotoxic state.

As mentioned in the conclusion of Chapter 3, there are also key differences between CD45 biology in mice and humans, primarily relating to isoform prevalence and its correlation with cell phenotype. In humans, CD45 isoform splicing often corresponds to specific activation states and phenotypes. Canonically, T cells will downregulate CD45RA and upregulate the shorter CD45RO isoform upon activation. Pending further expression analysis of CD45RA on bystander leukocytes, generating a CD45RO targeting cytokine fusion could enable systemic administration of this approach.

Because this approach hinges on intratumoral CD45 infiltration, we wanted to understand how the mouse models we used for our preclinical validation compare in their leukocyte fraction to established human tumors. Previous reports estimating leukocyte fraction from TCGA samples range from 5% to 30%, suggesting that even though many tumors have dysfunctional immune infiltrates or low lymphocyte counts, there are no leukocyte immune deserts(*117*). Using another resource for analyzing mouse syngeneic tumor models, the median baseline infiltration is around 10%(*118*).

Knowing that common mouse syngeneic tumors have commensurate CD45 infiltration as human tumors suggests that this approach could viable if it were to be translated.

Undoubtedly, we are in the middle of a cytokine engineering wave, with many exciting preclinical and clinical examples. This newest generation of engineered cytokines, including our cell-surface targeted immunocytokines, are spatiotemporally programmed in ways that will hopefully translate to better tolerated and more efficacious therapies.

Figures

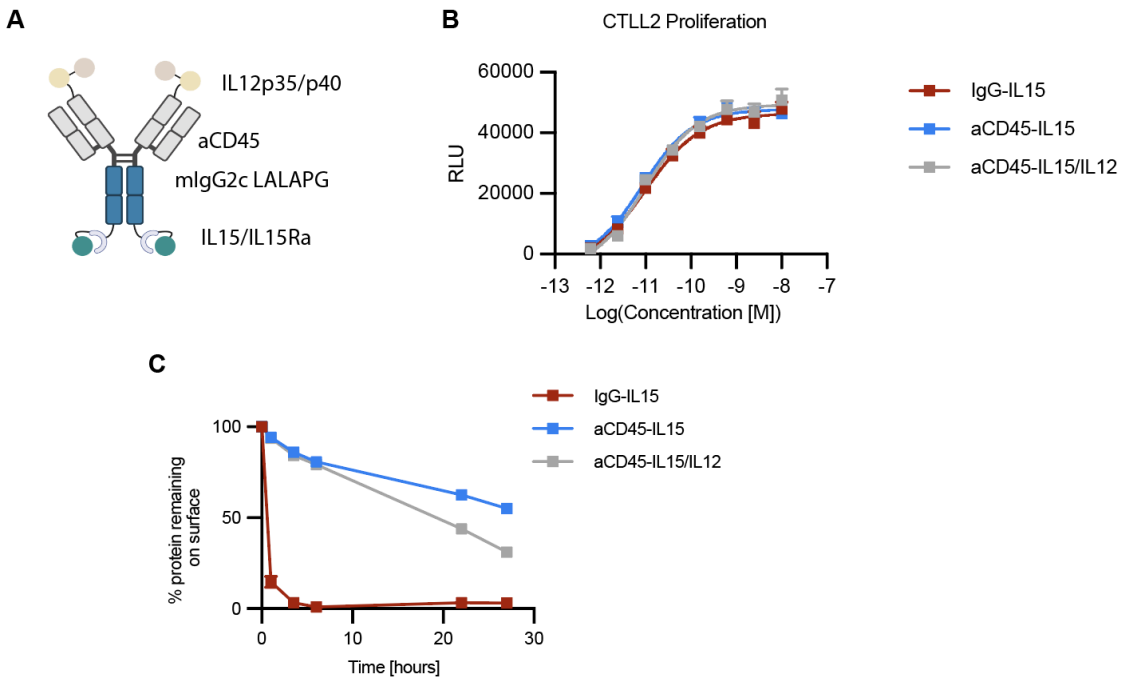

Figure 4.1. A single αCD45/IL15/IL12 fusion chimera is biofunctional and retained on the cell surface.

A, Schematic of αCD45-dual-IL. **B,** Luminescence measurement of CTLL-2 cell proliferation following 48 hr incubation with IgG-IL15, αCD45-IL15, or αCD45-dual-IL at indicated concentrations. **C,** Internalization kinetics of IgG-IL15, αCD45-IL15, or αCD45-dual-IL labeled with AF488 following binding to primary activated $CD8^+$ T cells. Data are mean ± s.d. from n = 3 biological replicates.

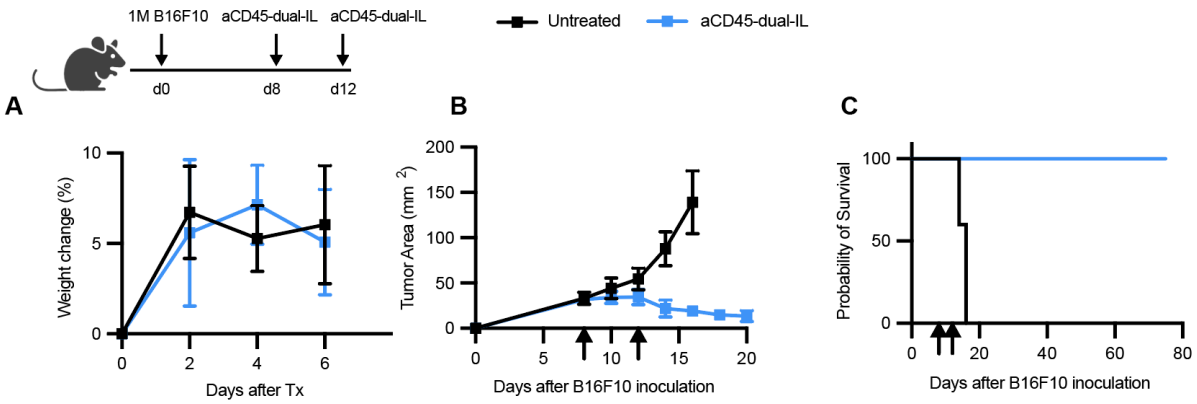

Figure 4.2. αCD45-dual-IL is safe and efficacious in B16F10 tumors.

C56BL/6 mice (n = 4-5/group) were inoculated with 1M B16F10 cells and treated on d8 and d12 with αCD45-dualIL at molar-matched doses to the original αCD45-Cyt paradigm. Shown are the **A**, weight, **B**, tumor growth curve, and **C**, overall survival.

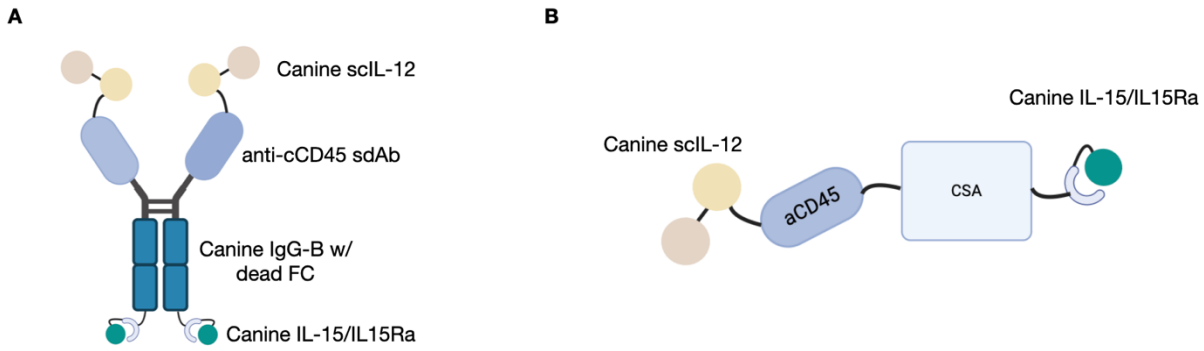

Figure 4.3. Sample architecture for canine surrogate αCD45-cytokine fusions.

A, Canine surrogate of αCD45-dual-IL mouse molecule described 4.1 and 4.2. **B,** monovalent canine cytokine-VHH-CSA fusion (CSA: canine serum albumin).

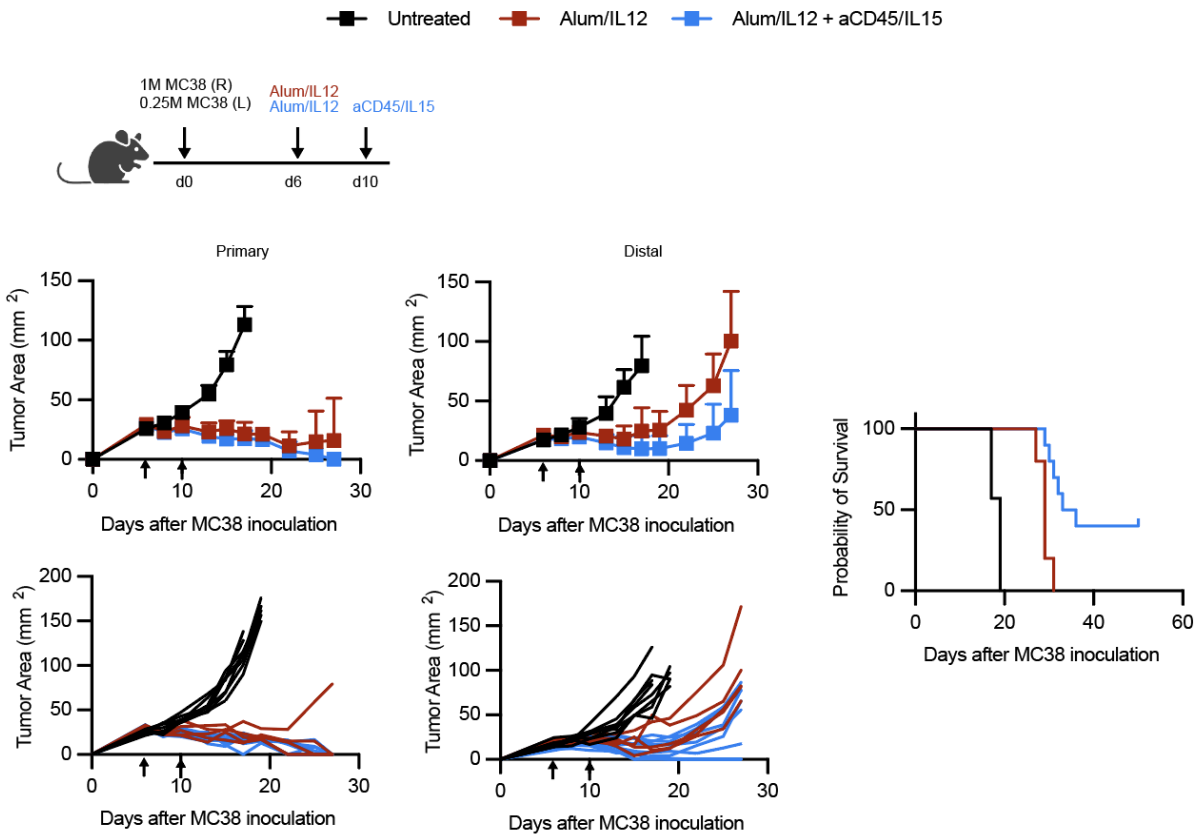

Figure 4.4. αCD45-IL15 elicits abscopal effects in combination with alum/IL-12.

C57BL/6 mice (n = 5-10/group) were inoculated with 1M and 0.25M MC38 cells on the right and left flank respectively on d0. Mice were treated on d6 with Alum/IL12 and d10 with αCD45/IL15. Shown are the primary and distal grouped and individual curves as well as overall survival.

Tables

Table 4.1. Amino acid sequences of αCD45-dual-IL fusion.

αCD45-dual-IL Light Chain (mCκ)	DIQLTQSPKSMSMSVGERVTLTCKASENVVTYVSWY QQKPEQSPKLLIYGASNRYTGVPDRFTGSGSATDFTL TISSVQAEDLADYHCGQGYSYPYTFGGGTKLEIK RAD AAPTVSIFPPSSEQLTSGGASVVCFLNNFYPKDINVKW KIDGSERQNGVLNSWTDQDSKDSTYSMSSTLTLTKDE YERHNSYTCEATHKTSTSPIVKSFNRNEC
αCD45-dual-IL Heavy Chain (mIgG2c LALA-PG)	MWELEKDVYVVEVDWTPDAPGETVNLTCDTPEEDDIT WTSDQRHGVIGSGKTLTITVKEFLDAGQYTCHKGGET LSHSHLLLHKKENGIWSTEILKNFKNKTFLKCEAPNYS GRFTCSWLVQRNMDLKFNIKSSSSSPDSRAVTCGMAS LSAEKVTLDQRDYEKYSVSCQEDVTCPTAEETLPIELAL EARQQNKYENYSTSFFIRDIIKPDPPKNLQMKPLKNSQV EVSWEYPDSWSTPHSYFSLKFFVRIQRKKEKMKETEEG CNQKGAFLVEKTSTEVQCKGGNVCVQAQDRYYNSSCS KWACVPCRVRSGGSGGGSGGGSGGGSRVIPVSGPAR CLSQSRNLLKTTDDMVKTAREKLKHYSCTAEDIDHEDITR DQTSTLKTCLPLELHKNESCLATRETSSTTRGSCLPPQK TSLMMTLCLGSIYEDLKMYQTEFQAINAALQNHNHQQIILD KGMLVAIDELMQSLNHNGETLRQKPPVGEADPYRVKMKL CILLHAFSTRVVTINRVMGYLSSA GGGGSGGGGSGGGGS QVQLLQSGGGLVQPGRSLKLSCLASGFIFSNYGMNWIRQ APGKGLEWVASISSTSSYIQYADTVKGRFTISRENAKNTLY LQMTSLISEDTALYYCARHGGYGYKGIWFAYWGQGTLV TVSS AKTTAPSVYPLAPVCGGTTGSSVTLGCLVKGYFPE PVTLTWNSGSLSSGVHTFPALLQSGLYTLSSSVTVTSNT WPSQTITCNVAHPASSTKVDKKIEPRVPITQNPCPPLKEC PPCAAPDAAGGPSVFIFPPKIKDVLMISLSPMVTCVVVDVS EDDPDVQISWFVNNVEVHTAQTQTHREDYNSTLRVVSALP IQHQDWMSGKEFKCKVNNRALGSPIEKTISKPRGPVRAP QVYVLPPPAEEMTKKEFSLTCMITGFLPAEIAVDWTSNGRT EQNYKNTATVLDSDGSYFMYSKLRVQKSTWERGSLFACSV VHEGLHNHLTTKTISRSLGK GGGGS GTTCPPPVSIEHADIRVKNYSVNSRERYVCNSGFKRKAGT STLIECVINKNTNVAHWTTPSLKCIRDPSLAGGSGGSGG SGGSGGSGGSGGNWIDVRYDLEKIESLIQSIHIDTTLYTD SDFHPSCKVTAMNCFLLELQVILHEYSNMTLNETVRNVLYLA NSTLSSNKNVAESGCKECEELEEKTFTEFLQSFIRIVQMFINTS

Methods

Fluorescence-quenching internalization assay

Internalization assays were performed and analyzed as described previously(*98*). Briefly, immunocytokines were conjugated with AlexaFluor 488 (AF488) using NHS ester chemistry (Invitrogen). Free dye was removed by Zeba spin desalting column purification (ThermoFisher). 100,000 primary CD8 T cells were seeded in 96-well plate and incubated with AF488-labeled immunocytokines at 10 µg/mL staggered at desired time points. Wells were then split such that one set was incubated with 25 µg/mL anti-AF488 quenching antibody (ThermoFisher, A-11094) for 25 minutes. For human $CD8^+$ T cell internalization assay, anti-human CD45 (clone: MEM-28) conjugated to AF488 (ThermoFisher) was used. Human CD8+ T cells were purchased from StemCell Technologies. Viability was assessed via DAPI staining. AF488 signal was measured using a BD LSR Fortessa and data were analyzed in Flowjo.

CTLL-2 proliferation

For IL-15 bioactivity, 10,000 CTLL-2 cells were seeded in a 96-well U-bottom plate in incomplete media per manufacturer's instructions with stated IL-15 immunocytokine dilutions for 48hrs at 37C. Proliferation was measured via CellTiter-Glo 2.0 Assay (Promega) following manufacturer's instructions. Luminescence was measured on a microplate reader (Tecan) with an integration time of 0.25 seconds.

Tumor inoculation and treatment.

See Chapter 2 and 3.

References

1. L. Santollani, K. D. Wittrup, Spatiotemporally programming cytokine immunotherapies through protein engineering. *Immunol. Rev.* **n/a**.

2. D. S. Chen, I. Mellman, Oncology meets immunology: the cancer-immunity cycle. *Immunity* **39**, 1–10 (2013).

3. M. J. Smyth, E. Cretney, M. H. Kershaw, Y. Hayakawa, Cytokines in cancer immunity and immunotherapy. *Immunol. Rev.* **202**, 275–293 (2004).

4. R. P. Donnelly, H. A. Young, A. S. Rosenberg, An Overview of Cytokines and Cytokine Antagonists as Therapeutic Agents. *Ann. N. Y. Acad. Sci.* **1182**, 1–13 (2009).

5. S. A. Rosenberg, IL-2: The First Effective Immunotherapy for Human Cancer. *J. Immunol.* **192**, 5451–5458 (2014).

6. J. R. Quesada, J. Reuben, J. T. Manning, E. M. Hersh, J. U. Gutterman, Alpha Interferon for Induction of Remission in Hairy-Cell Leukemia. *N. Engl. J. Med.* **310**, 15–18 (1984).

7. D. Briukhovetska, J. Dörr, S. Endres, P. Libby, C. A. Dinarello, S. Kobold, Interleukins in cancer: from biology to therapy. *Nat. Rev. Cancer* **21**, 481–499 (2021).

8. E. C. Borden, Interferons α and β in cancer: therapeutic opportunities from new insights. *Nat. Rev. Drug Discov.* **18**, 219–234 (2019).

9. E. C. Borden, Progress toward therapeutic application of interferons, 1979-1983. *Cancer* **54**, 2770–2776 (1984).

10. T. P. Cripe, Cancer gene therapy bears fruit. *Mol. Ther.* **31**, 303 (2023).

11. R. A. Saxton, C. R. Glassman, K. C. Garcia, Emerging principles of cytokine pharmacology and therapeutics. *Nat. Rev. Drug Discov.* **22**, 21–37 (2023).

12. P. G. Holder, S. A. Lim, C. S. Huang, P. Sharma, Y. S. Dagdas, B. Bulutoglu, J. T. Sockolosky, Engineering interferons and interleukins for cancer immunotherapy. *Adv. Drug Deliv. Rev.* **182**, 114112 (2022).

13. I. S. Pires, P. T. Hammond, D. J. Irvine, Engineering Strategies for Immunomodulatory Cytokine Therapies – Challenges and Clinical Progress. *Adv. Ther.* **4**, 2100035 (2021).

14. T. R. Malek, The Biology of Interleukin-2. *Annu. Rev. Immunol.* **26**, 453–479 (2008).

15. H. A. Martinez, I. Koliesnik, G. Kaber, J. K. Reid, N. Nagy, G. Barlow, B. A. Falk, C. O. Medina, A. Hargil, I. Vlodavsky, J.-P. Li, M. Pérez-Cruz, S.-W. Tang, E. H. Meyer, L. E. Wrenshall, J. D. Lord, K. C. Garcia, T. D. Palmer, L. Steinman, G. T. Nepom, T. N. Wight, P. L. Bollyky, H. F. Kuipers, FOXP3 + regulatory T cells use heparanase to access IL-2 bound to ECM in inflamed tissues. *BioRxiv Prepr. Serv. Biol.*, 2023.02.26.529772 (2023).

16. E. F. Zhu, S. A. Gai, C. F. Opel, B. H. Kwan, R. Surana, M. C. Mihm, M. J. Kauke, K. D. Moynihan, A. Angelini, R. T. Williams, M. T. Stephan, J. S. Kim, M. B. Yaffe, D. J. Irvine, L. M. Weiner, G. Dranoff, K. D. Wittrup, Synergistic innate and adaptive immune response to combination immunotherapy with anti-tumor antigen antibodies and extended serum half-life IL-2. *Cancer Cell* **27**, 489–501 (2015).

17. N. Momin, N. K. Mehta, N. R. Bennett, L. Ma, J. R. Palmeri, M. M. Chinn, E. A. Lutz, B. Kang, D. J. Irvine, S. Spranger, K. D. Wittrup, Anchoring of intratumorally administered cytokines to collagen safely potentiates systemic cancer immunotherapy. *Sci. Transl. Med.* **11** (2019).

18. B. Kwong, S. A. Gai, J. Elkhader, K. D. Wittrup, D. J. Irvine, Localized immunotherapy via liposome-anchored Anti-CD137 + IL-2 prevents lethal toxicity and elicits local and systemic antitumor immunity. *Cancer Res.* **73**, 1547–58 (2013).

19. J. T. Sockolosky, E. Trotta, G. Parisi, L. Picton, L. L. Su, A. C. Le, A. Chhabra, S. L. Silveria, B. M. George, I. C. King, M. R. Tiffany, K. Jude, L. V. Sibener, D. Baker, J. A. Shizuru, A. Ribas, J. A. Bluestone, K. C. Garcia, Selective targeting of engineered T cells using orthogonal IL-2 cytokine-receptor complexes. *Science* **359**, 1037–1042 (2018).

20. E. A. Lutz, Y. Agarwal, N. Momin, S. C. Cowles, J. R. Palmeri, E. Duong, V. Hornet, A. Sheen, B. M. Lax, A. M. Rothschilds, D. J. Irvine, S. Spranger, K. D. Wittrup, Alum-anchored intratumoral retention improves the tolerability and antitumor efficacy of type I interferon therapies. *Proc. Natl. Acad. Sci.* **119**, e2205983119 (2022).

21. K. Jung, J.-H. Ha, J.-E. Kim, J.-A. Kim, Y.-J. Kim, C.-H. Kim, Y.-S. Kim, Heterodimeric Fc-fused IL12 shows potent antitumor activity by generating memory CD8+ T cells. *Oncoimmunology* **7** (2018).

22. L. Baudino, Y. Shinohara, F. Nimmerjahn, J.-I. Furukawa, M. Nakata, E. Martínez-Soria, F. Petry, J. V. Ravetch, S.-I. Nishimura, S. Izui, Crucial Role of Aspartic Acid at Position 265 in the CH2 Domain for Murine IgG2a and IgG2b Fc-Associated Effector Functions1. *J. Immunol.* **181**, 6664–6669 (2008).

23. M. Lo, H. S. Kim, R. K. Tong, T. W. Bainbridge, J.-M. Vernes, Y. Zhang, Y. L. Lin, S. Chung, M. S. Dennis, Y. J. Y. Zuchero, R. J. Watts, J. A. Couch, Y. G. Meng, J. K. Atwal, R. J. Brezski, C. Spiess, J. A. Ernst, Effector-attenuating Substitutions

That Maintain Antibody Stability and Reduce Toxicity in Mice. *J. Biol. Chem.* **292**, 3900–3908 (2017).

24. N. Momin, J. R. Palmeri, E. A. Lutz, N. Jailkhani, H. Mak, A. Tabet, M. M. Chinn, B. H. Kang, V. Spanoudaki, R. O. Hynes, K. D. Wittrup, Maximizing response to intratumoral immunotherapy in mice by tuning local retention. *Nat. Commun.* **13**, 109 (2022).

25. J. Fallon, R. Tighe, G. Kradjian, W. Guzman, A. Bernhardt, B. Neuteboom, Y. Lan, H. Sabzevari, J. Schlom, J. W. Greiner, The immunocytokine NHS-IL12 as a potential cancer therapeutic. *Oncotarget* **5**, 1869–1884 (2014).

26. E. Gutierrez, M. Bigelow, C. LaCroix, J. Beech, P. Kirby, L. Markowitz, M. Shifrin, M. Naill, A. Braun, S. O'Neil, J.-M. Cuillerot, A. Cheung, A. Grinberg, N. Wagtmann, An optimized IL-12-Fc expands its therapeutic window, achieving strong activity against mouse tumors at tolerable drug doses. *Med*, S2666634023001034 (2023).

27. K. D. Moynihan, C. F. Opel, G. L. Szeto, A. Tzeng, E. F. Zhu, J. M. Engreitz, R. T. Williams, K. Rakhra, M. H. Zhang, A. M. Rothschilds, S. Kumari, R. L. Kelly, B. H. Kwan, W. Abraham, K. Hu, N. K. Mehta, M. J. Kauke, H. Suh, J. R. Cochran, D. A. Lauffenburger, K. D. Wittrup, D. J. Irvine, Eradication of large established tumors in mice by combination immunotherapy that engages innate and adaptive immune responses. *Nat. Med.* **22**, 1402–1410 (2016).

28. C. Wang, A. Cui, M. Bukenya, A. Aung, D. Pradhan, C. A. Whittaker, Y. Agarwal, A. Thomas, S. Liang, P. Amlashi, H. Suh, S. Spranger, N. Hacohen, D. J. Irvine, Reprogramming NK cells and macrophages via combined antibody and cytokine therapy primes tumors for elimination by checkpoint blockade. *Cell Rep.* **37**, 110021 (2021).

29. B. L. Osborn, M. Gu, K. J. Grzegorzewski, T. F. Logan, K. Crowder, G. R. Weiss, S. Syed, E. Rowensky, A. Tolcher, S. S. Agarwala, J. Kirkwood, R. M. Bukowski, P. Weiss, T. Olencki, R. Melder, Preliminary pharmacokinetic evaluation of Albuleukin; an interleukin-2 human serum albumin fusion protein, in solid tumor patients. *Cancer Res.* **64**, 1099–1099 (2004).

30. R. J. Melder, B. L. Osborn, T. Riccobene, P. Kanakaraj, P. Wei, G. Chen, D. Stolow, W. G. Halpern, T.-S. Migone, Q. Wang, K. J. Grzegorzewski, G. Gallant, Pharmacokinetics and in vitro and in vivo anti-tumor response of an interleukin-2-human serum albumin fusion protein in mice. *Cancer Immunol. Immunother.* **54**, 535–547 (2005).

31. E. Gutierrez, M. Bigelow, C. LaCroix, P. Kirby, L. Markowitz, M. Naill, S. O'Neil, P. A. Hull, J. Engelhardt, J.-M. Cuillerott, A. Cheung, A. Grinberg, N. Wagtmann, Abstract 1714: Preclinical characterization of DF6002/BMS-986415, a novel

differentiated IL-12 Fc-fusion protein with robust antitumor activity as monotherapy or in combination with anti-PD-1. *Cancer Res.* **81**, 1714 (2021).

32. B. Rogers, D. Dong, Z. Li, Z. Li, Recombinant Human Serum Albumin Fusion Proteins and Novel Applications in Drug Delivery and Therapy. *Curr. Pharm. Des.* **21**, 1899–1907 (2015).

33. A. Tzeng, B. H. Kwan, C. F. Opel, T. Navaratna, K. D. Wittrup, Antigen specificity can be irrelevant to immunocytokine efficacy and biodistribution. *Proc. Natl. Acad. Sci. U. S. A.* **112**, 3320–5 (2015).

34. E. A. Lutz, N. Jailkhani, N. Momin, Y. Huang, A. Sheen, B. H. Kang, K. D. Wittrup, R. O. Hynes, Intratumoral nanobody–IL-2 fusions that bind the tumor extracellular matrix suppress solid tumor growth in mice. *PNAS Nexus* **1**, pgac244 (2022).

35. B. Ribba, C. Boetsch, T. Nayak, H. P. Grimm, J. Charo, S. Evers, C. Klein, J. Tessier, J. E. Charoin, A. Phipps, P. Pisa, V. Teichgräber, Prediction of the Optimal Dosing Regimen Using a Mathematical Model of Tumor Uptake for Immunocytokine-Based Cancer Immunotherapy. *Clin. Cancer Res.* **24**, 3325–3333 (2018).

36. C. Hutmacher, D. Neri, Antibody-cytokine fusion proteins: Biopharmaceuticals with immunomodulatory properties for cancer therapy. *Adv. Drug Deliv. Rev.* **141**, 67–91 (2019).

37. F. Lansigan, R. Nakamura, D. P. Quick, D. Vlock, A. Raubitschek, S. D. Gillies, V. Bachanova, DI-Leu16-IL2, an Anti-CD20-Interleukin-2 Immunocytokine, Is Safe and Active in Patients with Relapsed and Refractory B-Cell Lymphoma: A Report of Maximum Tolerated Dose, Optimal Biologic Dose, and Recommended Phase 2 Dose. *Blood* **128**, 620 (2016).

38. G. Thurber, M. Schmidt, K. Wittrup, Factors determining antibody distribution in tumors. *Trends Pharmacol. Sci.*, S0165614707002854 (2008).

39. G. M. Thurber, M. M. Schmidt, K. D. Wittrup, Antibody tumor penetration: Transport opposed by systemic and antigen-mediated clearance. *Adv. Drug Deliv. Rev.* **60**, 1421–1434 (2008).

40. K. D. Wittrup, G. M. Thurber, M. M. Schmidt, J. J. Rhoden, “Chapter ten - Practical Theoretic Guidance for the Design of Tumor-Targeting Agents” in *Methods in Enzymology*, K. D. Wittrup, G. L. Verdine, Eds. (Academic Press, 2012; https://www.sciencedirect.com/science/article/pii/B9780123969620000100)vol. 503 of *Protein Engineering for Therapeutics, Part B*, pp. 255–268.

41. G. Garcin, F. Paul, M. Staufenbiel, Y. Bordat, J. Van der Heyden, S. Wilmes, G. Cartron, F. Apparailly, S. De Koker, J. Piehler, J. Tavernier, G. Uzé, High efficiency cell-specific targeting of cytokine activity. *Nat. Commun.* **5**, 3016 (2014).

42. K. Moynihan, D. Pappas, H. Sultan, T. Park, M. Kumar, R. Lan, I. Ni, J. Chen, M. Chin, T. Schumacher, A. Yeung, R. Schreiber, I. Djuretic, 1092 The CD8+ T cell selectivity of AB248 is essential for optimal anti-tumor activity and safety in nonclinical models. *J. Immunother. Cancer* **10** (2022).

43. L. Codarri Deak, V. Nicolini, M. Hashimoto, M. Karagianni, P. C. Schwalie, L. Lauener, E. M. Varypataki, M. Richard, E. Bommer, J. Sam, S. Joller, M. Perro, F. Cremasco, L. Kunz, E. Yanguez, T. Hüsser, R. Schlenker, M. Mariani, V. Tosevski, S. Herter, M. Bacac, I. Waldhauer, S. Colombetti, X. Gueripel, S. Wullschleger, M. Tichet, D. Hanahan, H. T. Kissick, S. Leclair, A. Freimoser-Grundschober, S. Seeber, V. Teichgräber, R. Ahmed, C. Klein, P. Umaña, PD-1-cis IL-2R agonism yields better effectors from stem-like CD8+ T cells. *Nature*, doi: 10.1038/s41586-022-05192-0 (2022).

44. S. C. Cowles, A. Sheen, L. Santollani, E. A. Lutz, B. M. Lax, J. R. Palmeri, G. J. Freeman, K. D. Wittrup, An affinity threshold for maximum efficacy in anti-PD-1 immunotherapy. *mAbs* **14**, 2088454 (2022).

45. Z. Ren, A. Zhang, Z. Sun, Y. Liang, J. Ye, J. Qiao, B. Li, Y.-X. Fu, Selective delivery of low-affinity IL-2 to PD-1$^+$ T cells rejuvenates antitumor immunity with reduced toxicity. *J. Clin. Invest.* **132** (2022).

46. R. Greer, H. Nguyen, P. Mesko, R. Lan, W. W. Prior, H. Sultan, M. Sukthankar, I. Ni, S. M. Chin, K. Moynihan, T. Schumacher, R. Schreiber, A. Yeung, I. Djuretic, 1083 AB821 is a CD8+ T cell selective IL-21 with enhanced bioavailability that mediates potent anti-tumor activity, cytotoxicity, and expansion of memory CD8+ T cells. *J. Immunother. Cancer* **10** (2022).

47. Y. Xu, L. C. Carrascosa, Y. A. Yeung, M. L.-H. Chu, W. Yang, I. Djuretic, D. C. Pappas, J. Zeytounian, Z. Ge, V. de Ruiter, G. R. Starbeck-Miller, J. Patterson, D. Rigas, S.-H. Chen, E. Kraynov, P. P. Boor, L. Noordam, M. Doukas, D. Tsao, J. N. Ijzermans, J. Guo, D. J. Grünhagen, J. Erdmann, J. Verheij, M. E. van Royen, P. G. Doornebosch, R. Feldman, T. Park, S. Mahmoudi, M. Dorywalska, I. Ni, S. M. Chin, T. Mistry, L. Mosyak, L. Lin, K. A. Ching, K. C. Lindquist, C. Ji, L. M. Londono, B. Kuang, R. Rickert, J. Kwekkeboom, D. Sprengers, T.-H. Huang, J. Chaparro-Riggers, An Engineered IL15 Cytokine Mutein Fused to an Anti-PD1 Improves Intratumoral T-cell Function and Antitumor Immunity. *Cancer Immunol. Res.* **9**, 1141–1157 (2021).

48. W. B. Coley, THE TREATMENT OF MALIGNANT TUMORS BY REPEATED INOCULATIONS OF ERYSIPELAS: WITH A REPORT OF TEN ORIGINAL CASES.1: BIBLIOGRAPHY. - ProQuest.

https://www.proquest.com/docview/125251850?pq-origsite=gscholar&fromopenview=true.

49. A. Marabelle, H. Kohrt, C. Caux, R. Levy, Intratumoral immunization: a new paradigm for cancer therapy. *Clin. Cancer Res. Off. J. Am. Assoc. Cancer Res.* **20**, 1747–56 (2014).

50. A. Marabelle, L. Tselikas, T. de Baere, R. Houot, Intratumoral immunotherapy: using the tumor as the remedy. *Ann. Oncol.* **28**, xii33–xii43 (2017).

51. S. Champiat, L. Tselikas, S. Farhane, T. Raoult, M. Texier, E. Lanoy, C. Massard, C. Robert, S. Ammari, T. De Baère, A. Marabelle, Intratumoral Immunotherapy: From Trial Design to Clinical Practice. *Clin. Cancer Res.* **27**, 665–679 (2021).

52. M. H. Cohen, J. M. Jessup, E. L. Felix, J. L. Weese, R. B. Herberman, Intralesional treatment of recurrent metastatic cutaneous malignant melanoma: a randomized prospective study of intralesional Bacillus Calmette-Guerin versus intralesional dinitrochlorobenzene. *Cancer* **41**, 2456–2463 (1978).

53. M. J. Silverstein, J. DeKernion, D. L. Morton, Malignant melanoma metastatic to the bladder. Regression following intratumor injection of BCG vaccine. *JAMA* **229**, 688 (1974).

54. M. M. Milhem, G. V. Long, C. J. Hoimes, A. Amin, C. D. Lao, R. M. Conry, J. Hunt, G. A. Daniels, M. Almubarak, M. F. Shaheen, T. M. Medina, M. A. Barve, S. K. Bishnoi, E. A. Abdi, M. J. Chisamore, B. Xing, A. Candia, E. Gamelin, R. Janssen, A. Ribas, Phase 1b/2, open label, multicenter, study of the combination of SD-101 and pembrolizumab in patients with advanced melanoma who are naïve to anti-PD-1 therapy. *J. Clin. Oncol.* **37**, 9534–9534 (2019).

55. H. M. Babiker, V. Subbiah, O. Maguire, S. Rahimian, H. Minderman, C. L. Haymaker, C. Bernatchez, E. Borazanci, J. Geib, S. K. Chunduru, P. M. Anderson, I. Puzanov, A. Diab, Abstract 4062: Activation of innate and adaptive immunity using intratumoral tilsotolimod (IMO-2125) as monotherapy in patients with refractory solid tumors: a phase Ib study (ILLUMINATE-101). *Cancer Res.* **79**, 4062 (2019).

56. A. Ribas, T. Medina, S. Kummar, A. Amin, A. Kalbasi, J. J. Drabick, M. Barve, G. A. Daniels, D. J. Wong, E. V. Schmidt, A. F. Candia, R. L. Coffman, A. C. F. Leung, R. S. Janssen, SD-101 in Combination with Pembrolizumab in Advanced Melanoma: Results of a Phase Ib, Multicenter Study. *Cancer Discov.* **8**, 1250–1257 (2018).

57. Y. Agarwal, L. E. Milling, J. Y. H. Chang, L. Santollani, A. Sheen, E. A. Lutz, A. Tabet, J. Stinson, K. Ni, K. A. Rodrigues, T. J. Moyer, M. B. Melo, D. J. Irvine, K. D.

Wittrup, Intratumourally injected alum-tethered cytokines elicit potent and safer local and systemic anticancer immunity. *Nat. Biomed. Eng.* **6**, 129–143 (2022).

58. B. Kwong, H. Liu, D. J. Irvine, Induction of potent anti-tumor responses while eliminating systemic side effects via liposome-anchored combinatorial immunotherapy. *Biomaterials* **32**, 5134–47 (2011).

59. A. Naba, K. R. Clauser, H. Ding, C. A. Whittaker, S. A. Carr, R. O. Hynes, The extracellular matrix: Tools and insights for the “omics” era. *Matrix Biol. J. Int. Soc. Matrix Biol.* **49**, 10–24 (2016).

60. J. Riegler, Y. Labyed, S. Rosenzweig, V. Javinal, A. Castiglioni, C. X. Dominguez, J. E. Long, Q. Li, W. Sandoval, M. R. Junttila, S. J. Turley, J. Schartner, R. A. D. Carano, Tumor Elastography and Its Association with Collagen and the Tumor Microenvironment. *Clin. Cancer Res. Off. J. Am. Assoc. Cancer Res.* **24**, 4455–4467 (2018).

61. J. Kemna, E. Gout, L. Daniau, J. Lao, K. Weißert, S. Ammann, R. Kühn, M. Richter, C. Molenda, A. Sporbert, D. Zocholl, R. Klopfleisch, H. Lortat-Jacob, P. Aichele, T. Kammertoens, T. Blankenstein, IFNγ binding to extracellular matrix prevents fatal systemic toxicity. *Nat. Immunol.* **24**, 414–422 (2023).

62. M. Hasan, S. Najjam, M. Y. Gordon, R. V. Gibbs, C. C. Rider, IL-12 is a heparin-binding cytokine. *J. Immunol. Baltim. Md 1950* **162**, 1064–1070 (1999).

63. B. Horton, M. Zagorulya, N. Momin, Y. Agarwal, K. Wittrup, S. Spranger, 1087 Addition of IL-2 overcomes lung tumor resistance to IL-12 by coordinating cytotoxic and regulatory T cell responses. *J. Immunother. Cancer* **10** (2022).

64. J. A. Stinson, A. Sheen, N. Momin, J. Hampel, R. Bernstein, R. Kamerer, B. Fadl-Alla, J. Samuelson, E. Fink, T. M. Fan, K. D. Wittrup, Collagen-anchored interleukin-2 and interleukin-12 safely reprogram the tumor microenvironment in canine soft tissue sarcomas. *Clin. Cancer Res.*, CCR-23-0006 (2023).

65. A. R. Chakravarti, C. E. Groer, H. Gong, V. Yudistyra, M. L. Forrest, C. J. Berkland, Design of a Tumor Binding GMCSF as Intratumoral Immunotherapy of Solid Tumors. *Mol. Pharm.* **20**, 1975–1989 (2023).

66. J. Ishihara, A. Ishihara, K. Sasaki, S. S.-Y. Lee, J.-M. Williford, M. Yasui, H. Abe, L. Potin, P. Hosseinchi, K. Fukunaga, M. M. Raczy, L. T. Gray, A. Mansurov, K. Katsumata, M. Fukayama, S. J. Kron, M. A. Swartz, J. A. Hubbell, Targeted antibody and cytokine cancer immunotherapies through collagen affinity. *Sci. Transl. Med.* **11**, eaau3259 (2019).

67. A. Mansurov, J. Ishihara, P. Hosseinchi, L. Potin, T. M. Marchell, A. Ishihara, J.-M. Williford, A. T. Alpar, M. M. Raczy, L. T. Gray, M. A. Swartz, J. A. Hubbell,

Collagen-binding IL-12 enhances tumour inflammation and drives the complete remission of established immunologically cold mouse tumours. *Nat. Biomed. Eng.* **4**, 531–543 (2020).

68. A. Mansurov, P. Hosseinchi, K. Chang, A. L. Lauterbach, L. T. Gray, A. T. Alpar, E. Budina, A. J. Slezak, S. Kang, S. Cao, A. Solanki, S. Gomes, J.-M. Williford, M. A. Swartz, J. L. Mendoza, J. Ishihara, J. A. Hubbell, Masking the immunotoxicity of interleukin-12 by fusing it with a domain of its receptor via a tumour-protease-cleavable linker. *Nat. Biomed. Eng.* **6**, 819–829 (2022).

69. B. E. Nelson, J. J. Adashek, S. H. Lin, V. Subbiah, The abscopal effect in patients with cancer receiving immunotherapy. *Med* **4**, 233–244 (2023).

70. A. Mukhopadhyay, J. Wright, S. Shirley, D. A. Canton, C. Burkart, R. J. Connolly, J. S. Campbell, R. H. Pierce, Characterization of abscopal effects of intratumoral electroporation-mediated IL-12 gene therapy. *Gene Ther.* **26**, 1–15 (2019).

71. H. L. Kaufman, T. Amatruda, T. Reid, R. Gonzalez, J. Glaspy, E. Whitman, K. Harrington, J. Nemunaitis, A. Zloza, M. Wolf, N. N. Senzer, Systemic versus local responses in melanoma patients treated with talimogene laherparepvec from a multi-institutional phase II study. *J. Immunother. Cancer* **4**, 12 (2016).

72. R. Danielli, R. Patuzzo, A. M. Di Giacomo, G. Gallino, A. Maurichi, A. Di Florio, O. Cutaia, A. Lazzeri, C. Fazio, C. Miracco, L. Giovannoni, G. Elia, D. Neri, M. Maio, M. Santinami, Intralesional administration of L19-IL2/L19-TNF in stage III or stage IVM1a melanoma patients: results of a phase II study. *Cancer Immunol. Immunother. CII* **64**, 999–1009 (2015).

73. A. Tzeng, M. J. Kauke, E. F. Zhu, K. D. Moynihan, C. F. Opel, N. J. Yang, N. Mehta, R. L. Kelly, G. L. Szeto, W. W. Overwijk, D. J. Irvine, K. D. Wittrup, Temporally Programmed CD8α + DC Activation Enhances Combination Cancer Immunotherapy. *Cell Rep.* **17**, 2503–2511 (2016).

74. A. Rothschilds, A. Tzeng, N. K. Mehta, K. D. Moynihan, D. J. Irvine, K. D. Wittrup, Order of administration of combination cytokine therapies can decouple toxicity from efficacy in syngeneic mouse tumor models. *Oncoimmunology* **8** (2019).

75. D. H. Barouch, S. Santra, T. D. Steenbeke, X. X. Zheng, H. C. Perry, M.-E. Davies, D. C. Freed, A. Craiu, T. B. Strom, J. W. Shiver, N. L. Letvin, Augmentation and Suppression of Immune Responses to an HIV-1 DNA Vaccine by Plasmid Cytokine/Ig Administration. *J. Immunol.* **161**, 1875–1882 (1998).

76. D. H. Barouch, A. Craiu, M. J. Kuroda, J. E. Schmitz, X. X. Zheng, S. Santra, J. D. Frost, G. R. Krivulka, M. A. Lifton, C. L. Crabbs, G. Heidecker, H. C. Perry, M.-E. Davies, H. Xie, C. E. Nickerson, T. D. Steenbeke, C. I. Lord, D. C. Montefiori, T. B. Strom, J. W. Shiver, M. G. Lewis, N. L. Letvin, Augmentation of immune responses

to HIV-1 and simian immunodeficiency virus DNA vaccines by IL-2/Ig plasmid administration in rhesus monkeys. *Proc. Natl. Acad. Sci.* **97**, 4192–4197 (2000).

77. D. H. Barouch, S. Santra, J. E. Schmitz, M. J. Kuroda, T.-M. Fu, W. Wagner, M. Bilska, A. Craiu, X. X. Zheng, G. R. Krivulka, K. Beaudry, M. A. Lifton, C. E. Nickerson, W. L. Trigona, K. Punt, D. C. Freed, L. Guan, S. Dubey, D. Casimiro, A. Simon, M.-E. Davies, M. Chastain, T. B. Strom, R. S. Gelman, D. C. Montefiori, M. G. Lewis, E. A. Emini, J. W. Shiver, N. L. Letvin, Control of Viremia and Prevention of Clinical AIDS in Rhesus Monkeys by Cytokine-Augmented DNA Vaccination. *Science* **290**, 486–492 (2000).

78. L. R. Baden, W. A. Blattner, C. Morgan, Y. Huang, O. D. Defawe, M. E. Sobieszczyk, N. Kochar, G. D. Tomaras, M. J. McElrath, N. Russell, K. Brandariz, M. Cardinali, B. S. Graham, D. H. Barouch, R. Dolin, the NIAID HIV Vaccine Trials Network 044 Study Team, Timing of Plasmid Cytokine (IL-2/Ig) Administration Affects HIV-1 Vaccine Immunogenicity in HIV-Seronegative Subjects. *J. Infect. Dis.* **204**, 1541–1549 (2011).

79. T. Mustelin, T. Vang, N. Bottini, Protein tyrosine phosphatases and the immune response. *Nat. Rev. Immunol.* **5**, 43–57 (2005).

80. N. Holmes, CD45: all is not yet crystal clear. *Immunology* **117**, 145–155 (2006).

81. I. S. Trowbridge, M. L. Thomas, CD45: an emerging role as a protein tyrosine phosphatase required for lymphocyte activation and development. *Annu. Rev. Immunol.* **12**, 85–116 (1994).

82. J. M. Penninger, J. Irie-Sasaki, T. Sasaki, A. J. Oliveira-dos-Santos, CD45: new jobs for an old acquaintance. *Nat. Immunol.* **2**, 389–396 (2001).

83. M. L. Hermiston, Z. Xu, A. Weiss, CD45: A Critical Regulator of Signaling Thresholds in Immune Cells. *Annu. Rev. Immunol.* **21**, 107–137 (2003).

84. S. M. Krummey, A. B. Morris, J. R. Jacobs, D. J. McGuire, S. Ando, K. P. Tong, W. Zhang, J. Robertson, S. A. Guasch, K. Araki, C. P. Larsen, B. D. Evavold, H. T. Kissick, M. L. Ford, CD45RB Status of CD8+ T Cell Memory Defines T Cell Receptor Affinity and Persistence. *Cell Rep.* **30**, 1282-1291.e5 (2020).

85. E. Krzywinska, A. Cornillon, N. Allende-Vega, D.-N. Vo, C. Rene, Z.-Y. Lu, C. Pasero, D. Olive, N. Fegueux, P. Ceballos, Y. Hicheri, M. Sobecki, J.-F. Rossi, G. Cartron, M. Villalba, CD45 Isoform Profile Identifies Natural Killer (NK) Subsets with Differential Activity. *PLoS ONE* **11** (2016).

86. J. Irie-Sasaki, T. Sasaki, W. Matsumoto, A. Opavsky, M. Cheng, G. Welstead, E. Griffiths, C. Krawczyk, C. D. Richardson, K. Aitken, N. Iscove, G. Koretzky, P.

Johnson, P. Liu, D. M. Rothstein, J. M. Penninger, CD45 is a JAK phosphatase and negatively regulates cytokine receptor signalling. *Nature* **409**, 349–354 (2001).

87. C. B. Carbone, N. Kern, R. A. Fernandes, E. Hui, X. Su, K. C. Garcia, R. D. Vale, In vitro reconstitution of T cell receptor-mediated segregation of the CD45 phosphatase. *Proc. Natl. Acad. Sci.* **114**, E9338–E9345 (2017).

88. R. A. Fernandes, L. Su, Y. Nishiga, J. Ren, A. M. Bhuiyan, N. Cheng, C. J. Kuo, L. K. Picton, S. Ohtsuki, R. G. Majzner, S. P. Rietberg, C. L. Mackall, Q. Yin, L. R. Ali, X. Yang, C. S. Savvides, J. Sage, M. Dougan, K. C. Garcia, Immune receptor inhibition through enforced phosphatase recruitment. *Nature* **586**, 779–784 (2020).

89. A. H. Lippert, C. Paluch, M. Gaglioni, M. T. Vuong, J. McColl, E. Jenkins, M. Fellermeyer, J. Clarke, S. Sharma, S. Moreira da Silva, B. Akkaya, C. Anzilotti, S. H. Morgan, C. F. Jessup, M. Körbel, U. Gileadi, J. Leitner, R. Knox, M. Chirifu, J. Huo, S. Yu, N. Ashman, Y. Lui, I. Wilkinson, K. E. Attfield, L. Fugger, N. J. Robertson, C. J. Lynch, L. Murray, P. Steinberger, A. M. Santos, S. F. Lee, R. J. Cornall, D. Klenerman, S. J. Davis, Antibody agonists trigger immune receptor signaling through local exclusion of receptor-type protein tyrosine phosphatases. *Immunity* **57**, 256-270.e10 (2024).

90. L. Tang, Y. Zheng, M. B. Melo, L. Mabardi, A. P. Castaño, Y.-Q. Xie, N. Li, S. B. Kudchodkar, H. C. Wong, E. K. Jeng, M. V. Maus, D. J. Irvine, Enhancing T cell therapy through TCR-signaling-responsive nanoparticle drug delivery. *Nat. Biotechnol.* **36**, 707–716 (2018).

91. K. D. Wittrup, H. L. Kaufman, M. M. Schmidt, D. J. Irvine, Intratumorally anchored cytokine therapy. *Expert Opin. Drug Deliv.* **19**, 725–732 (2022).

92. I. Melero, E. Castanon, M. Alvarez, S. Champiat, A. Marabelle, Intratumoural administration and tumour tissue targeting of cancer immunotherapies. *Nat. Rev. Clin. Oncol.* **18**, 558–576 (2021).

93. M. A. Aznar, N. Tinari, A. J. Rullán, A. R. Sánchez-Paulete, M. E. Rodriguez-Ruiz, I. Melero, Intratumoral Delivery of Immunotherapy—Act Locally, Think Globally. *J. Immunol.* **198**, 31–39 (2016).

94. L. Tang, Y. Zheng, M. B. Melo, L. Mabardi, A. P. Castaño, Y.-Q. Xie, N. Li, S. B. Kudchodkar, H. C. Wong, E. K. Jeng, M. V. Maus, D. J. Irvine, Enhancing T cell therapy through TCR-signaling-responsive nanoparticle drug delivery. *Nat. Biotechnol.* **36**, 707–716 (2018).

95. Y. Zheng, L. Tang, L. Mabardi, S. Kumari, D. J. Irvine, Enhancing Adoptive Cell Therapy of Cancer through Targeted Delivery of Small-Molecule Immunomodulators to Internalizing or Noninternalizing Receptors. *ACS Nano* **11**, 3089–3100 (2017).

96. E. L. Dane, A. Belessiotis-Richards, C. Backlund, J. Wang, K. Hidaka, L. E. Milling, S. Bhagchandani, M. B. Melo, S. Wu, N. Li, N. Donahue, K. Ni, L. Ma, M. Okaniwa, M. M. Stevens, A. Alexander-Katz, D. J. Irvine, STING agonist delivery by tumour-penetrating PEG-lipid nanodiscs primes robust anticancer immunity. *Nat. Mater.* **21**, 710–720 (2022).

97. J. J. Orozco, A. L. Kenoyer, Y. Lin, S. O'Steen, R. Guel, M. E. Nartea, A. H. Hernandez, M. D. Hylarides, D. R. Fisher, E. R. Balkin, D. K. Hamlin, D. S. Wilbur, K. D. Orcutt, K. D. Wittrup, D. J. Green, A. K. Gopal, B. G. Till, B. Sandmaier, O. W. Press, J. M. Pagel, Therapy of Myeloid Leukemia using Novel Bispecific Fusion Proteins Targeting CD45 and 90Y-DOTA. *Mol. Cancer Ther.* **19**, 2575–2584 (2020).

98. M. M. Schmidt, G. M. Thurber, K. D. Wittrup, Kinetics of anti-carcinoembryonic antigen antibody internalization: effects of affinity, bivalency, and stability. *Cancer Immunol. Immunother. CII* **57**, 1879–90 (2008).

99. S. Gaggero, J. Martinez-Fabregas, A. Cozzani, P. K. Fyfe, M. Leprohon, J. Yang, F. E. Thomasen, H. Winkelmann, R. Magnez, A. G. Conti, S. Wilmes, E. Pohler, M. van Gijsel Bonnello, X. Thuru, B. Quesnel, F. Soncin, J. Piehler, K. Lindorff-Larsen, R. Roychoudhuri, I. Moraga, S. Mitra, IL-2 is inactivated by the acidic pH environment of tumors enabling engineering of a pH-selective mutein. *Sci. Immunol.* **7**, eade5686 (2022).

100. N. Prokhnevska, M. A. Cardenas, R. M. Valanparambil, E. Sobierajska, B. G. Barwick, C. Jansen, A. Reyes Moon, P. Gregorova, L. delBalzo, R. Greenwald, M. A. Bilen, M. Alemozaffar, S. Joshi, C. Cimmino, C. Larsen, V. Master, M. Sanda, H. Kissick, CD8+ T cell activation in cancer comprises an initial activation phase in lymph nodes followed by effector differentiation within the tumor. *Immunity*, S1074761322006069 (2022).

101. B. E. Grace, C. M. Backlund, D. M. Morgan, B. H. Kang, N. K. Singh, B. D. Huisman, C. G. Rappazzo, K. D. Moynihan, L. Maiorino, C. S. Dobson, T. Kyung, K. S. Gordon, P. V. Holec, O. C. T. Mbah, D. Garafola, S. Wu, J. C. Love, K. D. Wittrup, D. J. Irvine, M. E. Birnbaum, Identification of Highly Cross-Reactive Mimotopes for a Public T Cell Response in Murine Melanoma. *Front. Immunol.* **13** (2022).

102. J.-C. Beltra, M. S. Abdel-Hakeem, S. Manne, Z. Zhang, H. Huang, M. Kurachi, L. Su, L. Picton, Y. Muroyama, V. Casella, Y. J. Huang, J. R. Giles, D. Mathew, J. Belman, M. Klapholz, H. Decaluwe, A. C. Huang, S. L. Berger, K. C. Garcia, E. J. Wherry, "Enhanced STAT5a activation rewires exhausted CD8 T cells during chronic stimulation to acquire a hybrid durable effector like state" (preprint, Immunology, 2022); https://doi.org/10.1101/2022.10.03.509766.

103. K. A. Connolly, M. Kuchroo, A. Venkat, A. Khatun, J. Wang, I. William, N. I. Hornick, B. L. Fitzgerald, M. Damo, M. Y. Kasmani, C. Cui, E. Fagerberg, I. Monroy,

A. Hutchins, J. F. Cheung, G. G. Foster, D. L. Mariuzza, M. Nader, H. Zhao, W. Cui, S. Krishnaswamy, N. S. Joshi, A reservoir of stem-like CD8+ T cells in the tumor-draining lymph node preserves the ongoing antitumor immune response. *Sci. Immunol.* **6**, eabg7836 (2021).

104. J. M. Schenkel, R. H. Herbst, D. Canner, A. Li, M. Hillman, S.-L. Shanahan, G. Gibbons, O. C. Smith, J. Y. Kim, P. Westcott, W. L. Hwang, W. A. Freed-Pastor, G. Eng, M. S. Cuoco, P. Rogers, J. K. Park, M. L. Burger, O. Rozenblatt-Rosen, L. Cong, K. E. Pauken, A. Regev, T. Jacks, Conventional type I dendritic cells maintain a reservoir of proliferative tumor-antigen specific TCF-1+ CD8+ T cells in tumor-draining lymph nodes. *Immunity* **54**, 2338-2353.e6 (2021).

105. S. V. Gearty, F. Dündar, P. Zumbo, G. Espinosa-Carrasco, M. Shakiba, F. J. Sanchez-Rivera, N. D. Socci, P. Trivedi, S. W. Lowe, P. Lauer, N. Mohibullah, A. Viale, T. P. DiLorenzo, D. Betel, A. Schietinger, An autoimmune stem-like CD8 T cell population drives type 1 diabetes. *Nature* **602**, 156–161 (2022).

106. D. Zehn, R. Thimme, E. Lugli, G. P. de Almeida, A. Oxenius, 'Stem-like' precursors are the fount to sustain persistent CD8+ T cell responses. *Nat. Immunol.* **23**, 836–847 (2022).

107. I. Siddiqui, K. Schaeuble, V. Chennupati, S. A. Fuertes Marraco, S. Calderon-Copete, D. Pais Ferreira, S. J. Carmona, L. Scarpellino, D. Gfeller, S. Pradervand, S. A. Luther, D. E. Speiser, W. Held, Intratumoral Tcf1+PD-1+CD8+ T Cells with Stem-like Properties Promote Tumor Control in Response to Vaccination and Checkpoint Blockade Immunotherapy. *Immunity* **50**, 195-211.e10 (2019).

108. G. Glatting, M. Müller, B. Koop, K. Hohl, C. Friesen, B. Neumaier, E. Berrie, P. Bird, G. Hale, N. M. Blumstein, H. Waldmann, D. Bunjes, S. N. Reske, Anti-CD45 Monoclonal Antibody YAML568: A Promising Radioimmunoconjugate for Targeted Therapy of Acute Leukemia. *J. Nucl. Med.* **47**, 1335–1341 (2006).

109. J. A. Stinson, M. M. P. Barbosa, A. Sheen, N. Momin, E. Fink, J. Hampel, K. Selting, R. Kamerer, K. L. Bailey, K. D. Wittrup, T. M. Fan, Tumor-localized interleukin-2 and interleukin-12 combine with radiation therapy to safely potentiate regression of advanced malignant melanoma in pet dogs. bioRxiv [Preprint] (2024). https://doi.org/10.1101/2024.02.12.579965.

110. C. McMahon, A. S. Baier, R. Pascolutti, M. Wegrecki, S. Zheng, J. X. Ong, S. C. Erlandson, D. Hilger, S. G. F. Rasmussen, A. M. Ring, A. Manglik, A. C. Kruse, Yeast surface display platform for rapid discovery of conformationally selective nanobodies. *Nat. Struct. Mol. Biol.* **25**, 289–296 (2018).

111. M. K. Rahim, T. L. H. Okholm, K. B. Jones, E. E. McCarthy, C. C. Liu, J. L. Yee, S. J. Tamaki, D. M. Marquez, I. Tenvooren, K. Wai, A. Cheung, B. R. Davidson, V. Johri, B. Samad, W. E. O'Gorman, M. F. Krummel, A. Van Zante, A. J. Combes, M.

Angelo, L. Fong, A. P. Algazi, P. Ha, M. H. Spitzer, Dynamic CD8+ T cell responses to cancer immunotherapy in human regional lymph nodes are disrupted in metastatic lymph nodes. *Cell* **186**, 1127-1143.e18 (2023).

112. J. A. Pai, M. D. Hellmann, J. L. Sauter, M. Mattar, H. Rizvi, H. J. Woo, N. Shah, E. M. Nguyen, F. Z. Uddin, A. Quintanal-Villalonga, J. M. Chan, P. Manoj, V. Allaj, M. K. Baine, U. K. Bhanot, M. Jain, I. Linkov, F. Meng, D. Brown, J. E. Chaft, A. J. Plodkowski, M. Gigoux, H. H. Won, T. Sen, D. K. Wells, M. T. A. Donoghue, E. de Stanchina, J. D. Wolchok, B. Loomis, T. Merghoub, C. M. Rudin, A. Chow, A. T. Satpathy, Lineage tracing reveals clonal progenitors and long-term persistence of tumor-specific T cells during immune checkpoint blockade. *Cancer Cell* **41**, 776-790.e7 (2023).

113. Z. Perez Horta, S. Saseedhar, A. L. Rakhmilevich, L. Carmichael, J. A. Hank, M. Boyden, S. D. Gillies, P. M. Sondel, Human and murine IL2 receptors differentially respond to the human-IL2 component of immunocytokines. *OncoImmunology* **8**, e1238538 (2019).

114. C. M. Van Herpen, R. Huijbens, M. Looman, J. De Vries, H. Marres, J. Van De Ven, R. Hermsen, G. J. Adema, P. H. De Mulder, Pharmacokinetics and immunological aspects of a phase Ib study with intratumoral administration of recombinant human interleukin-12 in patients with head and neck squamous cell carcinoma: a decrease of T-bet in peripheral blood mononuclear cells. *Clin. Cancer Res. Off. J. Am. Assoc. Cancer Res.* **9**, 2950–2956 (2003).

115. J. P. Leonard, M. L. Sherman, G. L. Fisher, L. J. Buchanan, G. Larsen, M. B. Atkins, J. A. Sosman, J. P. Dutcher, N. J. Vogelzang, J. L. Ryan, Effects of single-dose interleukin-12 exposure on interleukin-12-associated toxicity and interferon-gamma production. *Blood* **90**, 2541–2548 (1997).

116. S. Dow, A Role for Dogs in Advancing Cancer Immunotherapy Research. *Front. Immunol.* **10**, 2935 (2019).

117. V. Thorsson, D. L. Gibbs, S. D. Brown, D. Wolf, D. S. Bortone, T.-H. Ou Yang, E. Porta-Pardo, G. F. Gao, C. L. Plaisier, J. A. Eddy, E. Ziv, A. C. Culhane, E. O. Paull, I. K. A. Sivakumar, A. J. Gentles, R. Malhotra, F. Farshidfar, A. Colaprico, J. S. Parker, L. E. Mose, N. S. Vo, J. Liu, Y. Liu, J. Rader, V. Dhankani, S. M. Reynolds, R. Bowlby, A. Califano, A. D. Cherniack, D. Anastassiou, D. Bedognetti, Y. Mokrab, A. M. Newman, A. Rao, K. Chen, A. Krasnitz, H. Hu, T. M. Malta, H. Noushmehr, C. S. Pedamallu, S. Bullman, A. I. Ojesina, A. Lamb, W. Zhou, H. Shen, T. K. Choueiri, J. N. Weinstein, J. Guinney, J. Saltz, R. A. Holt, C. S. Rabkin, Cancer Genome Atlas Research Network, A. J. Lazar, J. S. Serody, E. G. Demicco, M. L. Disis, B. G. Vincent, I. Shmulevich, The Immune Landscape of Cancer. *Immunity* **48**, 812-830.e14 (2018).

118. Z. Zeng, C. J. Wong, L. Yang, N. Ouardaoui, D. Li, W. Zhang, S. Gu, Y. Zhang, Y. Liu, X. Wang, J. Fu, L. Zhou, B. Zhang, S. Kim, K. B. Yates, M. Brown, G. J. Freeman, R. Uppaluri, R. Manguso, X. S. Liu, TISMO: syngeneic mouse tumor database to model tumor immunity and immunotherapy response. *Nucleic Acids Res.* **50**, D1391–D1397 (2022).